Fundamental aspects of reactions in titanium-silicon thin films for integrated circuits

Citation for published version (APA):
Raaijmakers, I. J. M. M. (1988). *Fundamental aspects of reactions in titanium-silicon thin films for integrated circuits*. [Phd Thesis 1 (Research TU/e / Graduation TU/e), Applied Physics and Science Education]. Technische Universiteit Eindhoven. https://doi.org/10.6100/IR291927

DOI:
10.6100/IR291927

Document status and date:
Published: 01/01/1988

Document Version:
Publisher’s PDF, also known as Version of Record (includes final page, issue and volume numbers)

Please check the document version of this publication:

• A submitted manuscript is the version of the article upon submission and before peer-review. There can be important differences between the submitted version and the official published version of record. People interested in the research are advised to contact the author for the final version of the publication, or visit the DOI to the publisher's website.
• The final author version and the galley proof are versions of the publication after peer review.
• The final published version features the final layout of the paper including the volume, issue and page numbers.

Link to publication

General rights
Copyright and moral rights for the publications made accessible in the public portal are retained by the authors and/or other copyright owners and it is a condition of accessing publications that users recognise and abide by the legal requirements associated with these rights.

- Users may download and print one copy of any publication from the public portal for the purpose of private study or research.
- You may not further distribute the material or use it for any profit-making activity or commercial gain
- You may freely distribute the URL identifying the publication in the public portal.

If the publication is distributed under the terms of Article 25fa of the Dutch Copyright Act, indicated by the “Taverne” license above, please follow below link for the End User Agreement:

www.tue.nl/taverne

Take down policy
If you believe that this document breaches copyright please contact us at:

openaccess@tue.nl

providing details and we will investigate your claim.

Download date: 04. Oct. 2023

FUNDAMENTAL ASPECTS OF REACTIONS IN TITANIUM–SILICON THIN FILMS FOR INTEGRATED CIRCUITS

Ivo J. M. M. Raaijmakers

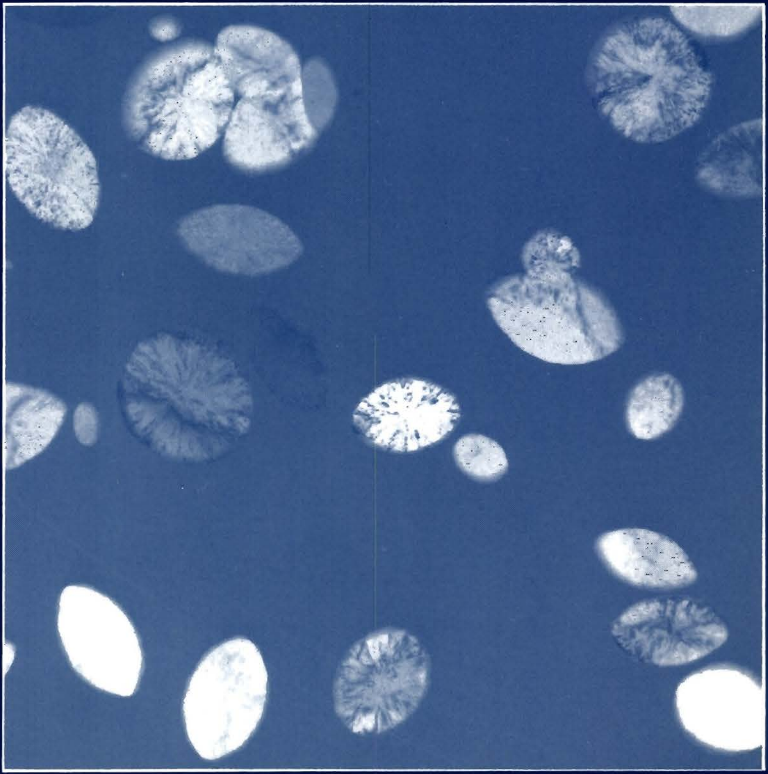

The photograph on the cover is obtained in a transmission electron microscope and shows titaniumsilicide crystals in an amorphous co-sputtered thin film.

FUNDAMENTAL ASPECTS OF REACTIONS IN TITANIUM–SILICON THIN FILMS FOR INTEGRATED CIRCUITS

PROEFSCHRIFT

ter verkrijging van de graad van doctor aan de Technische Universiteit Eindhoven, op gezag van de Rector Magnificus, Prof. Ir. M. Tels, voor een commissie aangewezen door het College van Decanen in het openbaar te verdedigen op dinsdag 8 november 1988 te 16.00 uur

door

Ivo Johannes Mechtildis Maria
RAAIJMAKERS

geboren te Almelo.

Dit proefschrift is goedgekeurd door de promotoren

Prof. Dr. H.H. Brongersma

and

Prof. Dr. F.W. Saris

The work described in this thesis has been carried out at the Philips Research Laboratories Eindhoven as part of the Philips Research program.

Aan Karin en mijn ouders.

FUNDAMENTAL ASPECTS OF REACTIONS IN TITANIUM–SILICON THIN FILMS FOR INTEGRATED CIRCUITS

Ivo J. M. M. Raaijmakers

Contents

List of Publications and Conference Contributions

A large part of this thesis has been published or is submitted for publication in literature. The following presents a list of publications and conference contributions.

- I.J.M.M. Raaijmakers, A.H. Reader and H.J.W. van Houtum,
  'Nucleation and Growth of Titanium Silicide Studied by In-Situ Annealing in a Transmission Electron Microscope.'
  J. Appl. Phys. **61**, 2527 (1987).

- I.J.M.M. Raaijmakers, A.H. Reader and H.J.W. van Houtum,
  'Nucleation and Growth of Silicides Studied by In-Situ Annealing in a Transmission Electron Microscope.', paper presented by IJMMR at the European Workshop on Refractory Metals and Silicides, Aussois, France (1987).
  Le Vide, les Couches Minces **236**, 75 (1987).

- I.J.M.M. Raaijmakers, A.H. Reader and P.H. Oosting,
  'The Formation of an Amorphous Silicide by Thermal Reaction of Sputter-deposited Ti and Si layers.'
  J. Appl. Phys. **63**, 2790 (1988).

- I.J.M.M. Raaijmakers, P.H.Oosting and A.H. Reader,
  'A Solid State Amorphisation Reaction in Ti-Si Diffusion Couples: the Phase Field.', paper presented by IJMMR at the Materials Research Society Fall Meeting, Boston MA (1987).
  Mater. Res. Soc. Proc. **xx**, xxx (1988) (Materials Research Society Pittsburgh).

- I.J.M.M. Raaijmakers, A.H. Reader and A.H. van Ommen,
  'Crystallisation of Amorphous Ti - Si alloy Thin Films: Microstructure and Resistivity.'
  accepted for publication in J. Appl. Phys. (1988).

- H.J.W. van Houtum and I.J.M.M. Raaijmakers,
  'Nucleation and Growth of Titanium Silicide with an Emphasis on the influence of Oxygen.', paper presented by IJMMR at the Materials Research Society Fall Meeting, Boston MA (1985).
  Mater. Res. Soc. Symp. Proc. **54**, 37 (1986), (Materials Research Society, Pittsburgh).

- H.J.W. van Houtum, I.J.M.M. Raaijmakers and T.J. Menting,
  'Influence of Grain Size on the Transformation Temperature of C49 $TiSi_2$ to C54 $TiSi_2$.'
  J. Appl. Phys. 61, 3116 (1987).

- A.H. Reader, I.J.M.M. Raaijmakers and H.J.W. van Houtum,
  'Stacking Faults and Precipitates in Annealed Co-sputtered C49 $TiSi_2$ Films.' paper presented by AHR at the Microscopy Semiconductor Conf., Oxford (1987).
  Inst. Phys. Conf. Ser. **87**, 523 (1987).

- H.J.W. van Houtum, A.A. Bos, A.G.M. Jonkers and I.J.M.M. Raaijmakers,
  '$TiSi_2$ Strap Formation by Ti and Amorphous Si Reaction', paper presented by AAB at the Workshop on Metals, Dielectrics and Interfaces for VLSI, San Juan Bautista (CA) (1988).
  Accepted for publication in J. Vac. Sci. Technol. **B**, scheduled for Nov/Dec issue (1988).

Dankwoord

De leiding van het Philips Natuurkundig Laboratorium wil ik bedanken voor de vrijheid die ik heb mogen genieten tijdens het uitvoeren van het onderzoek voor dit proefschrift. Roel Kramer, Wolter Gelling en Chris Werkhoven hebben mij in deze altijd gesteund.
Velen hebben hun bijdrage aan de totstandkoming van dit proefschrift geleverd. Ik plaats hier een welgemeend woord van dank aan allen die hun bijdrage in dit proefschrift herkennen.

Samenvatting

Het verkleinen van de karakteristieke dimensies in een geintegreerde schakeling tot in het submicron gebied maakt het noodzakelijk nieuwe hittebestendige materialen met een zo laag mogelijke elektrische weerstand te ontwikkelen. Silicides, dat zijn chemische verbindingen tussen een (overgangs)metaal en silicium, zijn veelbelovende materialen voor toepassing in een geintegreerd circuit. De vormingsmechanismes en de eigenschappen van deze verbindingen zijn dan ook intensief bestudeerd gedurende het laatste decennium. Nog veel is echter onbekend of onverklaard in deze relatief recentelijk in de belangstelling gekomen verbindingen.

In dit proefschrift worden de vormingsmechanismen en de elektrische eigenschappen van titaansilicide beschreven. Vrijwel zeker is titaandisilicide ($TiSi_2$) een van de eerste silicides die op grote schaal toegepast zal worden in de halfgeleiderindustrie. In essentie zijn er twee methoden om een silicide stap in het bestaand fabrikageproces te implementeren: *(i)* een hittebehandeling van een gecodeponeerde (meestal amorfe) dunne film legering van Ti en Si wat tot kristallisatie leidt en *(ii)* een hittebehandeling van een dunne film Ti - Si diffusiekoppel, wat tot chemische interdiffusie van het Ti en het Si leidt. In de hoofdstukken 2 tot en met 4 wordt de vorming van een silicide volgens het eerste proces beschreven. In hoofdstuk 5 wordt de tweede preparatiemethode behandeld.

In hoofdstuk 2 starten we met de beschrijving van de kristallisatie van amorfe Ti - Si binaire legeringen, zoals deze bestudeerd kan worden door de amorfe dunne films te verhitten tot ongeveer 300 ^{O}C in een elektronenmicroscoop. Met behulp van deze methode kan de kiemvorming en de groei van het kristallijne materiaal in de amorfe matrix *gescheiden* bestudeerd worden en wel *tijdens* het proces. Aangetoond is dat de kristallen kiemen volgens een toevalsproces met een constante snelheid. Voorts zal aangetoond worden dat de groeisnelheid constant is bij een bepaalde temperatuur. Dit is te verwachten, aangezien geen atomaire diffusie over lange afstanden nodig is; het Ti en Si was immers gecodeponeerd in dezelfde dunne film legering. In het gekristalliseerde materiaal blijken wel zeer veel kristalfouten aanwezig te zijn. Het karakter van deze zogenaamde stapelfouten is in wat meer detail geanalyseerd.

Dit soort kristalfouten is niet gewenst in een silicide daar ze de elektrische weerstand van het materiaal zullen verhogen. In hoofdstuk 3 gaan we daarom in op de invloed van kristalfouten op de elektrische weerstand. Daartoe wordt de weerstand van een gecodeponeerde dunne film gemeten gedurende de relevante reacties. Met behulp van deze methode waren er duidelijk drie reactiestadia te herkennen: *(i)* de kiemvorming en groei van de zogenaamde C49 $TiSi_2$ fase bij een temperatuur van ongeveer 300 ^oC zoals ook in hoofdstuk 2 wordt beschreven; *(ii)* een voorheen nog niet geïdentificeerde precipitatiereactie in het temperatuur gebied van 300 tot 750 ^oC en *(iii)* een polymorfe fasetransformatie van de C49 fase naar de zogenaamde C54 fase bij ongeveer 800 ^oC.

Gedurende een typische hittebehandeling van het $TiSi_2$ is er een grote maar vrij geleidelijke weerstandsafname waar te nemen gedurende de precipitatiereactie. Voor een gedeelte kon deze weerstandsafname verklaard worden uit een afname van de dichtheid van de genoemde stapelfouten. Voor de eerste maal is er aangetoond dat het faseveld van de C49 $TiSi_2$ fase een behoorlijke breedte bezit. Hieruit kon geconcludeerd worden dat een afname in het aantal puntdefecten, veroorzaakt door stoichiometrie-afwijkingen, het andere gedeelte van de weerstandsafname moest verklaren. Van groot technologisch belang is ook de transformatie naar de C54 fase. Het blijkt dat gedurende deze faseovergang vrijwel alle defecten geëlimineerd worden, zodat uiteindelijk een materiaal met een reproduceerbare en lage kamertemperatuur-weerstand ontstaat.

De kinetiek van de verschillende fasetransformaties zoals beschreven in de vorige hoofdstukken kan heel gemakkelijk gemeten worden met behulp van een weerstandsmeting tijdens de hittebehandeling. De informatie die we zo kunnen krijgen zegt alleen iets over de totale reactie omdat de som van de invloed van vele groeiende kristallen op de weerstand gemeten wordt. Dit maakt dat de interpretatie van dit soort metingen met enige omzichtigheid moet geschieden. Hieraan wordt aandacht besteed in hoofdstuk 4. Het blijkt dat de twee fasetransformaties, amorf - C49 en C49 - C54, zeer goed beschreven worden met de zogenaamde Johnson–Mehl–Avrami vergelijking en een constante kiemvormingssnelheid en groeisnelheid. De activeringsenergie voor de C49 - C54 faseovergang is extreem groot, waaruit geconcludeerd kon worden dat de kiemvorming van deze fase waarschijnlijk moeilijk plaatsvindt.

Met behulp van de weerstandsmetingen kan ook de kristallisatietemperatuur als functie van de samenstelling van de laag bepaald worden. Amorfe Ti - Si legeringen met een Si gehalte tussen 20 en 60 atoom % kristalliseren pas bij vrij hoge temperatuur: ongeveer 500 ^oC. Deze temperatuur is hoger dan die welke nodig is om een aanzienlijke interactie in een Ti - Si diffusiekoppel te doen plaatsvinden (zie verder). Het is dan ook niet verwonderlijk dat het eerste reactieproduct in een Ti - Si diffusiekoppel een amorfe fase is. Er is door ons ook een merkwaardig minimum in de kristallisatietemperatuur gevonden voor legeringen met een compositie dicht bij die van $TiSi_2$. Waardes tot 270 °C zijn gemeten. Deze verschijnselen zijn bediscussieerd aan de hand van bestaande modellen voor de kristallisatie van amorfe legeringen.

In hoofdstuk 5 tenslotte behandelen we de reacties tussen discrete Si en Ti lagen. Er is nu lange afstands-diffusie nodig om een aanzienlijke hoeveelheid silicide te vormen. Er wordt begonnen met een overzicht van de literatuur. Uit dit overzicht volgt een aantal zeer in het oog springende dubbelzinnigheden. Bijvoorbeeld, er worden verschillen gerapporteerd in de reactie van Ti met kristallijn en die met amorf Si waarvoor een afdoende verklaring nog ontbreekt. Het is zelfs zo dat een gedetailleerde studie naar de kinetiek van de faseformatie in Ti - kristallijn Si diffusiekoppels nog ontbreekt, waarschijnlijk vanwege reproduceerbaarheidsproblemen.

De verschillende reacties tussen Ti en kristallijn Si en die met amorf Si worden bestudeerd met Auger elektronenspectroscopie, Rutherford He-ionenterugstrooiing en cross-sectie transmissie elektronenmicroscopie. Bij lage temperaturen ($\leq 475°C$) blijkt er weinig of geen verschil te bespeuren in de reacties van een Ti laag met amorf of die met kristallijn Si. In beide gevallen wordt er een metastabiele amorfe fase gevormd, bestaande uit ongeveer even grote hoeveelheden Ti en Si. Verschillen treden pas op na reactie bij ongeveer 500 °C. Op het amorfe Si kiemt nu heel duidelijk de C49 $TiSi_2$ fase terwijl dit op kristallijn Si zeker niet gebeurt. Hoogstwaarschijnlijk is daar kristallijn monosilicide aanwezig. De kiemvormingsmoeilijkheden van het disilicide uit het monosilicide op een kristallijn substraat schrijven we toe aan de zeer grote bijdrage van de kristallisatiewarmte van amorf Si aan de totale reactiewarmte.

De hierboven beschreven kiemvormingsmoeilijkheden komen ook tot uiting in het gedrag van Ti - kristallijn Si diffusiekoppels bij de iets hogere groeitemperaturen (550 °C tot 700 °C) welke in de fabrikage normaal gebruikt worden. In dit temperatuur gebied kon de reactie gescheiden worden in een gedeelte waar de kiemvorming van $TiSi_2$ een dominante rol speelt en een gedeelte waar alleen diffusie door de silicidefase belangrijk is. Dit laatste stuk blijkt zeer reproduceerbaar. Het eerste, door kiemvorming gedomineerde, stuk van de reactie is zeer gevoelig voor allerlei nauwelijks controleerbare parameters. Er wordt aannemelijk gemaakt dat de gerapporteerde reproduceerbaarheidsproblemen van de Ti - Si reactie hun oorsprong voornamelijk vinden in de kiemvormingsmoeilijkheden van de disilicide-fase.

De bedoeling van dit onderzoek was om een bijdrage te leveren aan de kennis van Ti–silicides en de reacties in het Ti - Si systeem. Vanuit technologisch standpunt is een van de meest belangrijke vindingen het overheersen van kiemvormingsverschijnselen in diverse stadia van de reactie. Zowel in de vorming van $TiSi_2$ op een kristallijn Si substraat als in de vorming van de C54 fase uit de C49 fase blijkt kiemvorming een belangrijke rol te spelen. Deze kennis kan leiden tot een andere benadering van enkele technologische problemen. Vanuit wetenschappelijke standpunt lijkt het zinvol om de kristallisatiereacties in amorfe gecodeponeerde silicides systematischer aan te pakken. Een interessant verschijnsel is bijvoorbeeld de grote afname in de kristallisatietemperatuur dichtbij de kompositie van het disilicide. Aangezien we ook het voorkomen van een vaste stof amorfisatiereactie in het Ti - Si systeem hebben aangetoond, zal meer gedetailleerde kennis van kristallisatiereacties mogelijk leiden tot een beter begrip van metaal - Si reacties in het algemeen.

Chapter 1

General Introduction

1.1 Silicides in Integrated Circuits

The continuous increase in packing density and minimum feature size in bipolar and Metal Oxide Semiconductor (MOS) integrated circuits leads to an increase in the switching speed of the transistors [Gar83,Bac84]. Simultaneously however, the delay of signal propagation through the interconnection increases due to the increase in length (larger circuit complexity and size) [Sin82,Sar82] and due to the increase of interconnect resistance and specific capacitance (thinner layers, smaller lateral size). These opposing influences on the device access or switching time eventually lead to a so-called interconnection limited circuit [Gar83].

Since the early 1970's doped polycrystalline silicon is used as a high temperature resistant gate electrode and gate level interconnect in MOS devices. It has several advantages over pure metal gates which were used in the first MOS devices: it is stable to the vulnerable SiO_2 gate dielectricum, it can easily be deposited by chemical vapour deposition techniques, and it can be oxidized to yield an excellent insulating dielectric. The major drawback of polycrystalline Si is its high resistivity (500 - 1000 $\mu\Omega$cm), and the associated large signal propagation delay times.

An MOS device not only degrades in performance with downscaling because of increasing interconnection related delay times, but also because of increasing device series resistances. This series resistance is composed of two major contributions: the contact resistance of the metal–semiconductor contacts in the source and drain, and the sheet resistance of the source and drain regions [Ng 87]. The contact resistance scales approximately with the inverse square of the contact area which leads to unacceptably high contact resistances for contact hole sizes in the micrometer regime. Moreover, as junction depths have to be scaled down in conjunction with the lateral sizes in order to maintain acceptable device characteristics, the sheet resistance of the shallow doped regions in the source and drain areas of the transistor becomes unacceptably high.

Both of the above mentioned problems require new, high temperature resistant, contact and interconnect materials with a lower resistivity than that of doped Si. In the late 1970's and 1980's the application of *silicides*, i.e. compounds between a (transition) metal and silicon, has been proposed to alleviate the problems associated with downscaling and increasing complexity of integrated circuits. In order to decrease gate signal propagation delay, silicides may be applied directly as a gate electrode [Moc78] or, if it is desired to preserve the favourable Si/SiO_2 interface properties, as a polycide (from ***poly***crystalline Si and sili***cide***, a silicide used as an electrical shunt on top of the high resistivity polycrystalline Si gate) [Cro79,Cho83]. A decrease in transistor series resistance may be reached with the application of a silicide in the contact hole. In order to cover the entire contact hole with silicide and to avoid an additional and expensive lithographic step the salicide technology (from *s*elf *a*ligned si*licide*) [Shi81,Tin82] has become quite popular.

Practically all transition metals form silicides when they are allowed to react with Si [Mur83,Ott84]. Every single metal in turn may form several silicides with different stoichiometries. For example in the Ti - Si system the existence of the stoichiometric compounds Ti_3Si, Ti_5Si_3, TiSi, Ti_5Si_4 and $TiSi_2$ is reported [Mas87]. The diversity in silicides is still larger because a particular stoichiometric compound may crystallize in different crystal structures, for example the two polytypes of $TiSi_2$ (see further). In view of the point that the supply of Si is practically unlimited in a Si–based device, the most Si–rich silicides will be the thermodynamically stable ones. Thus for most metals, primarily the disilicides need consideration for their application in Si-based devices.

The primary criterion to choose a particular silicide is that it should have a resistivity as low as possible. Other important criteria depend somewhat on the specific application. In a polycide technology one desires plasma etchability, good adhesion to polycrystalline Si, good high temperature stability and ability to form a dielectric by oxidation. The disilicides of Mo [Fuk84], W [Cro79], Ta [Mur80a] and Ti [Mur80,Mur80a] are considered to be the most viable alternatives in a polycide technology. The resistivities of the above silicides are in the range of 15 to 80 $\mu\Omega$cm [Mur83,Nic83], which is an order of magnitude lower than the resistivity of doped polycrystalline Si.

The criteria for choosing a silicide for a salicide technology include ease of forming a smooth silicide by thermal reaction with crystalline Si, existence of a selective metal etch, good thermal stability and minimal lateral overgrowth over oxide regions. From the silicides which are candidates in a salicide process $TiSi_2$ [Tin82,Lau82,Mur80a] and $CoSi_2$ [Hov88,Mor87] has the lowest resistivity (about 15 $\mu\Omega$cm [Mur83,Nic83]), although silicides of other (near noble) transition metals are also reported to be used for a salicide process in integrated circuit technology [Tin84,Shi81]. The position of $TiSi_2$ as the first candidate for a self aligned process is now firmly established [Hov88,Mor87,Alp85] however. Since $TiSi_2$ is a material which in principle can be used in both a salicide and a polycide technology, a study on nucleation and growth of silicides in the Ti - Si system, and electrical properties of the formed titanium silicides seems appropiate.

1.2 Silicide Preparation Methods

In practice several methods are used to prepare a silicide thin film. The most common methods to arrive at a low resistivity, crystalline silicide thin film are: *(i)* the (re)-crystallization of an amorphous or microcrystalline co-deposited thin film of metal and silicon of the desired composition; *(ii)* a solid state reaction of a metal thin film on silicon (amorphous, poly-, or monocrystalline) and *(iii)* chemical vapour deposition.

The first method is for example used in the polycide technology and may also be used to create a short range interconnect [Cro79,Mur80a,Fuk84] 4 [Cho83,Mur80]. The metal - silicon alloy may be deposited by evaporation or sputtering from two independent sources or alternatively, sputtering from a compound target of the appropiate composition. The as-deposited alloy thin film is usually amorphous or microcrystalline and has a high resistivity. By an anneal treatment at temperatures between about 0.2 T_m to about 0.5 T_m (where T_m is the melting temperature of the silicide) [Cho83] the alloy (re)-crystallizes to a crystalline silicide having the desired low resistivity. Mechanistic reaction steps which are important during such a crystallization process are: *(i)* the nucleation of crystalline material in the amorphous matrix; *(ii)* the subsequent growth of these crystalline nuclei and *(iii)* phase transformations, grain growth and precipitation in the crystallized thin film. Since an intimate mixture of metal and Si is obtained in co-deposited samples, no macroscopic concentration gradients are required and long range diffusion is not an important transport mechanism in steps *(i)* and *(ii)*. In chapters 2, 3 and 4 of this thesis the crystallization of such amorphous metal - silicon alloy thin films is described.

The second preparation method, i.e. reacting a discrete metal thin film with Si, is applied in the salicide technology to form a silicided contact (or gate) [Shi81,Lau82,Alp85,Tin82,Mur80a]. For that purpose a metal layer is deposited on an appropiately cleaned Si substrate or a polycrystalline Si layer by sputtering, evaporation or chemical vapour deposition. The as-deposited metal layer is usually polycrystalline. The diffusion couple is next reacted at temperatures of about 0.3 T_m to about 0.5 T_m [Gur77,Heu86,Mur83,Heu82] to convert the metal layer into silicide. Recently, the Ti - salicide technology was also combined with a technique to create short interconnect stripes over oxide regions ('straps') in the same salicidation process sequence [Jon87,Won87,Hou88]. In that case an additional Si layer is sputter-deposited on the Ti layer. The as-deposited Si layer is usually amorphous. Thus the important solid state reactions to be studied are the reaction of a discrete Ti layer with *crystalline* Si and the reaction of Ti with *amorphous* Si. We note here that pronounced differences in reaction rate and mechanism have been reported for these two reactions [Hun83,Lin86], and that the exact reason for these differences is still a matter of dispute. An important reaction step in thin film diffusion couples is the nucleation of the first compound phase at the Ti - Si interface. In contrast to the previously introduced case of a co-deposited alloy, where an intimate mixture of metal and Si atoms is already present in the as-deposited case, the spatial separation of Ti and Si in discrete layers now requires long range diffusion as a necessary transport process. In chapter 5 of this thesis the reactions of Ti with two structurally different crystalline forms of Si (monocrystalline and amorphous) will be described.

A very trendy technique of creating a silicide is chemical vapour deposition of WSi_2 from a WF_6 - SiH_4 mixture [Wel87]. This technology is competitive to the salicide technology in that the silicide may be formed selectively on Si. However the technique is still in its infancy and, although promising, it will require more time to incorporate it in the established process flow. This silicide preparation method will not be discussed further in this thesis.

1.3 Objectives and Outline

We will start out with the presentation of a study which describes the crystallization process of amorphous Ti - Si alloys as observed in a transmission electron microscope. For that purpose, samples will be heated within the electron microscope so that they can be observed simultaneously. This technique offers the possibility to distinguish between the nucleation stage, the growth of separate nuclei and subsequent precipitation reactions. The velocity of the crystallization front and the nucleation rate can in principle be determined quantitatively from electron microscopy. Such kinetic parameters are useful if the time and temperature of the annealing step to crystallize the amorphous alloy are to be estimated. The measured nucleation and growth rate can be compared with rates which are calculated from simple models for the crystallization reactions. The operational crystallization mechanisms and the growth morphologies of crystallites will be correlated with, for example, the composition of the starting material.

As was outlined in the first sections of this introduction, one of the most important properties of a silicide is its resistivity. Many investigators have emphasized the importance of structural defects on the resistivity of a particular silicide. Of course the density and nature of these defects, and consequently the resistivity, is dependent on the preparation conditions of the silicide thin film. $TiSi_2$ in its C49 ($ZrSi_2$) polytype (see further) is usually highly defective and has a very high (defect related) residual resistivity. Therefore a study of the resistivity and defect behaviour of the crystalline silicide as a function of the anneal treatment is useful. From such a study will be reported in chapter 3. In that chapter the nature and the density of these defects will be determined with (amongst other techniques) electron microscopy. Measured defect densities will be correlated with electrical parameters like the resistivity and the Hall effect.

Several processes play a role before the desired low resistivity C54 $TiSi_2$ phase is obtained from for example a co-deposited alloy. These different processes will be identified in chapter 3 with the aid of direct measurements of the resitivity *during* the anneal treatment *(in-situ* resistivity measurements), electron microscopy and X-ray diffraction.

It is of scientific and technological interest to determine the kinetics of the phase transformations in the Ti - Si system. Usually solid state phase transformations are associated with appreciable resistivity changes. Thus it should be possible to analyze the kinetics of such a phase transformation in the solid state by measuring the resistivity during the reaction.

In chapter 4 a detailed study on the kinetics of the different processes occurring during the formation of low resistivity $TiSi_2$ from a co-deposited alloy will be described. The interpretation of such measurements of the overall kinetics is not as straight forward as the interpretation of the *in-situ* electron microscopy work described in chapter 2. This is mainly so because the measurement of a single macroscopic parameter as the resistivity does not relate uniquely to a particular kinetic parameter, for example a fraction of transformed material. Particular attention will be paid to the problem of interpretation of the resistivity measurements. If care is exercized in the interpretation of the measurements we estimate that the kinetical parameters which will be derived from such *in-situ* resistivity measurements will significantly increase our knowledge on the kinetics of processes in the Ti - Si system.

Moreover, the relatively fast and simple measurement of resistivity during an anneal treatment allows one to do many measurements in a relatively short time. The crystallization temperature of such amorphous metal - Si alloy thin films is for example a parameter which can be measured in such a way. In order to arrive at a more complete picture of the crystallization of Ti - Si alloys, the crystallization temperatures for different alloys with compositions ranging from very Si–rich to moderately Ti–rich were determined and discussed in terms of existing models for crystallization kinetics.

Finally our attention will be turned to the reactions in Ti - Si diffusion couples in chapter 5. The silicidation reactions now require long range diffusion because of the spatial separation of the Ti and Si atoms. The reactions of Ti with *amorphous* Si and *crystalline* Si will both be investigated. A considerable amount of work on the reactions in Ti - Si diffusion couples has already been published. Therefore it seems appropiate to start out with a review of the relevant literature. This review led to many ambiguities and questions which never have been solved in detail in many silicides, and especially not in Ti–silicides. The main objectives of the research described in chapter 5 is to resolve these ambiguities. For the first time we will demonstrate the importance of nucleation phenomena in the reaction of Ti with crystalline Si. Moreover it will be shown that in Ti - Si diffusion couples a metastable amorphous phase may be grown. The existence of such an amorphous reacted layer in the Ti - Si system provides a link between the crystallization studies described in chapters 2 to 4 and the reactions in diffusion couples described in chapter 5.

1.4 Structure of Titanium Silicides

This thesis deals with the silicides of Ti and the kinetics of their formation. However, many effects which are identified and investigated here for the Ti - Si system can at least qualitatively be transposed to other silicide forming systems and in particular to the systems of Si with Hf and Zr. The purpose of the present part of the introduction is to give a short impression on some general structural and chemical properties of silicides and more specifically the silicides of the group IV-A elements (Ti, Zr and HF).

Fig. 1.1 records the phase diagrams of the Ti - Si system and the Zr - Si system [Mas87]. The phase diagram of the Hf - Si system is very much like that of the Zr - Si system and has been omitted here. In the Ti - Si phase diagram the intermetallic phases Ti_3Si, Ti_5Si_3, TiSi, Ti_5Si_4 and $TiSi_2$ are found. In the Zr - Si system some additional intermetallic phases are present in the central part of the diagram, but the shape of the solidus is very similar in both diagrams. Let us consider now the silicides with stoichiometry of M_5Si_3, M_5Si_4, MSi and MSi_2 for M = Hf,Zr and Ti. In the three mentioned systems the M_5Si_3, M_5Si_4 and MSi phases crystallize

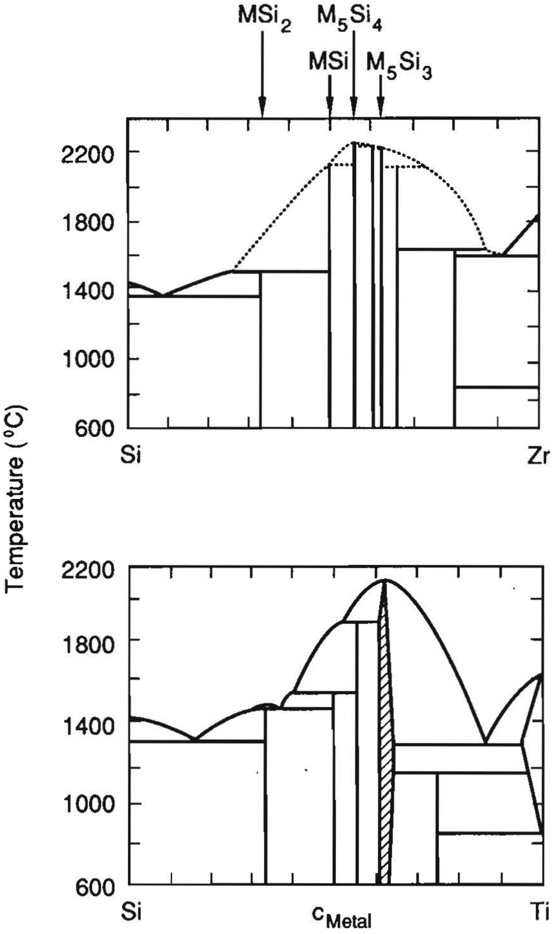

Fig. 1.1. Binary phase diagrams of the Ti - Si system (bottom) and the Zr - Si system (top). Note the similarity of both diagrams, especially on the Si–rich (left) side.

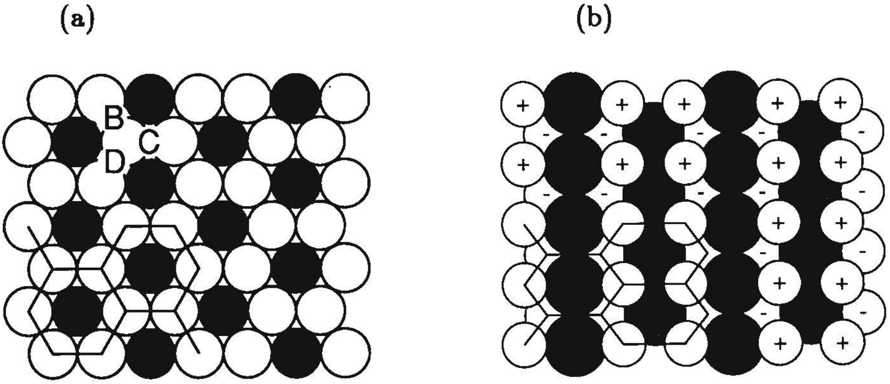

Fig. 1.2. (a) Structure of planar stoichiometric building layers of typical refractory metal disilicides; (b) non-planar building blocks of the C49 disilicide phase; + and – denote atoms above and below the plane of the page respectively. Filled and open circles correspond to Ti and Si atoms respectively.

in the same crystal structure. (M_5Si_3 has the $D8_8$ or Mn_5Si_3 structure, M_5Si_4 has the Zr_5Si_4 structure and MSi has the B27 or FeB structure [Mas87,Now54a].) In the Hf and Zr system the disilicide crystallizes in the C49 ($ZrSi_2$) structure, and the disilicide in the Ti - Si system crystallizes in a slightly different structure in equilibrium: the C54 ($TiSi_2$) structure [Mas87,Lav39]. However, it has recently been shown [Bey85,Hou86] that $TiSi_2$ exhibits polytypism. At low temperatures ($< 600^oC$) it appeared that $TiSi_2$ crystallizes in the C49 structure too, i.e. the same structure as that of $HfSi_2$ and $ZrSi_2$. Moreover, small amounts of contaminants may stabilize $TiSi_2$ in the C49 structure. For example, Cotter et al. [Cot56] prepared an apparently stable but Al contaminated [Bru61] form of the C49 $TiSi_2$ phase by aluminothermic reduction. Thus the structural analogy in the Hf, Zr and Ti systems is quite convincing if it is considered that $TiSi_2$ may crystallize in a C49 structure. After an anneal at higher temperatures ($> 700\ ^oC$) the C49 phase recrystallizes to the C54 equilibrium phase. Since it was not possible until now to induce the reverse transition [Hou86,Bey85] the C49 $TiSi_2$ phase is suspected to be metastable. With the present information however, it might as well be a low temperature modification of the C54 $TiSi_2$ structure.

The structure of most refractory metal silicides is conveniently described by a stacking of fundamental building layers of a close packed hexagonal structure (see Fig. 1.2) and of the correct 1/2 stoichiometry [Heu82,Now54a]. A layer consists of metal atoms, each surrounded by 6 Si atoms within the plane. Sequential layers are stacked on the positions

B,C and D indicated in Fig. 1.2a. Dependent on the stacking sequence the structures of the tetragonal $MoSi_2$ type (ABAB... stacking), the hexagonal $CrSi_2$ type (ABCABC... stacking) or orthorombic (but nearly hexagonal) $TiSi_2$ type (ABCD... stacking) are obtained. The C54 $TiSi_2$ structure is orthorombic because the stoichiometric plane needs to be distorted a little bit in order to accomodate the large Ti atom.

This distortion is continued much more heavily in the C49 $ZrSi_2$ structure [Sch54], where the metal atom is so large that it can not be accomodated at all by the Si network. As a consequence the planar Si network must buckle up to form the non-planar building blocks of Fig. 1.2b. In the C49 $ZrSi_2$ structure stoichiometric layers are less easily recognized because of the non-planar structure of the building block, rather, non-stoichiometric layers consisting of pure Si and layers consisting of both metal and Si atoms can be distinguished. (This will be treated in more detail in chapter 2.)

The structure of the disilicides of the refractory metals thus evolves from the hexagonal/tetragonal structures in which the rather small metal atoms are readily accomodated by the Si network, all the way to the orthorombic C49 $ZrSi_2$ structure where the metal atom is much too large to fit into the Si network. Considering the radii of the refractory metal atoms [Gol67] one anticipates that Ti occupies an intermediate position in the above sequence. Then it is not surprising that $TiSi_2$ shows polytypism, at low temperatures forming the C49 phase as a precursor to the C54 phase.

The C49 and C54 phases are quite similar from a chemical point of view. The molar volume of $TiSi_2$ in the C54 structure is equal to that in the C49 structure: $42.4 * 10^{-3}$ nm^3 [Lav39,Hou86]. In both structures all Ti atoms occupy equivalent positions and show a similar ten-fold coordination of Si–atoms. The Ti - Si atomic distance in the C49 structure varies between 0.256 nm and 0.279 nm with an average value of 0.266 nm [Vau55,Sch54]. In the C54 structure the Ti - Si interatomic distance is between 0.254 nm and 0.275 nm with a similar average value of 0.267 nm [Lav39]. The similarities between the C54 and C49 structure are further substantiated by the fact that $ZrSi_2$ (C49 structure) dissolves upto 60 % of $TiSi_2$ (C54 structure) whereby the planar building layers of $TiSi_2$ readily transform to the buckled building blocks of the C49 structure [Now54b].

To summarize, it is argued that the Hf, Zr and Ti - Si systems show many structural and chemical similarities. This means that many of the present findings for the Ti - Si system may carefully be applied to the Hf and Zr - Si systems too, at least in a qualitative way. On the basis of a review of the structure of the refractory metal disilicides and the intermediate size of the Ti atom it seems quite logical that $TiSi_2$ crystallizes in two polytypes: the C49 or $ZrSi_2$ structure (in which the analogons Hf and Zr crystallize too), and the C54 or $TiSi_2$ structure. It is considered that the chemical differences between the two polytypes are small.

Bibliography

[Alp85] M.E. Alperin, T.C. Holloway, R.A. Haken, C.D. Gosmeyer, R.V. Karnaugh and W.D. Parmantie, IEEE Trans. Electron. Devices **ED32**, 141 (1985).

[Bac84] G. Baccarini, M.R. Wordeman and R.H. Dennard, IEEE Trans. Electron. Dev. **ED 31**, 452 (1984).

[Bey85] R. Beyers and R. Sinclair, J. Appl. Phys. **57**, 5240 (1985).

[Bru61] C. Brukl, H. Nowotny, O. Schob and F. Benesovsky, Mh. Chem. **92**, 781 (1961).

[Cho83] T.P. Chow and A.J. Steckl, IEEE Trans. Electron Devices **ED30**, 1480 (1983).

[Cot56] P.G. Cotter, J.A. Kohn and R.A. Potter, J. Am. Cer. Soc. **39** 11 (1956).

[Cro79] B.L. Crowder and S. Zirinsky, IEEE Trans. Electron Devices **ED26**, 369 (1979).

[Fuk84] M. Fukomoto, A. Shinokara, S. Okado, K. Kugimiya, IEEE Trans. Electron. Devices **ED31**, 1432 (1984).

[Gar83] P.A. Gargini, Inst. Phys. Conf. Ser. **69**, 141 (1984), ed. by E.H. Rhoderick (The Institute of Physics, London, 1984).

[Gol67] H.J. Goldschmidt in 'Interstitial Alloys' (Butterworths, London 1967).

[Gur77] G.J. van Gurp, Semiconductor Silicon **77**-2, 342 (1977), ed. by H.R. Huff and E. Sirtl (Electrochem. Soc., Princeton N.J., 1977).

[Heu82] F.M. d'Heurle in 'VLSI Science and Technology', ed. by C. Dell'Oca and W.M. Bullis, p. 194, Electrochemical Soc., Pennington (1982).

[Heu86] F.M. d'Heurle and P. Gas, J. Mater. Res. **1**, 205 (1986). . **3**, 167 (1988).

[Hou86] H.J.W. van Houtum and I.J.M.M. Raaijmakers, Mater. Res. Soc. Symp. Proc. **54**, 37 (1986).

[Hou88] H.J.W. van Houtum, A.A. Bos, A.G.M. Jonkers and I.J.M.M. Raaijmakers, accepted for publication in J. Vac. Sci. Technol. **B XX**, xxx (1988).

[Hov88] L.J. Van Den Hove, PhD thesis, University of Leuven (Leuven, Belgium 1988).

[Hun83] L.S. Hung, J. Gyulai, J.W. Mayer, S.S. Lau and M.A. Nicolet, J. Appl. Phys. **54**, 5076 (1983).

[Jon87] A.G.M. Jonkers, H.J.W. van Houtum and A. Moet, Proc. Workshop on Refr. Metals and Silicides. Aussois (France) 1987, published in: le Vide, les Couches Minces **42**, 103 (1987).

[Kem82] M.J.H. Kemper and P.H. Oosting, J. Appl. Phys. **53**, 6214 (1982)

[Lau82] C.K. Lau, Y.C. See, D.B. Scott, J.M. Bridges, S.M. Perna and R.D. Davies, I.E.D.M. Techn. Digest, San Fransisco CA, 13 - 15 Dec. (1982), p. 714 (IEEE, New York 1982).

[Lav39] F. Laves and H.J. Wallbaum, Z. Kristallogr. **101**, 78 (1939).

[Lin86] C.D. lien, M.A. Nicolet and S.S. Lau, Thin Solid Films **143**, 63 (1986).

[Mas87] Th.B. Massalsky, J.L. Murray, L.H. Benett and H. Baker, eds., 'Binary Alloy Phase Diagrams' **2** (Am. Soc. Metals., Metals Park, Ohio 1986).

[Moc78] T. Mochizuki, K. Shibata, T. Inoue, K. Ohuchi, Japan J. Appl. Phys. **17** Suppl. 1, 37 (1978).

[Mor87] A.E. Morgan, , E.K. Broadbent, M. Delfino, B. Coulman and D.K. Sadana, J. Electrochem. Soc. **134**, 925 (1987).

[Mur80a] S.P. Murarka, D.B. Fraser, A.K. Sinha and H.L. Levenstein, IEEE Trans. Electron. Devices **ED27**, 1409 (1980).

[Mur80b] S.P. Murarka and D.B. Fraser, J. Appl. Phys. **51**, 350 (1980).

[Mur80c] S.P. Murarka and D.B. Fraser, J. Appl. Phys. **51**, 342 (1980).

[Mur83] S.P. Murarka, 'Silicides for VLSI Applications' (Ac. Press, New York, 1983).

[Ng 87] K.K. Ng and W.T. Lynch, IEEE trans. Electron Dev. **ED 34**, 503 (1987).

[Nic83] M.A. Nicolet and S.S. Lau, in VLSI Electronics,**6**, edited by N.G. Einspruch (Academic, New York, 1983) .

[Now54a] H. Nowotny and E. Parthé, Planseeber. Pulvermet. **2**, 34 (1954).

[Now54b] H. Nowotny, R. Machenschalk, R. Kieffer and F. Benesovsky, Mh. Chem. **85**, 241 (1954).

[Ott84] G. Ottaviani, Mat. Res. Soc. Symp. Proc. **25**, 21 (1984).

[Sar82] K.C. Saraswat and F. Mohammadani, IEEE Trans. Electron. Dev. **ED 29**, 645 (1982).

[Sch54] H. Schachner, H. Nowotny and H. Kudielka, Mh. Chem. **85**, 1141 (1954).

[Shi81] T. Shibata, K.Hieda, M. Sato, M. Konaka, R.L.M. Dang and H. Izuka, I.E.D.M. Techn. Digest, Washington DC, 7 - 9 dec (1981), p. 647 (IEEE, New York 1981).

[Sin82] A.K. Sinha, J.A. Cooper, jr, and H.J. Levinstein, IEEE Electron. Dev. Lett. **EDL 3**, no. 4, 90 1982.

[Tin82] C.Y. Ting, S.S. Iyer, C.M. Osburn, G.J. Hu and A.M. Schweighart, Proc. Electrochem. Soc. Meeting **82**-2, 224 (1982).

[Tin84] C.Y. Ting, I.E.D.M. Techn. Digest, San Fransisco CA, 9 - 12 dec. (1984), p. 110 (IEEE, New York 1984).

[Vau55] P.A. Vaughan and A. Bracuti, Progr. and Abstr. Amer. Crystallogr. Assn. Summer Meeting, June 27 - July 2 (1955), p. 8.

[Wel87] V.A. Wells, ed., 'Tungsten and other Refractory Metals for VLSI Application III (Materials Research Society, Pittsburgh 1987).

[Won87] S.S. Wong, D.C. Hen, P. Merchant, T.R. Cass and J. Amano, IEEE Transactions on Electron Devices **ED34**, 587 (1987).

Chapter 2

Crystallization of Ti - Si Alloys Studied by In-Situ Annealing in an Electron Microscope

2.1 Introduction

The formation mechanism of refractory or near-noble metal silicides has recently received considerable attention [Mur83,Heu86]. Whereas there have been numerous studies on first phase nucleation [Wal76,Ben87] and growth mechanisms or growth kinetics [Heu86] by techniques such as x-ray diffraction (XRD), Rutherford backscattering spectrometry (RBS), Auger electron spectroscopy (AES) and transmission electron microscopy (TEM), only a few papers have been published on the formation of silicides studied by *in-situ* annealing in a TEM [Wei86,Kem82]. This technique, however, offers a unique possibility to follow the growth of the silicide in real time and to distinguish between *(i)* the nucleation stage, *(ii)* the subsequent growth of the nuclei, and *(iii)* possible recrystallization or precipitation phenomena.

We have started with a study on the crystallization of amorphous Ti - Si alloy thin films with compositions in the range Ti/Si = 1/1 to Ti/Si = 1/3. This range includes the technologically important composition of the disilicide. The crystallization phenomena were investigated by annealing the samples *in-situ* in a transmission electron microscope. Kinetic parameters like the crystallization temperature, the velocity of the crystallization front (or the 'growth rate') and the nucleation rate can be determined quantitatively by simple measurements from electron microscopy micrographs. To explain the observed magnitudes of kinetic parameters semiquantitatively, they will be compared with values derived from simple models.

There are ample indications from literature [But84,Her83,Hol87,Raa88a] that in the initial reaction of Ti layers with silicon, the first metastable phase formed is an amorphous alloy with a composition close to that of the lowest eutectic [Wal76] or to that of the mono-silicide [Raa88b,Hol87] (see also chapter 5). Therefore, both of the above mentioned and technologically relevant silicide preparation methods must include the same reaction step, i.e. the crystallization of an amorphous silicide. Thus, it is expected that a study on the crystallization behaviour of amorphous silicides will not only yield information on the nucleation and growth of silicide crystals in an amorphous metal - Si matrix, but will also supply more general knowledge on silicide growth.

As was introduced in chapter 1, the formation of $TiSi_2$ in its equilibrium C54 ($TiSi_2$) [Lav39] crystal structure is preceeded [Hou86,Bey85] by the formation of $TiSi_2$ in the C49 ($ZrSi_2$) [Cot56] crystal structure. The final phase transformation to the low resistivity C54 $TiSi_2$ structure occurs at fairly high temperatures (above about 700 ^oC) [Hou86,Hou87,Bey85]. We could not reach these specimen temperatures routinely in the electron microscope, so this chapter presents results on the crystallization of amorphous thin films to C49 $TiSi_2$ thin films. The C49 to C54 recrystallization process will be treated later in chapter 4.

The results reported in this study are obtained from thin-film samples. Therefore, results cannot be applied immediately to bulk samples (like for example melt spun or ball rolled amorphous alloys).

2.2 Experimental

The structure of the specimens used for the *in-situ* annealing experiments in the transmission electron microscope (TEM) is depicted in Fig. 2.1. Si wafers were processed to yield amorphous Si_3N_4 membranes, supported by Si [Jac86]. The size of the membranes was 50 μm x 50 μm, the thickness was approximately 30 nm. On these wafers a stack of approximately 400 alternating layers of Ti and Si, up to a total thickness of about 200 nm, was deposited in a Perkin-Elmer '2400' RF-diode sputter-deposition system. Before deposition the residual gas pressure was $5 * 10^{-5}$ Pa. The argon pressure during deposition was 0.7 Pa. The substrate was not intentionally heated before or during deposition, the estimated temperature during deposition did not exceed 60 ^oC. Since the Si_3N_4 membranes and thin films to be studied are transparent to 100 keV electrons, the specimens can be observed in the electron microscope without further processing. Through-

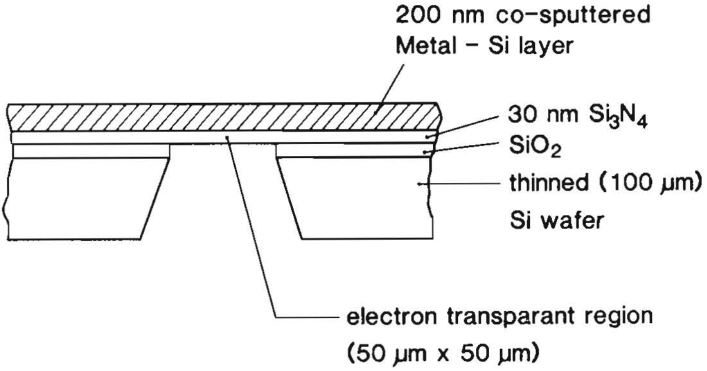

Fig. 2.1. Structure of the samples used in the present investigation. The silicide layer to be studied (thickness about 200 nm) and the central window are transparent to the 100 keV electrons.

out all experiments, one surface of the thin film was in contact with the Si_3N_4 membrane.

The composition of the thin films was derived from Rutherford backscattering spectrometry (RBS). In addition some samples were analyzed with Auger electron spectroscopy (AES) combined with sputter-depth profiling (Ar^+, 3keV ion bombardment) in a Perkin Elmer PHI 600 scanning Auger microprobe.

The growth experiments were performed in a Philips EM300 electron microscope, equipped with a tungsten filament heated hot stage and thermocouple. It was found that the effect of the electron beam was to increase the growth speed and nucleation rate in the observed area. We determined a correction for this effect by comparing measured growth speeds (see further) with and without electron beam irradiation. In the latter case, the electron beam was only switched on for a reletively short period of time when a micrograph was made. If the electron beam has a thermal effect only, it was determined that the correction was equivalent to a temperature rise of the observed area of (35 ± 5) °C above the thermocouple temperature in the range of (250 °C - 450 °C). In practice it is very inconvenient to switch the beam off between exposures, and it was decided to perform all experiments with the beam permanently switched on. Consequently all reported temperatures have been corrected for the effect of the electron beam.

A typical experiment to measure the growth rate of a crystal in the matrix was performed by heating the sample until the first nuclei were visible. When enough nuclei were present, the temperature was reduced to the desired value. After temperature equilibrium was reached, a series of micrographs at fixed time intervals (of the order of minutes) were made. Each micrograph showed several separate crystals from which the growth rate could be determined simultaneously. To avoid erroneous results all growth measurements were performed on crystals which were well separated from neighboring crystalline regions so that the growth rate remained unaffected by interference from other crystals.

The nucleation rate was estimated by counting the number of nuclei nucleated in unit area and unit time.

More detailed structural investigations were performed *ex-situ* in a Philips EM400 microscope operating at 120 kV. This microscope was equipped with an electron microprobe.

2.3 Results and Discussions

2.3.1 General

The chemical composition and thickness of the as-deposited layers were derived from RBS measurements (Table 2.1). An estimate for the geometrical thickness of the samples was calculated with the assumption that the molar volume of Ti equals its bulk value ($V_m^{Ti} = 18 * 10^{-24}$ cm^3) and that the molar volume of Si equals its 'metallic' or 'silicide' value ($V_m^{Si} = 12 * 10^{-24}$ cm^3). In the Si–richest samples some argon was incorporated during the sputter-deposition process (about 3 at. % maximum for the most Si–rich sample). No significant levels of other impurities were found in the as-deposited or annealed samples with Rutherford backscattering spectrometry (RBS) or Auger electron spectroscopy (AES) (detection limit about 0.5 at. % for O and C). In the remainder of this chapter samples will be referred to by their entry in Table 2.1.

Sample ($Ti_{1-x}Si_x$)	**Composition** (c_{Si})	**Thickness** (10^{16} atoms/cm^2)	**Thickness (estimate)** (nm)
$\alpha Ti_{45}Si_{55}$	0.55	140 ± 7	210 ± 10
$\alpha Ti_{31}Si_{69}$	0.69	138 ± 7	190 ± 10
$\alpha Ti_{29}Si_{71}$	0.71	124 ± 6	170 ± 10
$\alpha Ti_{23}Si_{77}$	0.77	126 ± 6	170 ± 10

Table 2.1: The thicknesses and composition of the amorphous alloy thin films as measured with RBS. The geometrical thickness in the last column is calculated from the RBS result. It can be used as a rough estimate only.

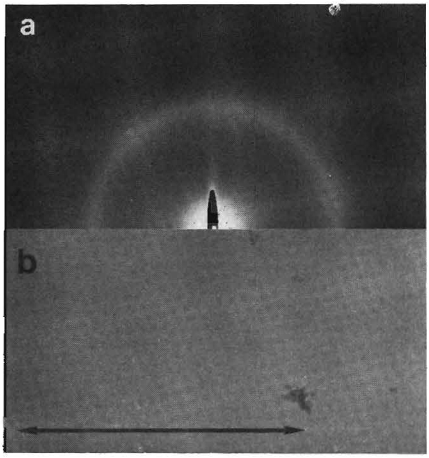

Fig. 2.2. The as-deposited $Ti_{31}Si_{69}$ sample. (a) selective area diffraction pattern; (b) bright field micrograph. The arrow corresponds to a length of 1 μm. (The contrast in the bright field micrograph is a little dust particle only used for focussing the microscope.)

The structure of an as-deposited sample $Ti_{31}Si_{69}$ is revealed in Fig. 2.2. Selective area electron diffraction (SAD) in the transmission electron microscope (TEM) showed only one very broad diffraction band corresponding to a mean interatomic spacing of about 0.22 nm. The crystal size determined from the width of the diffraction band in Fig. 2.2a was about 1 nm, i.e., of the order of the unit cell dimensions of C49 $TiSi_2$ [Hou86]. Moreover, the bright field micrograph corresponding to the diffraction pattern (Fig. 2.2b) shows no contrast. Similar results were obtained for samples with other compositions too. Thus, it can be concluded that the as-deposited samples were amorphous.

The samples were now slowly heated in the electron microscope and, in order to prevent complete crystallization of the specimens, the samples were cooled again as soon as a reasonable number of crystals was obtained. We will first discuss the morphology and microstructure of the crystals in the samples $\alpha Ti_{31}Si_{69}$ and $\alpha Ti_{29}Si_{71}$ whose composition is fairly close to that of the disilicide. Later we will turn our attention to the crystallization of the other samples, with compositions remote from that of $TiSi_2$.

Figs. 2.3a and b show TEM micrographs of silicide crystals in the samples $\alpha Ti_{31}Si_{69}$ and $\alpha Ti_{29}Si_{71}$. The crystals in Fig. 2.3 could be identified by selective area diffraction (SAD) as C49 $TiSi_2$ [Cot56,Hou86]. No other crystalline compounds were detected. The morphology of the C49 $TiSi_2$ crystals in the $\alpha Ti_{31}Si_{69}$ and $\alpha Ti_{29}Si_{71}$ samples is similar (see Fig. 2.3). Both samples were found to have square and ellipsoidal shaped crystals. In the case of the $\alpha Ti_{29}Si_{71}$ samples, however, the crystals were closer to a circular shape, the corners of squares and ellipsoids being blunted. Throughout all growth experiments these characteristic shapes were preserved.

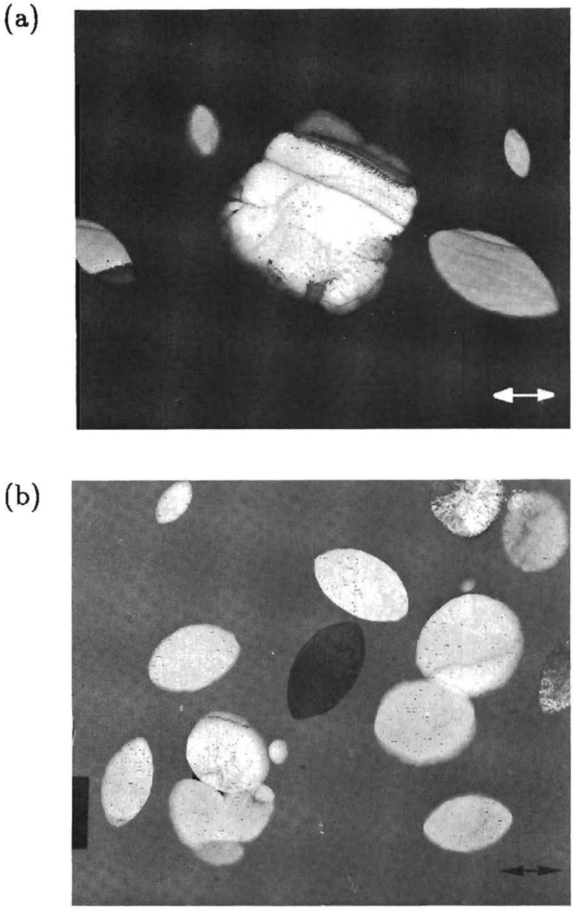

Fig. 2.3. C49 $TiSi_2$ single crystals in an amorphous matrix, (a): $\alpha Ti_{31}Si_{69}$; (b): $\alpha Ti_{29}Si_{77}$ The arrows in the micrographs correspond to a length of 1 μm.

The typical growth shape of the C49 $TiSi_2$ crystals in the samples $\alpha Ti_{31}Si_{69}$ and $\alpha t Ti_{29}Si_{71}$ points to an anisotropy in the velocity of the crystallization front and is probably related to the crystallographic structure of the C49 phase. In order to investigate this issue in more detail the crystallographic directions in the C49 $TiSi_2$ crystals were identified in the TEM (see Fig. 2.4). As expected, the orientation of the square and ellipsoidal crystals shows a unique correlation with the position of the crystallographic axes of the C49 unit cell in the crystals. Fig. 2.4a shows square and ellipsoidal crystals in $\alpha Ti_{31}Si_{69}$ with the proper crystallographic directions as determined in the TEM. The schematic drawing in Fig. 2.4b shows the three-dimensional shape of the $TiSi_2$ crystals as 'cushions'. Depending on the orientation of the crystals with respect to the boundaries of the thin film, squares (truncated perpendicular to the b–axis) or ellipsoids (truncated parrallel to the b–axis) are seen.

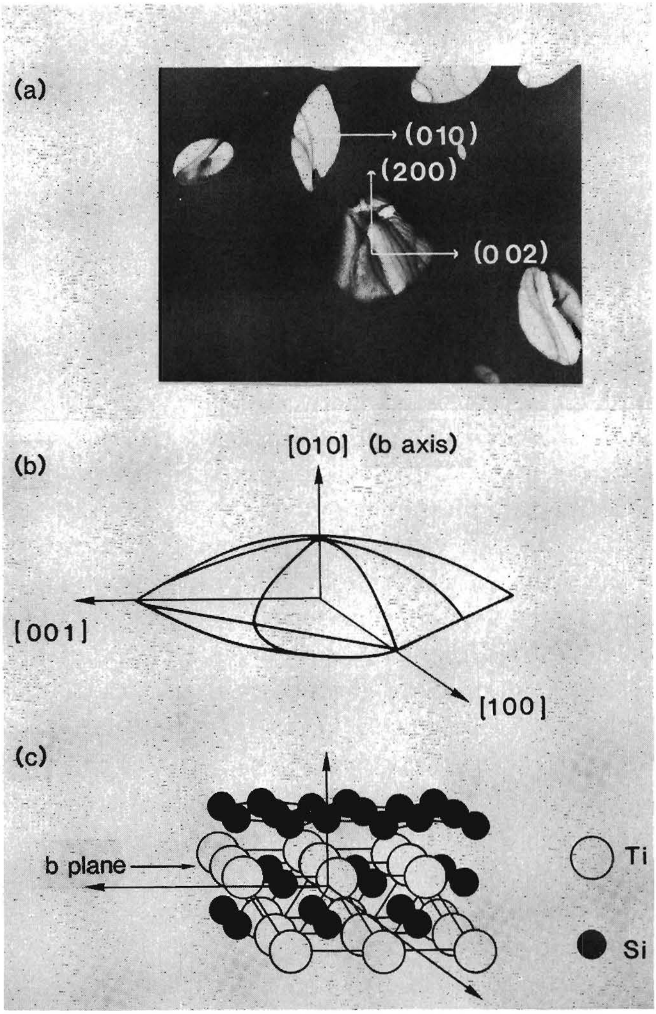

Fig. 2.4. (a) Crystallographic directions in C49 $TiSi_2$ crystals as found by TEM diffraction. (b) In three dimensions a C49 $TiSi_2$ crystal in an amorphous matrix would be 'cushion' shaped. Dependent on the orientation of the crystal with respect to the thin film boundaries, elliptical or square cross sections are obtained. (c) The crystallographic structure of the C49 $TiSi_2$ phase. The {010} planes consist of flat close packed planes of Si atoms alternated with planes consisting of both Ti and Si atoms.

Fig. 2.4c shows a model of the C49 structure in the same orientation as the cushion depicted in Fig. 2.4b. Discrete layers consisting of Si atoms and layers consisting of both Ti and Si atoms in an equiatomic ratio can be distinguished perpendicular to the b–axis (which was previously identified with the short axis of the cushions or ellipsoids). To maintain this typical cushion shape, the crystals have to grow more slowly along the b–axis than they do perpendicular to that direction. Considering the fact that the Si–layers are nearly close packed, one anticipates that these b–planes are smoother and have a lower step density. The observed anisotropy in velocity and typical shape of the C49 crystals can thus be explained from the crystal structure if the velocity of the crystallization front is dependent on the step density on the crystalline - amorphous interface.

It was difficult to obtain partially transformed $\alpha Ti_{31}Si_{69}$ regions (as shown in the micrograph of Fig. 2.3a) for further investigations after cooling to room temperature. During cooling of specimens which showed only isolated crystals in the amorphous matrix, a very fast crystallization reaction of the remaining part of the specimen occurred sometimes. The temperature at which this crystallization took place was about 100 ^oC, which is considerably lower than normal growth and nucleation temperatures. Additionally, some $Ti_{31}Si_{69}$ samples were already completely crystallized before any heating took place. We observed that the nitride membrane from these specimens was broken. These observations may indicate that stress influences the crystallization process.

In all ellipsoidal crystals (see Figs. 2.3a and b) a prominent faultlike feature was observed along the long axis of the crystals (see Figs. 2.3 and 2.5). Fault analyses [Rea87b] showed that this contrast originates from an array of stacking faults, with an approximate spacing of 3 to 5 nm. The displacement vector of these faults is in the direction $< 620 >$. It is found that the faults arise from the omission of an atomic layer parallel to the b–plane. This requires also a shift in the [100] direction to accommodate adjacent atoms on either side of the fault [Rea87b]. We observed that this kind of stacking fault was present throughout the entire $TiSi_2$ crystals, but in a somewhat smaller concentration than along the axis. Stacking fault contrast was not observed in the square crystals, but it is likely that these crystals contain similar faults which are not visible because they are not in a suitable orientation with respect to the incoming electron beam. These stacking faults may be one of the defects which cause the residual resistivity of the C49 phase to be high, which will be treated in detail in chapter 3.

Figs. 2.6a and b show crystalline regions in the most Si–rich sample ($\alpha Ti_{23}Si_{77}$) and in the Ti–rich sample ($\alpha Ti_{45}Si_{55}$). In the Si–rich sample the crystals could be identified by selective area diffraction (SAD) as

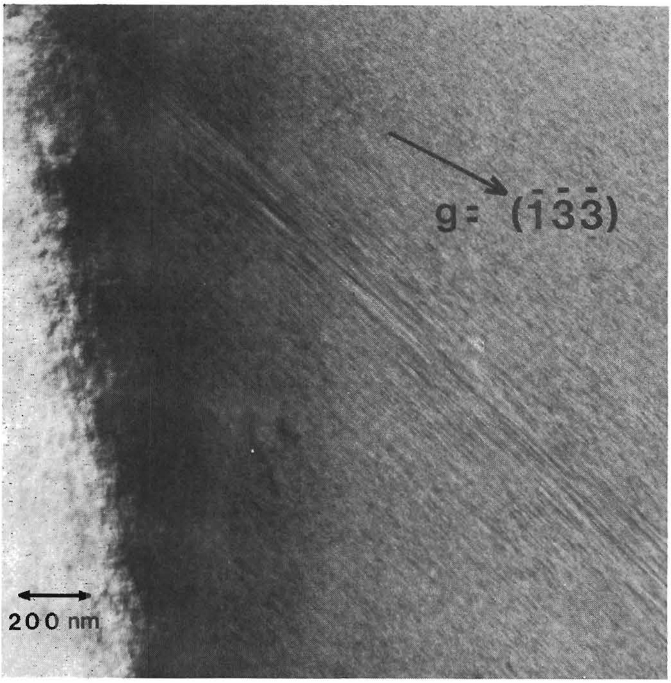

Fig. 2.5. High magnification, bright - field ($B = [\bar{3}01]$) micrograph of the center of an ellipsoidal crystal. Stacking faults can be seen. The stacking fault spacing in the center of the crystal is about 5 nm.

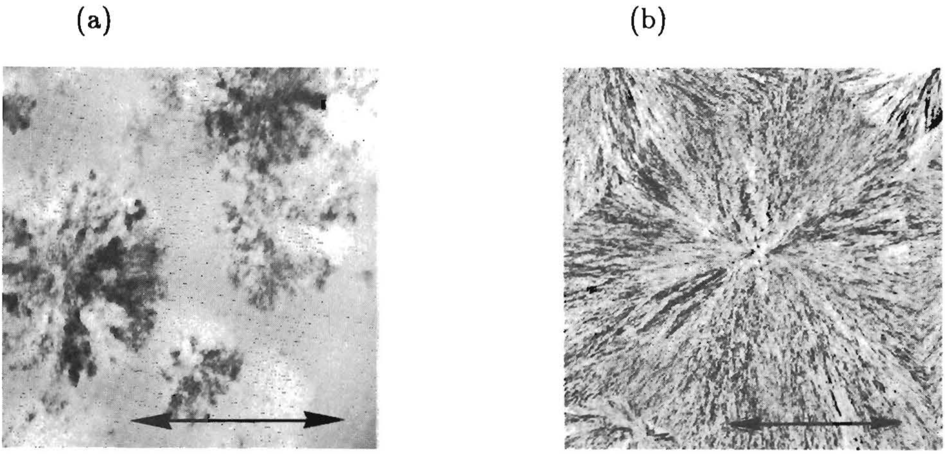

Fig. 2.6. (a) C49 $TiSi_2$ crystals in the Si–rich sample $\alpha Ti_{23}Si_{77}$. The arrow denotes a length of 1 μm. (b) Crystalline regions in the Ti–rich sample $\alpha Ti_{45}Si_{55}$. The arrow denotes a length of 10 μm.

C49 $TiSi_2$ [Cot56,Hou86], just like the crystals in Fig. 2.3. In the Ti-rich ($\alpha Ti_{45}Si_{55}$) sample unambiguous phase identification was impossible as will be discussed later in chapter 4. The morphology of the crystals in the $\alpha Ti_{23}Si_{77}$ and the $\alpha Ti_{45}Si_{55}$ sample is significantly different from that of the crystals in the other two samples. Figs. 2.6a and b show that the morphology is more or less circular (spherulitic [Kos75,Duh80,Her78]). While only a weak radial symmetry can be discerned in the Si-rich sample (Fig. 2.6a), this radial symmetry is much more pronounced in the micrograph of the Ti-rich sample (Fig. 2.6b). It was not possible to obtain isolated crystals in the $\alpha Ti_{45}Si_{55}$ alloy. Rather, when crystallization started, usually on the sides of the specimens membrane, the whole observed area crystallizes rapidly into one or a few crystalline regions in which no or only a few grain boundaries can be discerned.

For the Si-rich sample ($\alpha Ti_{23}Si_{77}$) depicted in Fig. 2.6a we investigated the location of the excess silicon. Using Auger electron spectroscopy (depth profile) and electron micro-analyses in the TEM (lateral profile), we were unable to locate Si concentration gradients in the crystals, the amorphous matrix, and at the interfaces between crystalline and amorphous material. No segregation of Si on either the vacuum - film interface or the film - Si_3N_4 interface was found after the present (low-temperature) anneals. Although some of the excess Si may be incorporated in a metastable solid solution (see also chapter 4) we do not expect that all of the excess Si in the $\alpha Ti_{23}Si_{77}$ sample can be incorporated in the lattice. Instead, the excess Si will be present as little precipitates within the crystals. We suggest that the black point-like contrast (see Fig. 2.6a) is due to these Si precipitates [Rea87b]. The size of these precipitates is estimated to be about 5 to 10 nm.

2.3.2 Growth Rates

We will at first describe the growth of crystallites in the Si-rich samples, i.e. those corresponding to the micrographs of Figs. 2.3 and 2.6a. Later we will make some qualitative remarks on the crystallization reaction in the Ti-rich sample, corresponding to the micrograph of Fig. 2.6b.

In all Si-rich samples we found that the velocity of the crystallization front or the linear growth rate (expressed in m/s) was constant with time at a given temperature. This is consistent with the fact that no macroscopic concentration gradients are found. The rate of the crystallization process is thus controlled at the crystalline-amorphous interface.

Of course, the observed anisotropy in the case of $\alpha Ti_{31}Si_{69}$ and $\alpha Ti_{29}Si_{71}$ causes the value of the growth rate to depend on the direction along which the diameter of the crystals is measured. For the determination of the growth rate of the ellipsoidal crystals we used the half length of their long

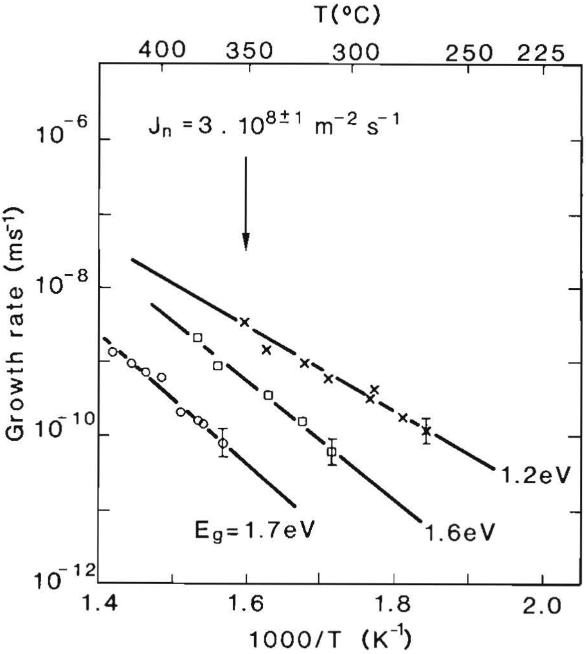

Fig. 2.7. Arrhenius plot of the growth rate for crystals in $\alpha Ti_{31}Si_{69}$ (crosses), $\alpha Ti_{29}Si_{71}$ (squares) and $\alpha Ti_{23}Si_{77}$ (circles). The activation energy E_g for growth is indicated along the straight lines. The inaccuracy in the activation energy is estimated to be 0.1 eV. The temperature at which nucleation becomes significant is indicated with the arrow and is found approximately the same for the depicted compositions.

axis, while for the square crystals we used the half length of the diagonal. The growth rates which were determined from the first time derivative of these two sizes were equal within the measurement error. The growth rate at a particular temperature was determined from at least three crystals. The random error in the growth rate is about 50 % which partly can be ascribed to small temperature variations (5 ^oC) during the experiments.

Fig. 2.7 shows a plot of the logarithm of the growth rate of C49 $TiSi_2$ crystals versus reciprocal temperature (an Arrhenius plot). The slope of the straight lines in the Arrhenius plot equals the activation energy for growth. Note that the growth of $TiSi_2$ crystals in the Si–richer amorphous alloys ($\alpha Ti_{29}Si_{71}$ and $\alpha Ti_{23}Si_{77}$) exhibits a significantly higher activation energy than the growth in the nearly stoichiometric alloy $\alpha Ti_{31}Si_{69}$. This may indicate that the crystallization process is governed by different mechanisms in the stoichiometric or Si–rich alloys.

Generally three possible crystallization mechanisms are considered (primarily composition determines which process is dominant) [Hor80,Kos81]:

(i) polymorphous crystallization

(ii) eutectic crystallization

(iii) primary crystallization of one of the components
(in our case Si or $TiSi_2$).

These processes are exemplified in the hypothetical free-energy diagram of Fig. 2.8, together with the composition of the present Si–rich alloys and the composition of the Si - $TiSi_2$ eutectic.

In the case of the $\alpha Ti_{31}Si_{69}$ alloy, the most probable reaction path is a polymorphous crystallization to C49 $TiSi_2$. No diffusion is necessary over distances larger than a few interatomic spacings. Christian [Chr81] proposed that the activation energy E_g for the interface velocity in a polymorphous transition will be close to the activation energy for grain-boundary diffusion. A comparison between the magnitude of E_g (1.2 eV) and the ac-

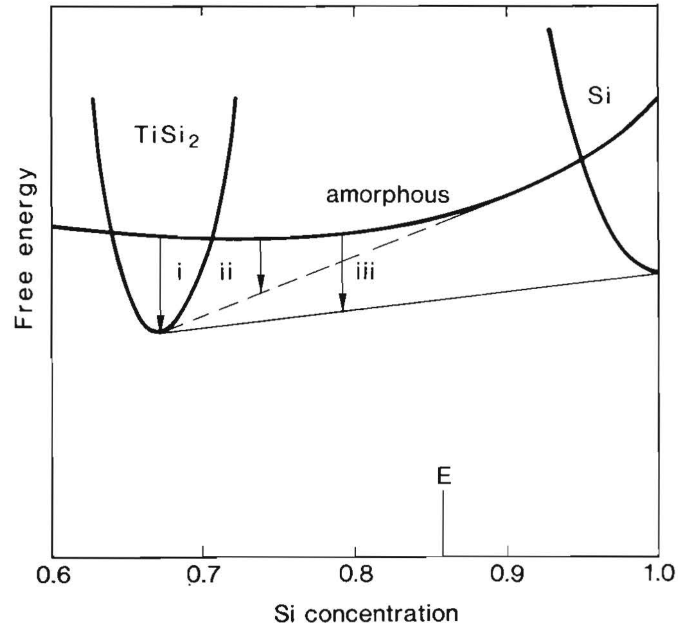

Fig. 2.8. Tentative free-energy diagram of the binary system Ti - Si for a temperature lower than the eutectic temperature (only the Si - side of the diagram is shown). E denotes the Si - $TiSi_2$ eutecticum (14 at.% Ti). The three possible crystallization paths are indicated by arrows : polymorphous crystallization *(i)*, primary crystallization of $TiSi_2$ *(ii)*, and eutectic crystallization *(iii)*.

tivation energy for Si diffusion in crystalline $TiSi_2$ (1.80 - 2.20 eV, [Aum85] [Hun83], chapter 5) supports this point of view.

The temperature dependence of the growth rate is frequently described in the form of a simple Arrhenius type relation [Gre85,Kos81,Ran81,Hei81], viz:

$$\Gamma = \Gamma_0 exp[-\frac{E_g}{kT}] \tag{2.1}$$

where E_g denotes the activation energy for the growth process and Γ_0 is a preexponential factor which depends in detail on the operational crystallization mechanism and growth process; k is the Boltzmann constant and T is the absolute temperature. In the case of step assisted polymorphous growth the preexponential factor can be estimated by [Chr81]:

$$\Gamma_0 \approx \hat{n}\Omega^{1/3}\nu \tag{2.2}$$

where $\hat{n}$ the dimensionless step density (expressed in interatomic distances), Ω the average atomic volume and $\nu = kT/h$ the atomic vibration frequency. Substituting $\Omega = 14 * 10^{-24}$ cm^3 for $TiSi_2$, $\nu = 10^{13}$ s^{-1} and a reasonable value for n̂, say 10^{-1}, yields a preexponential factor of about 250 m/s. Kóster et al. [Kos81] quote a similar value of about 10^3 m/s for polymorphous crystallization reactions in many different amorphous alloys. At a temperature of 350 °C a growth rate of $\Gamma = 4 * 10^{-9}$ m/s is observed. Calculating the activation energy from this growth speed and the estimated preexponential factor of 250 m/s yields an activation energy of 1.3 eV, a value close to the value derived from the slope of the Arrhenius plot. Thus for the polymorphous phase transformation the absolute value and the activation energy of the velocity of the crystallization front are consistent with a step assisted growth mechanism.

An excess of Si increased the activation energy to a value of about 1.7 eV, indicating that in the Si–rich alloys a different crystallization process may prevail. The $\alpha Ti_{23}Si_{77}$ sample undergoes an eutectic crystallization reaction (see Fig. 2.8). A reaction path by primary crystallization of Si or $TiSi_2$ is excluded because a decreasing growth rate with time (which is typical for a primary crystallization reaction) is not observed. An eutectic crystallization mechanism results in the observed characteristic microstructure (see Figs. 2.6a). Crystals are observed to consist of lamellae of the two crystallizing phases and assume a so-called spherulitic shape [Kos75,Duh80,Her78]. A weak radial symmetry can be discerned in the crystals in the $\alpha Ti_{23}Si_{77}$ alloy. A typical width of an eutectic lamella may be estimated from the size of the Si precipitates: 5 to 10 nm. The fact that such eutectic lamellae are of considerable width as compared to the interatomic distance necessitates diffusion of both elements to take place, probably through the amorphous matrix. This may increase the value of the activation energies of the eutectic reaction above that of the polymorphous reaction. As an order of magnitude estimate of the preexponential factor in Eq. 2.1 one might take for the eutectic reaction [Kos81]:

$$\Gamma \approx \frac{\Omega^{2/3}\nu}{s} \tag{2.3}$$

where s is the spacing of the eutectic lamellae. Substituting for s a value of 10 nm in the case of the $\alpha Ti_{23}Si_{77}$ alloy yields a preexponential factor of about 50 m/s. At a temperature of 350 °C a growth rate of $\Gamma = 3 * 10^{-11}$ m/s is observed. Calculating the activation energy from this growth speed and the estimated preexponential factor yields an activation energy of 1.5 eV. This estimate is in agreement with the value derived from the slope of the Arrhenius plot ((1.7 ± 0.1) eV), and the growth rates are consistent with an eutectic crystallization mechanism.

The micrograph of the Ti–rich sample $\alpha Ti_{45}Si_{55}$ in Fig. 2.6b shows a microstructure typical to an eutectically crystallized alloy. Lamellae parallel to the growth direction are very clearly visible. It was not possible to determine the velocity of the crystallization front for this Ti–rich alloy as was done for the other three alloys. It appeared that the growth was very fast once the crystalline material had nucleated. For the same reason only one or two different crystals are seen on the entire electron transparent region of the specimen (typical dimension 50 μm). Typical temperatures at which the growth and nucleation of crystalline material takes place are about 600°C. Note that this temperature is much higher than the typical growth and nucleation temperatures of the other alloys (300 °C to 400 °C), whose composition was closer to the $TiSi_2$ stoichiometry. These differences in crystallization temperature will be addressed in more detail in chapter 4.

2.3.3 Nucleation

In the higher temperature range ($\geq$ 300 °C), the nucleation rate was appreciable for the Si–rich samples and the nearly stoichiometric samples. Estimates of the nucleation rate at 350 °C yielded $J = 3*10^{8\,\pm\,1}$ $m^{-2}s^{-1}$ (indicated in Fig. 2.7). This value was about the same for the $\alpha Ti_{31}Si_{69}$, $\alpha Ti_{29}Si_{71}$ and $\alpha Ti_{23}Si_{77}$ alloys. The temperature dependence of the nucleation rate could not be determined because of the high growth rates at temperatures where the nucleation rate was high enough to be measured.

One might argue that the nuclei are already present in the amorphous thin film before it is heated in the electron microscope. Then the only barrier to crystallization is the limited atomic mobility at low temperatures. In that case, one expects all crystals to start growing at the same time, i.e. as soon as the temperature reaches values were the growth rate is appreciable, say 10^{-9} m/s. Consequently one expects all crystals to have approximately the same size if they start growing from preexisting nuclei and to have widely different sizes if they grow from random (in time) nucleated nuclei [Bla85]. In the micrograph of Fig. 2.3a crystals of many different sizes are observed which shows that random nucleation is important. In chapter 4 additional evidence in favor of a random nucleation process will be presented.

In order to explain the magnitude of the above determined random nucleation rate at 350 °C let us consider the classical Volmer - Weber expression for the steady state nucleation rate J [Chr81]:

$$J = J_0 exp[-\frac{E_n}{kT}] = N exp[-\frac{E_c}{kT}] * \nu exp[-\frac{E_g}{kT}] \qquad (2.4)$$

where J_0 is a preexponential factor (expressed in $m^{-2}s^{-1}$), E_n an effective activation energy, N the number of possible nucleation sites (expressed in m^{-2}), E_c the free energy needed to form a critical nucleus and E_g and ν are defined earlier in Eqs. 2.1 and 2.2. Note that in quoting N and J as a rate per unit surface, we implicitly assumed that nucleation is heterogeneous (i.e. nucleation occurs on either of the surfaces of the thin film). This is a reasonable assumption for nucleation in thin films [Chr81]. The effective activation energy for nucleation E_n thus is equal to the sum of the activation energy for growth and the energy needed to form a critical nucleus.

From the measurements of growth speeds of the polymorphous crystallization reaction one calculates that the second exponential in Eq.2.4 is about $10^{-11 \pm 1}$ at a temperature of 350 °C. At that temperature the nucleation rate was measured to be about $J = 3 * 10^{8 \pm 1}$ $m^{-2}s^{-1}$. An upper and a lower limit for N can be determined from the following considerations. As a lower limit for N one may take the number of crystallites per unit area in a completely crystallized sample. For the present samples the grain size is of the order of 1 μm, hence a lower limit for N is about 10^{12} m^{-2}. As an upper limit for N one may use the surface density of $TiSi_2$ which is about 10^{18} m^{-2}. Thus as a reasonable range of values for N we will use $10^{15 \pm 3}$ m^{-2}. With the above estimated range for N and a frequency factor $\nu = kT/h = 10^{13}$ s^{-1} one calculates for E_c the value of (1.2 ± 0.5) eV which seems reasonable. The total activation energy for nucleation equals the sum of the free energy to form a critical nucleus and the activation energy for growth, viz: $E_n = E_c + E_g = (2.4 \pm 0.6)$ eV.

2.4 Conclusions

We studied the crystallization of amorphous Ti - Si binary alloy thin films with compositions ranging from Ti/Si = 1/1 through the stoichiometric composition Ti/Si = 1/2 to more Si–rich alloy thin films Ti/Si = 1/3 by *in-situ* annealing in a transmission electron microscope. The line of research followed here allows the possibility to discriminate between phenomena occurring in the nucleation stage and the subsequent growth stage.

In alloys with a composition close to or richer in Si than the disilicide it was found that $TiSi_2$ in the C49 ($ZrSi_2$) polytype was the growing crystalline phase at temperatures in the range of 250 °C to 450 °C.

The velocity of the crystallization front was measured from TEM micrographs. In all cases the growth was independent of time at a specific temperature until the crystals touched each other. This is consistent with the fact that no macroscopic chemical composition gradients were present during the crystallization process. Alloys with a composition close to the stoichiometry of $TiSi_2$ crystallized through a polymorphous phase transformation with a low activation energy (1.2 eV) at a temperature of about 300 °C. Si–rich alloys crystallized through eutectic decomposition. The difference in reaction mechanism was clearly reflected in a higher activation energy for the growth of crystalline material (1.6 to 1.7 eV) and somewhat higher crystallization temperatures (about 330 °C to 380 °C). The absolute magnitude of the growth rates could be explained with order of magnitude estimates from simple growth models for both reaction mechanisms.

For the alloys with a composition near that of the disilicide and for Si–rich alloys the nucleation rate was appreciable at temperatures exceeding about 300 °C. From the presence of crystals with many different sizes it was concluded that nucleation was random. Only a very rough estimate for the activation energy for nucleation could be determined from the Volmer - Weber expression for the steady state nucleation rate: (2.4 ± 0.6) eV.

The C49 $TiSi_2$ crystals contained two kinds of defects. Firstly, the $TiSi_2$ crystals were found to contain a high density of stacking faults parallel to the b–plane. The occurrence of these stacking faults could be explained on the basis of the crystal structure of the C49 phase. An effect of these stacking faults on the resistivity of the C49 $TiSi_2$ phase was anticipated. Secondly, in the alloy with compositions of 77 % Si, which is significantly richer in Si than the disilicide (67 % Si), at least a part of the excess Si was found to be present within the crystals in the form of small (with sizes of 5 to 10 nm) precipitates.

In contrast to the low temperatures required for nucleation and growth in the Si–rich or near stoichiometric amorphous alloys, much higher temperatures (about 600 °C) were needed to crystallize the alloy with a composition near to that of the monosilicide. The latter sample crystallized through an eutectic mechanism. Unfortunately, quantitative kinetic measurements for this sample could not be obtained.

Bibliography

[Aum85] C.E. Aumann, J.R. Jacobs, M.S. Phipps, C. Pico, N.C. Tran and M.G. Lagally, in Proceedings of the VLSI Multilevel Conference, Santa, Clara, 1985 (IEEE, New York, 1985), pp. 363-372.

[Ben87] R.W. Bené, J. Appl. Phys. **61**, 1826 (1987).

[Bey85] R. Beyers and R. Sinclair, J. Appl. Phys. **57**, 5240 (1985).

[Bla85] H. Blanke and U. Kóster in 'Rapidly Quenched Metals', **1**, 227, ed. by S. Steeb and H. Warlimont, (North-Holland, Amsterdam 1985).

[But84] R. Butz, G.W. Rubloff, T.Y. Tan and P.S. Ho, Phys. Rev. **B30**, 5421 (1984).

[Chr81] J.W. Christian, The Theory of Transformations in Metals and Alloys, 2nd ed. Part I (Pergamon, Oxford, 1981).

[Cot56] P.G. Cotter, J.A. Kohn and R.A. Potter, J. Am. Cer. Soc. **39** 11 (1956).

[Duh80] P. Duhay, Sci. Technol. **2**, 29 (1980).

[Gre85] A.L. Greer, Proc 5Th Int. Conf. Rapidly Quenched Metals, Wúrzburg, Germany, Sept. 1984, ed. by S. Steeb and H. Warlimont, **1**, p 215, North Holland, Amsterdam (1985).

[Hei81] M. von Heimendahl and G. Kuglstatter, J. Mater. Sci. **16**, 2405 (1981).

[Her78] U. Herold and U. Kóster, Proceedings of the 3rd International Conference on Rapidly Quenched Metals, Brighton (1978) (Metals Society, London, 1978), Vol. 1, p.281.

[Her83] S.R. Herd, K.Y. Ahn and K.N. Tu, Mater. Res. Symp. Proc. **18**, 197 (1983).

[Heu86] F.M. d'Heurle and P. Gas, J. Mater. Res. **1**, 205 (1986).

[Hol87] K. Holloway and R. Sinclair, J. Appl. Phys. **61**, 1359 (1987).

[Hor80] E. Hornbogen and I. Schmidt, in Liquid and Amorphous Metals, edited by E. L scher and H. Coufal (Sythoff and Noordhoff, Alphen aan den Rijn, The Netherlands, 1980).

[Hou86] H.J.W. van Houtum and I.J.M.M. Raaijmakers, Mater. Res. Soc. Symp. Proc. **54**, 37 (1986).

[Hou87] H.J.W. van Houtum, I.J.M.M. Raaijmakers and T.J.M. Menting J. Appl. Phys. **61**, 3116 (1987).

[Hun83] L.S. Hung, J. Gyulai, J.W. Mayer, S.S. Lau and M.A. Nicolet, J. Appl. Phys. **54**, 5076 (1983).

[Jac86] J.W.M. Jacobs and J.F.C.M. Verhoeven, J. Micros. **143**, 103 (1986).

[Kem82] M.J.H. Kemper and P.H. Oosting, J. Appl. Phys. **53**, 6214 (1982)

[Kos75] U. Kóster and P. Weiss, J. Non-Cryst. Solids **17**, 359 (1975).

[Kos81] U. Kóster and U. Herold in 'Glassy Metals I, Ionic Transport, Electronic Transport and Crystallization', ed. by H.J. Gúntherodt and H. Beck, p. 225 (Springer Verlag, Berlin 1981).

[Lav39] F. Laves and H.J. Wallbaum, Z. Kristallogr. **101**, 78 (1939).

[Mur80a] S.P. Murarka and D.B. Fraser, J. Appl. Phys. **51**, 350 (1980).

[Mur80b] S.P. Murarka and D.B. Fraser, J. Appl. Phys. **51**, 342 (1980).

[Mur83] S.P. Murarka, 'Silicides for VLSI Applications' (Ac. Press, New York, 1983).

[Raa88a] I.J.M.M. Raaijmakers, A.H. Reader and P.H. Oosting, J. Appl. Phys. **63**, 2790 (1988)

[Raa88b] I.J.M.M. Raaijmakers, P.H.Oosting and A.H. Reader, Mater. Res. Soc. Symp. Proc. XX, xxx (1988), Materials Research Society Pittsburgh.

[Ran81] S. Ranganathan and M. von Heimendahl, J. Mater. Sci. **16**, 2401 (1981).

[Rea87a] A.H. Reader, I.J.M.M. Raaijmakers and H.J.W. van Houtum, proc. Microsc. Semicond. Mater. conf., Oxford (1987); published in Inst. Phys. conf. Ser. **87**, section 7, 523 (1987).

[Wal76] R.M. Walser and R.W. Bene, Appl. Phys. Lett. **28**, 624 (1976).

[Wei86] B.Z. Weiss, K.N. Tu and D.A. Smith, Acta Metall. **34**, 1491 (1986).

Chapter 3

Crystallization of Amorphous Ti - Si Alloys: Microstructure and Resistivity

3.1 Introduction

In very large scale integrated circuits silicides can be used as contact material or interconnect material [Cho83,Heu82,Mur83]. High temperature resistant, low resistivity interconnects can for example be formed from a co-deposited alloy of metal and Si. Deposition of this material on polycrystalline Si (polycide [Cro79]) or directly on SiO_2 (as a gate electrode [Moc78]) is feasible. The as-deposited alloys are usually amorphous. Although the alloys crystallize readily at moderate temperatures (200 to 500 °C), the desired low resistivities are only achieved after anneals at a much higher temperature (700-1000 °C).

In the last five years several studies have been devoted to the crystallization of such amorphous metal-Si alloy thin films. For example, Raaijmakers et al. [Raa87c,Raa87d] (see also chapter 2) and Weiss et al. [Wei86] annealed amorphous Ti - Si and Cr - Si alloy thin films in a TEM to elucidate the crystallization process. Weiss et al. [Wei86], Thompson et al. [Tho87], Nava et al. [Nav86a,Nav86b,Nav85a,Nav85b] and Tien et al. [Tie83] used *in-situ* resistivity measurements to study the crystallization behaviour of various refractory metal-Si alloys. The *in-situ* resistivity studies show many common features. One of the most salient similarities is that, with increasing anneal temperature, a sometimes small but very sharp drop in resistivity (associated with crystallization) is followed by a more gradual decrease in resistivity. This gradual decrease in resistivity is usually attributed to the annealing of defects, grain growth, recrystallization or elimination of remnants of amorphous material. Due to the fact that the resistivity decreases only slowly after crystallization, a high temperature anneal is required to achieve the minimum possible room temperature resistivity of a particular silicide. This calls for a more detailed study of this stage of the crystallization process.

In the quest for low resistivity materials, $TiSi_2$ is usually considered as being one of the winners [Mur83,Nic83]. In its C54 structure it shows a room temperature resistivity of 15 - 20 $\mu\Omega$cm. This value is even lower than the resistivity of the pure metal. However, it is now well established [Bey85,Hou86] that the Ti - Si reaction, whether in co-sputtered alloys or in diffusion couples, first produces a crystalline form of $TiSi_2$ which exhibits a much higher resistivity. This particular polytype of $TiSi_2$ is isomorphous with ZrSi2 (C49 structure) and has a room temperature resistivity of about 100 $\mu\Omega$cm. Only a high temperature anneal converts the C49 polytype to the low resistivity C54 polytype of $TiSi_2$. The temperature at which this transition occurs is ususally about 700 to 800 °C and is reported to depend on impurities [Bey85], film thickness [Hou86] or grain size [Hou87].

Reader et al. [Rea87b] recently reported that the resistivity of the C49 phase itself depends on the preparation method. It was found that C49 $TiSi_2$ films prepared from co-sputtered material had a significantly higher resistivity than C49 $TiSi_2$ films prepared from Ti - Si diffusion couples. The material prepared from co-sputtered material had a stacking fault density which was an order of magnitude larger than the material prepared from Ti - Si diffusion couples. The resistivity differences were attributed to these large differences in stacking fault density. The deleterious effect of a high density of stacking faults on the resistivity is also known for other silicides. For example, d'Heurle and co-workers [Heu82,Heu86,Kro87] attributed a resistivity maximum during the hexagonal to tetragonal phase transformation in WSi_2 and $MoSi_2$ to large densities of stacking faults.

In this chapter the resistivity behaviour of co-sputtered Ti - Si alloy thin films upon annealing is discussed. We will chiefly deal with the slow decrease of resistivity just after the crystallization of the amorphous Ti - Si alloy to the C49 polytype of $TiSi_2$. It will be shown that C49 $TiSi_2$ films with very different resistivities can be prepared from the same co-sputtered material. The observed resistivity behaviour will be explained from the microstructure of the crystallized specimens. For the first time evidence will be presented which supports the contention that the phase field of the C49 $TiSi_2$ phase is of substantial width.

3.2 Experimental

(100) oriented Si-wafers, 100 mm in diameter were thermally oxidized to grow approximately 0.6 μm SiO_2. Thin films of a Ti - Si alloy were co-sputtered on to these oxidized Si wafers as described previously (see chapter 2). For the present investigations the nominal thickness of the co-sputtered Ti - Si alloy thin film was 200 nm. The composition of the alloy thin film was targetted to be slightly Si–rich as compared to the composition of the disilicide ($TiSi_2$). The actual thickness and composition of the alloy thin films were derived from Rutherford backscattering spectrometry (RBS) using a 2 MeV He^+ ion beam and a scattering angle of 170 degrees. The wafers were cut into squares approximately 20 x 20 mm^2 on a side for heat treatment and *in-situ* resistivity measurements.

Heat treatment of the samples was performed in a turbomolecular pumped high-vacuum furnace. To avoid excessive degassing of the system walls during the anneals the walls were cooled efficiently with water. Anneals were started when a total pressure lower than 10^{-5} Pa had been reached. During heat treatment the pressure in the system increased to a maximum of 5 * 10^{-5} Pa. The heaters in the furnace consisted of two resistively heated hot plates facing each other (see below and Fig. 3.1). The sample was pressed gently to the bottom hot plate by four tungsten springs which

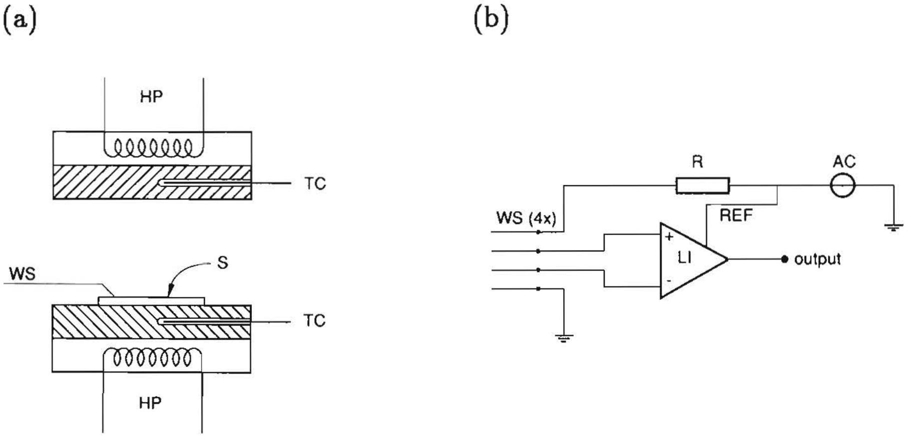

Fig. 3.1. Experimental setup to measure the resistivity of a thin film during anneal in high vacuum. (a) furnace assembly: S = sample; WS = tungsten contact springs TC = thermocouples; HP = resistively heated hot plate. The distance between the furnaces is exagerated in the figure.
(b) electrical diagram: LI = lock-in differential amplifier; AC = AC generator R = current limiting resistor; REF = reference signal.

served as contacts for the *in-situ* resistivity measurements. The temperature of the hot plates was measured with a chromel-alumel thermocouple inserted in a 1 mm diameter, 20 mm deep hole in the hot plates.

The hot plate temperature was controlled digitally with a proportional-integrative-derivative (PID) controller consisting of an Apple II-E microcomputer. Any desired temperature - time sequence could be programmed. Evidently the temperature of the sample does not necessarily equal the hot plate temperature. To relate sample and hot plate temperature a calibration was performed. For that purpose a small chromel-alumel thermocouple consisting of 0.1 mm diameter leads was glued to a sample with high-temperature-resistant ceramic adhesive.

The resistivity was measured *in-situ* with the aid of a four-point probe consisting of four 0.35 mm diameter tungsten springs spaced approximately 3 mm apart. To avoid erroneous resistivity readings caused by thermovoltages an AC technique was used consisting of an 80 Hz, 1 V_{eff} AC voltage source in series with a 1 kΩ resistor and a lock-in amplifier. (see Fig. 3.1b) Since the maximum resistivity of our samples (as measured between the outer probes) is only of the order of 10 Ω, the measurement current is constant within a few percent and equals 1 mA_{eff}. The frequency of the AC voltage source was chosen sufficiently low to allow capacitive coupling with the Si substrate through the SiO_2 layer to be neglected. The room temperature resistivities of the as-deposited and annealed samples were also measured *ex-situ* with a standard four-point probe. All resistivity-temperature curves obtained with the *in-situ* measurements were normalized to the resistivity of the as-deposited sample as measured with the standard four-point probe.

After cooling, the samples were further investigated with plan-view transmission electron microscopy (TEM), scanning electron miscroscopy (SEM), X-ray diffraction (XRD) and Hall effect measurements. Plan view TEM specimens were prepared using jet-etching from the backside of the wafer. Specimens were investigated in a Philips EM400T transmission electron microscope operating at 120 kV. X-ray diffraction was performed with a conventional 2 Θ diffractometer (Philips) equipped with a Cu-Kα X-ray source. Hall measurements were carried out on van der Pauw structures using a magnetic field strength of 0.6 T and a measurement current of 7.5 mA.

3.3 Results

3.3.1 As-deposited Material

The as-deposited alloy thin films are amorphous as was evidenced by selective area diffraction in the electron microscope and X-ray diffraction. This result is in agreement with previous investigations where similar layers on Si_3N_4 substrates were used [Raa87c,Raa87d] (see chapter 2).

The composition and thickness of the as-deposited thin films was determined with RBS. The total amount of Si and Ti atoms in the alloy thin film is $(95 \pm 3) * 10^{16}$ Si/cm^2 and $(42 \pm 3) * 10^{16}$ Ti/cm^2 respectively. (The inaccuracies are representative for the sample to sample variations in composition.) The composition of the alloy can thus be calculated to correspond to a Si concentration of 0.69 ± 0.02 (Ti/Si $= 0.44 \pm 0.04$), i.e. slightly Si–rich as compared with the composition of $TiSi_2$. The thickness of the silicide films can be determined from the total amount of Ti atoms, giving (180 ± 10) nm assuming bulk molar volume of $TiSi_2$ ($42.4 * 10^{-24}$ cm^3). In fact the present thin films is similar to the one on the $\alpha Ti_{31}Si_{69}$ specimen from the previous chapter.

3.3.2 Resistivity Behaviour

If the Ti - Si alloy thin film described above is heated in high vacuum at a constant heating rate of 1 ^{o}C/s the resistivity-temperature curve depicted in Fig. 3.2 is measured. Different samples were produced by heating a specimen to the desired temperature with a constant heating rate of 1 ^{o}C/s, keeping it at that temperature for approximately 200 s and then cooling it down in vacuum. This procedure yielded samples (b) through (g) which are characterized by the curves (b) through (g) in Fig. 3.2. We will at first describe the general form of the resistivity - temperature curve (Fig. 3.2) and the results obtained with X-ray diffraction (see further in Figs. 3.3 and 3.4). After that we will turn our attention to the electron microscopy results and the Hall measurements.

A few phenomena are immediately apparent from Fig. 3.2. For the as-deposited amorphous sample the temperature coefficient of resistivity (TCR) is slightly negative at room temperature. Kemper and Oosting [Kem82] attributed this anomalous behaviour of the temperature coefficient to the heavily disordered nature of these concentrated alloys (Mooij‘s rule [Moo73]). Mooij showed that in many disordered concentrated metal alloys Mathiessen's rule is not obeyed, instead the carrier mean free path reaches a limiting value of the order of interatomic dimensions.

At approximately 390 ^{o}C the resistivity suddenly drops, indicative of a crystallization process. This finding is confirmed with the X-ray diffrac-

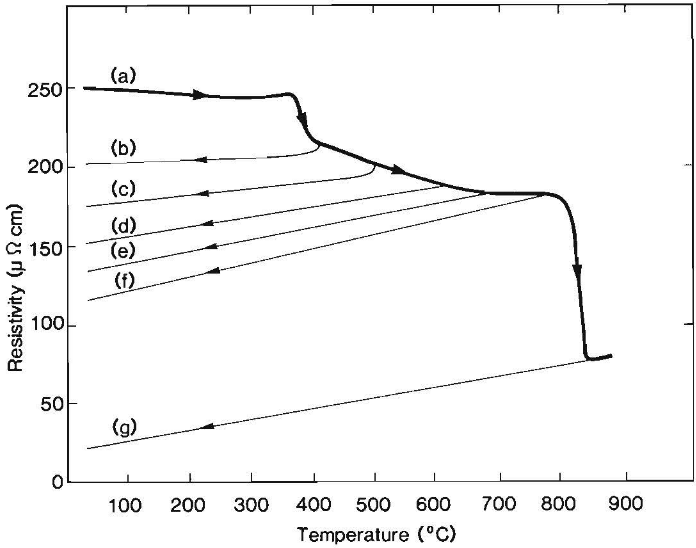

Fig. 3.2. Resistivity versus temperature curves. The thick curve (a) is obtained while heating the samples, while the thin curves (b) through (g) are obtained during cooling. The heating rate was approximately 1 °C/s. The sudden drops in resistivity are associated with crystallization of the sample to C49 $TiSi_2$ (at about 390 °C) and the transformation to C54 $TiSi_2$ (at about 820 °C).

tion results presented in Fig. 3.3. While no reflections are observed in the as-deposited sample, a sample annealed at 415 °C, i.e. just after the precipitous drop in resistivity (Fig. 3.2, curve (b)), shows clear reflections originating from $TiSi_2$ in its C49 polytype [Cot56,Bey85,Hou86]. Upon annealing at temperatures between 415 °C and 755 °C the resistivity decreases gradually. The temperature coefficient of resistivity and the slope of the cooling curves increases from a small positive value for sample (b) to a much higher value for sample (f).

Although clear changes in electrical transport properties are apparent, no differences in peak height nor in peak width were found in the diffraction patterns from samples (b)-(f). However, slight changes in peak position were found (Fig. 3.4). While the a and c - axis of the C49 unit cell are of constant length, the length of the b - axis increases with increasing anneal temperature. In samples annealed at temperatures of 700 °C or higher the values of the lattice constants are found to agree with the values determined by van Houtum et al. [Hou86] for C49 $TiSi_2$ prepared from Ti - Si diffusion couples. In samples annealed at low temperatures the value for the lattice constant b and the volume of the unit cell is (1.0 ± 0.2) % lower than the values found in the same material annealed at higher temperature.

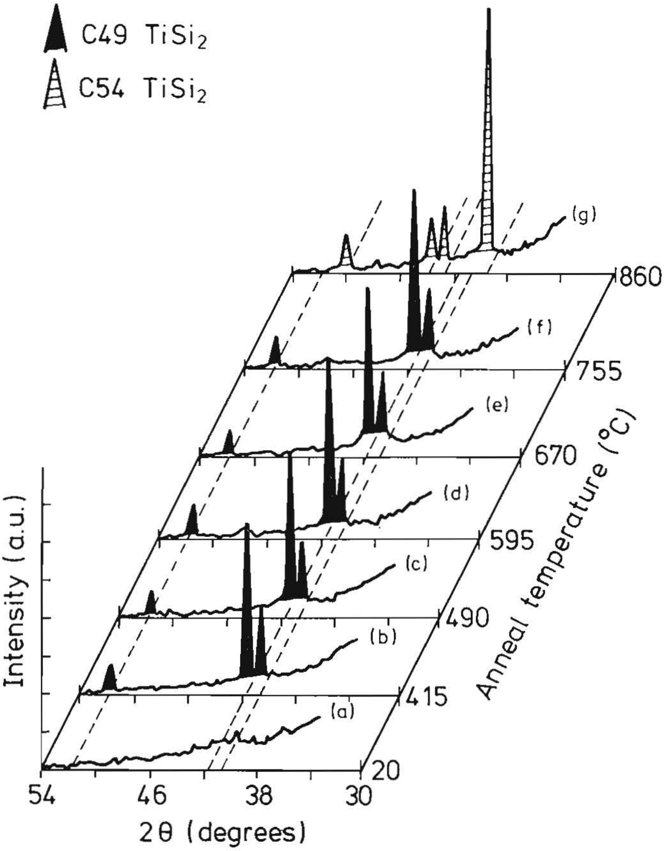

Fig. 3.3. X-ray diffraction diagrams of an as-deposited sample and annealed samples. Note that the as-deposited sample (a) is amorphous. Samples (b) through (f) show the same X-ray diffraction diagram corresponding to the C49 TiSi$_2$ phase. Sample (g) consists of the C54 TiSi$_2$ phase.

At a temperature of approximately 800 °C a second sharp drop in resistivity is observed. X-ray diffraction of sample (g) confirms that at this temperature the high-resistivity C49 phase is converted to the low resistivity C54 TiSi$_2$ phase [Lav39]. The room temperature resistivity of the C54 TiSi$_2$ phase is found to be (18 ± 1) $\mu\Omega$cm which is within the range of reported values [Nic83].

Note that the temperature dependence of the resistivity of the C54 phase is different from that of the C49 phase. Although the temperature coefficient of resistivity (i.e. $\frac{1}{\rho}\frac{d\rho}{dt}$) *increases* upon the transformation to the C54 phase, the slope of the cooling curve (i.e. $\frac{d\rho}{dt}$) *decreases* upon transformation. A similar observation can be made from the work

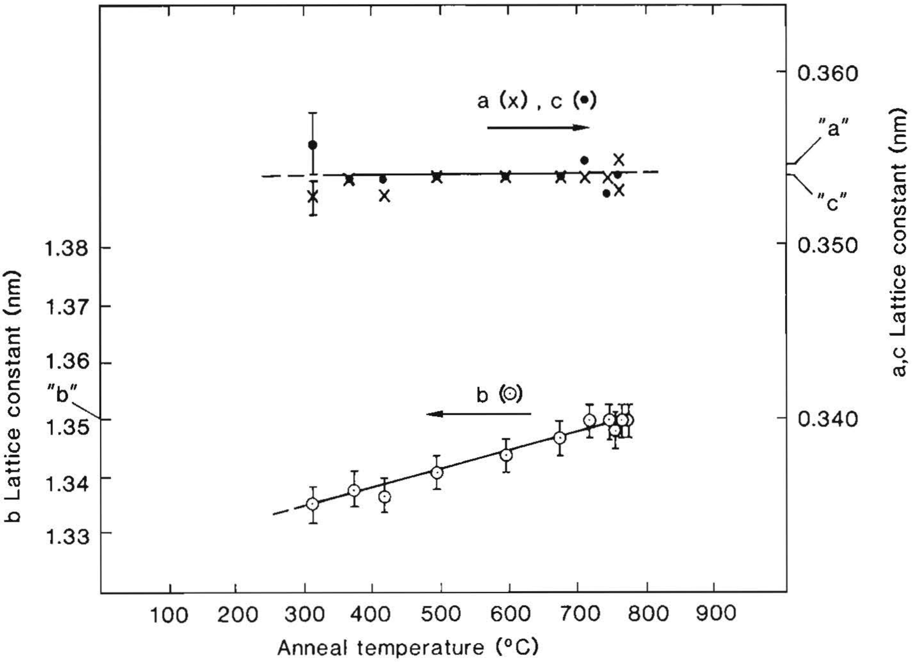

Fig. 3.4. Lattice constants for the C49 phase as a function of anneal temperature derived from the positions of the X-ray diffraction maxima. The values for the lattice constants as reported by van Houtum et al. [Hou86] are indicated along the axes with 'a', 'b' and 'c'.

of Hensel et al. [Hen86,Hen87b]. From their work we derived the slope to decrease from about 15 $* 10^{-2}$ $\mu\Omega$cm/K for the C49 phase to about 5 $* 10^{-2} \mu\Omega$cm/K for the C54 phase. From Fig. 3.2 we derive a decrease from about 9 $* 10^{-2}$ $\mu\Omega$cm/K (curve (f)) to about 6 $* 10^{-2}$ $\mu\Omega$cm/K (curve (g)).

The results of the *in-situ* resistivity measurements and X-ray diffraction are summarized in Fig. 3.5. The most essential feature of the figure is that the C49 $TiSi_2$ phase prepared from the same co-sputtered alloy may have a room temperature resistivity between 210 and 110 $\mu\Omega$cm with a concurrent increase in temperature coefficient from nearly zero to about 1 $* 10^{-3}$/K.

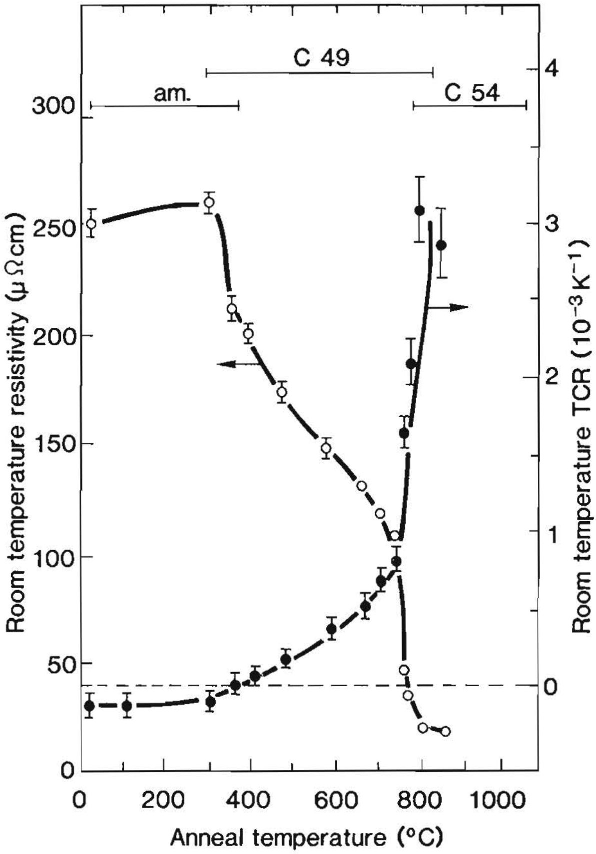

Fig. 3.5.
Room temperature resistivities and temperature coefficients of resistivity (TCR) as a function of anneal temperature. In the top of the figure the phases as identified with X-ray diffraction are indicated (am.= amorphous).

3.3.3 Microstructure

The microstructure and surface morphology of the crystallized alloy thin films was investigated with transmission electron microscopy (TEM) and scanning electron microscopy (SEM). Plan view TEM micrographs of samples (b) to (f) consisting of the C49 phase are shown in Fig. 3.6, while Fig. 3.7 shows a micrograph of sample (g) which consists of the C54 phase.

From this series of micrographs it can be concluded that all samples displayed are fully crystallized. C49 $TiSi_2$ grains approximately 1.2 μm in diameter are formed. In chapter 2 it was reported that at a particular temperature the velocity of the crystallization front is constant until the crystallites start to touch each other. For example, at a temperature of 415 ^oC (corresponding to the anneal temperature of sample (b)), the crystallization front moves with a constant velocity of approximately 30 nm/s (see Fig. 2.7). A particular $TiSi_2$ crystallite would be able to grow to the observed size of 1.2 μm in only 40 s. At temperatures exceeding 415 ^oC even shorter times are required to reach the observed grain size. We kept our samples at the anneal temperature for about 200 s, therefore it is unlikely that the present films will contain remnants of amorphous material. The grain size of samples (b) through (f) was determined from the micrographs of Fig. 3.6 to be independent of the anneal temperature and equal to 1.2 μm. X-ray diffraction too (Fig. 3.3) revealed no differences in peak width or peak height for the C49 $TiSi_2$ reflections. Thus, annealing our layers at temperatures exceeding the crystallization temperature does not result in grain growth or recrystallization. Only after the formation of C54 $TiSi_2$ at approximately 800 ^oC did the grain size increase to about 3 μm (see Fig. 3.7).

The high magnification sections of Fig. 3.6 reveal the presence of stacking faults in the C49 $TiSi_2$ grains just like the faults which were found in the crystallites in chapter 2. The average stacking fault density was determined from a number of such higher magnification micrographs. Stacking faults are only visible if the displacement vector of the faults has an appreciable component perpendicular to the incoming electron beam. With the specimen surface perpendicular to the electron beam, vertical or almost vertical stacking faults were seen in about 1/4 of the grains. Hence the stacking fault density could only be determined in these grains. Other grains presumably contain similar stacking faults [Rea87a].

Fig. 3.8 depicts the stacking fault density versus the anneal temperature. It is observed that the stacking fault density in the C49 phase material decreases from $2.8 * 10^6$/cm to $1.9 * 10^6$/cm with increasing anneal temperature. Upon phase transformation to the C54 polytype practically no stacking faults remain, regardless of the fault density in the material from

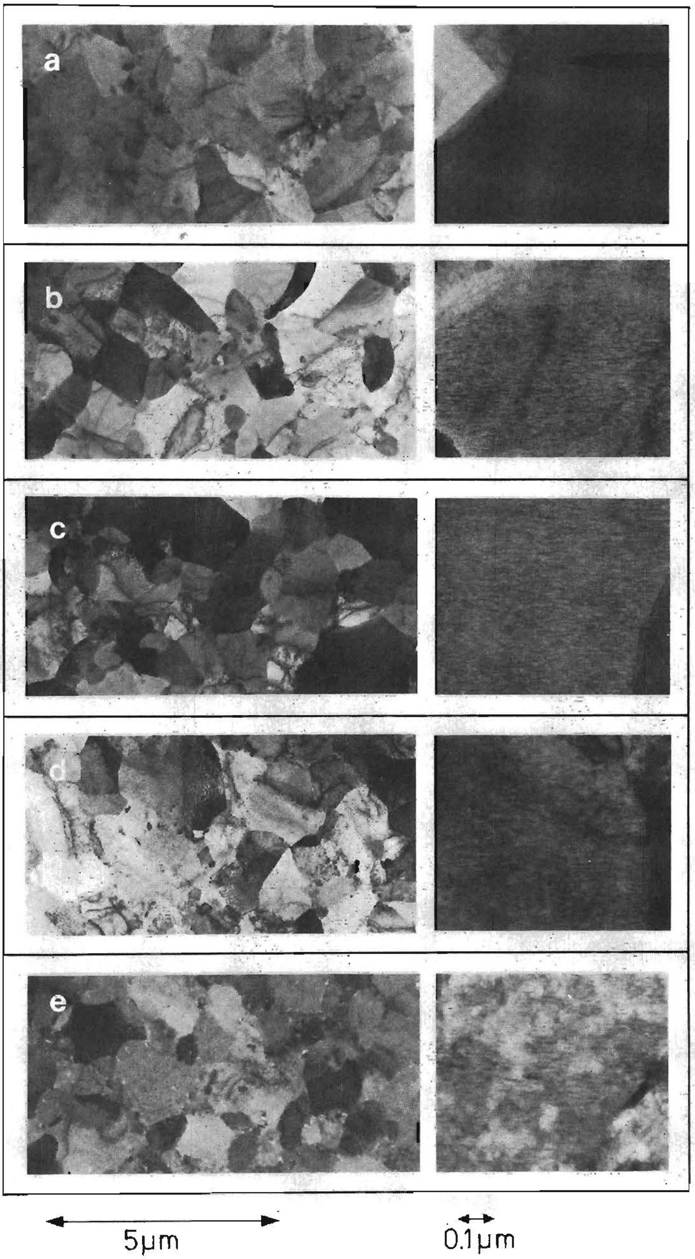

Fig. 3.6. TEM micrographs of C49 $TiSi_2$ samples annealed at different temperatures. (a) 415 °C; (b) 490 °C; (c) 595 °C; (d) 670 °C; (e) 755 °C. The micrographs shown at the right side of the figure are a strongly magnified section of the overviews at the left side of the figure. In the high magnification part of the figure stacking faults are visible.

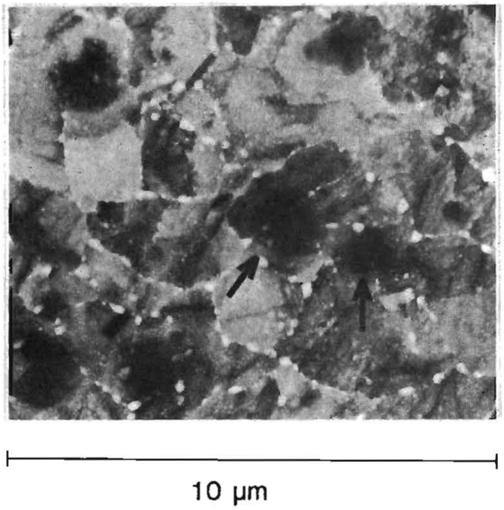

Fig. 3.6. TEM micrograph of a sample annealed at 860 °C. The sample consists of C54 $TiSi_2$. The arrows point to Si precipitates (black dots). (The holes at the grain boundaries are artefacts of TEM specimen preparation.)

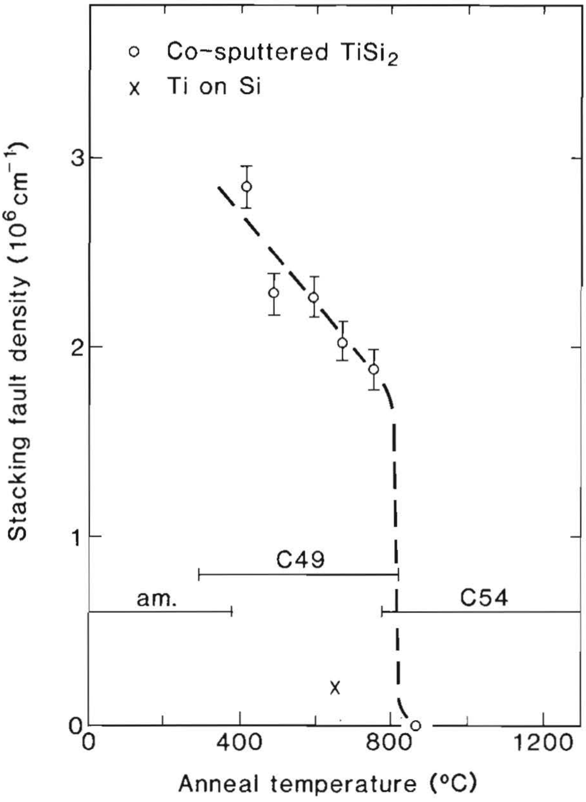

Fig. 3.8. Stacking fault densities in $TiSi_2$ layers versus annealing temperature (circles). Note the low fault densities in the C54 phase and the C49 phase prepared from a diffusion couple (cross).

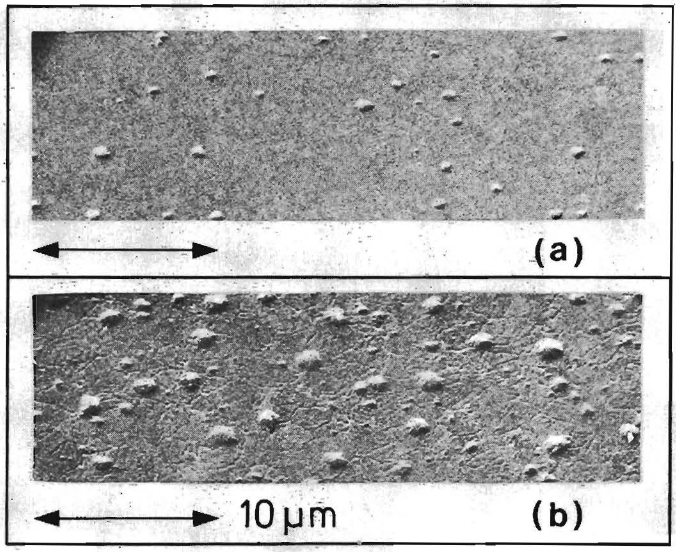

Fig. 3.9. SEM micrographs of samples annealed at (a) 755 °C (C49 $TiSi_2$) and (b) 860 °C (C54 $TiSi_2$). The features on the surface are Si precipitates. Note the drastic increase in the amount of precipitated Si when the C54 phase forms.

which it is prepared. Since the lowest value for the stacking fault density in the C49 polytype ($1.9 * 10^6$/cm) is still surprisingly high, we have tried to reduce this value by prolonged annealing at temperatures just below the transition temperature to the C54 phase. However, these attempts turned out to be unsuccessfull. It seemed as if for some (unknown) reason a certain number of faults were 'stable' in the C49 structure.

Recall now that our samples were slightly Si–rich as compared to the composition of $TiSi_2$ ($Ti/Si = 0.44 \pm 0.04$). The TEM micrographs in Fig. 3.6 show indications of an increasing amount of precipitates with increasing anneal temperature. In samples annealed for longer periods of times it was found [Rea87a] that the precipitates consisted of Si. Moreover, X-ray diffraction of the samples annealed in the higher temperature regime showed a reflection which could be ascribed to the (111) planes of crystalline Si (not shown in Fig. 3.3).

In Fig. 3.9 scanning electron microscopy (SEM) micrographs are shown of sample (f), consisting of C49 $TiSi_2$ and sample (g), consisting of C54 $TiSi_2$ respectively. After an anneal at a temperature of 755 °C Si precipitates are very clearly present at the surface of the C49 $TiSi_2$ film. Precipitate densities determined from TEM micrographs and SEM micrographs were similar, so most precipitates must indeed be situated at the surface. This observation correlates nicely with the fact that Si shows a tendency to segregate

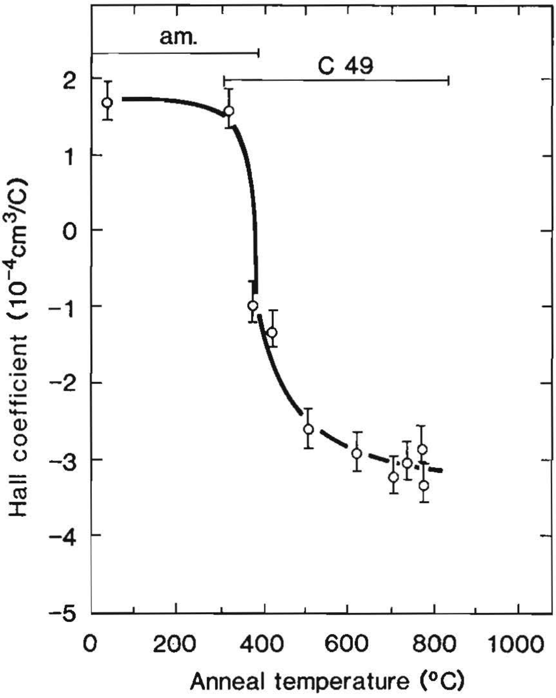

Fig. 3.10. Hall constant as a function of anneal temperature. After annealing at temperatures of 450 °C or higher, the Hall effect of C49 $TiSi_2$ shows a nearly constant magnitude.

at the $TiSi_2$ surface [Kui85]. It is also evident from the SEM micrograph of the sample annealed at 860 °C that the phase transformation to the C54 phase is associated with a large increase in the amount of precipitated Si. The same conclusion could be drawn from TEM micrographs of a C54 phase sample (shown in Fig. 3.7).

A rough estimate of the amount of Si which is present in the form of precipitates can be obtained from our SEM or TEM micrographs. Assuming the precipitates to be present as hemispheres on the surface, one estimates that for sample (f) an amount of $(1.9 \pm 0.7) * 10^{16}$ Si/cm^2 is present in the form of precipitates. When all Ti in our thin films ($(42 \pm 3) * 10^{16}$ Ti/cm^2) is reacted to stoichiometric $TiSi_2$, from the originally present $(95 \pm 3) * 10^{16}$ Si/cm^2 an amount of $(11 \pm 7) * 10^{16}$ Si/cm^2 would remain unreacted. This amount is much more than can be accounted for by the precipitates. However, after the transition to the C54 phase, for sample (g) we found an amount of $(10 \pm 3) * 10^{16}$ Si/cm^2 to be present in the form of precipitates. This value compares well with the actual Si excess determined from Rutherford backscattering, and is also in accordance with the phase diagram of the Ti - Si system [Mas87] where the C54 $TiSi_2$ phase is recorded as a line compound. The amount of Si present as precipitates in C49 $TiSi_2$ samples was always much smaller than the actual excess of Si.

In order to get an indication whether the differences in resistivity for the various C49 $TiSi_2$ films were due to differences in carrier density or their effective mean free path, Hall effect measurements were performed at room temperature. Fig. 3.10 records the Hall coefficient as a function of the anneal temperature. The as-deposited (amorphous) thin films are observed to have a positive Hall coefficient, indicating that holes are mainly responsible for charge transport. Near the crystallization temperature the Hall coefficient drops rapidly and changes sign, indicating that transport by electrons is dominant in C49 $TiSi_2$. The Hall coefficient decreases further with increasing anneal temperature until a nearly constant value of $-(3.0 \pm 0.3) * 10^{-4}$ cm^3/C is obtained for samples which were annealed at temperatures ranging from 490 ^oC to 755 ^oC. A Hall effect of constant magnitude is *likely* to be related to a constant carrier density. We acknowledge that it is *in principle* possible to have changes in carrier densities which are exactly compensated by for example changes in mobility [Bad87] or the shape of the Fermi surface. The latter situations however would represent rare coincidences. A constant carrier density suggests that the observed resistivity decrease after the crystallization to the C49 phase is caused by changes in the carrier mobility or their effective mean free path.

To estimate the mean free path in C49 $TiSi_2$ from the Hall coefficient we will assume that a single band contributes to conduction. Using the rough approximation of the classical free electron theory we find from the Hall effect and the resistivity effective mean free paths ranging from 1.8 nm for sample (c) to 3.6 nm for sample (f). The latter value is close to the value of 4.0 nm calculated by Hensel et al. [Hen87b] for C49 $TiSi_2$. If the rather simplifying approximations underlying the above calculation are valid, these values of the mean free path should give us an indication of the spacing of the defects which are thought to be responsible for the observed resistivity effects. The effective mean free path is much smaller than the observed grain size (about 1.2 μm) or the film thickness (about 180 nm). This implies that grain boundary scattering or surface scattering (with scattering probablities of order unity) can be excluded as contributions to the resistivity.

Summarizing, it was found that there are two possible microstructural defects which may contribute to the resistivity of the C49 $TiSi_2$ phase. Firstly, as was pointed out by Reader et al. [Rea87b] and d'Heurle et al. [Heu82,Heu86], the large density of stacking faults gives rise to an increased resistivity. Secondly, there is excess Si in the form of a (super-)saturated solid solution in the C49 phase. During annealing the excess Si in the C49 phase is partially removed by a precipitation reaction. The dissolved Si will affect the materials resistivity as impurities do in pure metals. On the other hand it was found that the transformation to the C54 phase eliminates the larger part, if not all of the excess Si in solid solution and practically all stacking faults.

3.4 Discussions

3.4.1 Stoichiometry

The resistivity effects which were described in the previous section cannot be understood adequately without a more detailed knowledge of the crystallization process and the role of the excess Si in the thin films. Therefore we will start our discussion with a description of relevant phenomena which occurr during and directly after the crystallization process. The crystallization of an initially amorphous Ti - Si alloy thin film with a composition which is reasonably close to that of the disilicide occurs through a polymorphous reaction (see chapter 2). The microstructure of the crystalline alloys, as evident from the transmission electron microscopy micrographs from Fig. 3.6, indeed showed that a polymorphous reaction had occurred.

Polymorphous crystallization of a thin film which is richer in Si than dictated by the solid solubility limit of Si in C49 $TiSi_2$ will initially result in a non-equilibrium super-saturated solid solution of Si in C49 $TiSi_2$. The excess Si may for example be accounted for by Ti vacancies or antisite defects (a Si atom substituted on the Ti sublattice).

When a super-saturated solid solution of Si in C49 $TiSi_2$ is annealed for a sufficiently long time at sufficiently high temperature, equilibrium will be established between Si and a saturated solid solution of Si in $TiSi_2$. It will mainly depend on anneal temperature whether the C49 polytype of $TiSi_2$ remains or whether the C54 polytype of $TiSi_2$ will be formed. In the first case the equilibrium between Si and the saturated solid solution of Si in C49 $TiSi_2$ may be of a metastable nature since the C49 phase itself is thought [Bey85] to be metastable. The Si in excess of the solubility limit in either two polytypes of $TiSi_2$ will now precipitate as a second phase. Transmission and scanning electron microscopy micrographs (Figs. 3.6 and 3.9) indeed revealed the presence of Si precipitates, most of which were found to be situated at the surface of the $TiSi_2$ thin film after annealing in the higher temperature regime. Moreover, the removal of excess dissolved Si from the C49 matrix by precipitation was observed to result in an increase in the lattice constants of the C49 phase.

A first estimate for the variations in lattice constant with composition may sometimes be obtained from Vegard's law [Tay61]. Vegard's law relates values for the lattice constants or atomic volume to the lattice constants or atomic volume of the terminal solid solutions through a simple linear interpolation. The average atomic volume of C49 $TiSi_2$ is $14 * 10^{-24}$ cm^3

(1/3 of the molar volume). For the value of the Si atomic volume in $TiSi_2$ one must use that in its 'metallic' form rather than the much larger value in its covalent binding state. In all refractory metal silicides the Si atomic volume is about $12 * 10^{-24}$ cm^3. Assuming a linear dependence of atomic volume on composition one calculates a decrease of about 0.14 % in atomic volume for every at. % of Si in solid solution. The actual excess of Si in our samples is (8 ± 5) at. %, derived from Rutherford backscattering spectrometry. If this Si is present as a (super-saturated) solid solution one would expect the value of the atomic volume of the C49 phase to be smaller than the value of stoichiometric $TiSi_2$ by (1.1 ± 0.7) %. The latter value is close to the observed deviation of the atomic volume of the C49 phase: from Fig 3.4 we derived a deviation of b (or atomic volume) just after crystallization by (1.0 ± 0.2) %.

The actual Si concentration in the equilibrated $TiSi_2$ layer (which is now a saturated solid solution) will generally not be equal to that of the stoichiometric $TiSi_2$ phase but is dictated by the solubility limit of Si in the $TiSi_2$. The phase diagram of the Ti - Si system [Mas87] records C54 $TiSi_2$ as a true line compound (i.e. a compound with a very narrow phase field). The narrow phase field of the C54 phase explains the observation that after recrystallization of the C49 phase to the C54 phase the excess Si had all precipitated (Fig. 3.9). No data on the width of the phase field for the C49 $TiSi_2$ phase can be found in literature. When the film consisted of the C49 phase the amount of Si present as precipitates was always much less than the actual excess of Si. So we conclude that the solubility of Si in the C49 phase may be significant, possibly upto a few percent.

One should now also realize that, when the C49 $TiSi_2$ phase is prepared from Ti - Si diffusion couples, once all Ti is consumed and *equilibrium* is established it would form a saturated solid solution of Si in $TiSi_2$ too. With respect to the actual concentration of Si in the C49 phase we do not expect a large difference between material prepared from Si–rich co-sputtered alloys in which the precipitation reaction is complete or Ti - Si diffusion couples in which all Ti has been consumed.

Badoz et al. [Bad87] recently reported that when W is reacted with (100) Si in a UHV environment a systematic excess of Si is found to be present in the WSi_2 layer. Moreover, the Hall coefficient for these WSi_2 films was found to have a negative value at room temperature. WSi_2 prepared from Si–rich co-sputtered material showed a negative Hall coefficient as well, while WSi_2 prepared from W-rich co-sputtered material showed a Hall coefficient of the opposite sign. To explain these observations they doubted whether the WSi_2 phase they formed during UHV annealing of W thin films on Si was stoichiometric and proposed that the excess Si was present at the grain boundaries. Considering the above discussion for $TiSi_2$, the systematic Si excess may also be related to a finite solid solubility of Si in the WSi_2 crystal itself.

In the above discussion on the crystallization mechanisms of an amorphous alloy we have elucidated the role of the excess Si. It was argued that the solubility of Si in the C49 $TiSi_2$ phase may be substantial, while it is negligible in the C54 $TiSi_2$ phase. The precipitation of the excess Si out of the crystalline material may contribute to the resistivity decrease after crystallization. In the next section we will discuss the different contributions to the resistivity of the silicide.

3.4.2 Resistivity

Figures 3.2 and 3.5 show the resistivity behaviour of the Ti - Si alloy thin films during annealing as a function of temperature. Annealing of the amorphous alloy resulted in an irreversible drop in resistivity at a temperature of 390 ^oC. X-ray diffraction and transmission electron microscopy showed that at this point the film fully crystallizes into the C49 $TiSi_2$ structure with a grain size of 1.2 μm, and that this grain size remains invariable upon further annealing. By annealing at higher temperatures and/or longer anneal times, the resistivity of the C49 phase could be reduced while simultaneously the temperature coefficient of the resistivity increased. The decrease in resistivity was accompagnied by a decreasing stacking fault density and a decreasing amount of dissolved Si, forming Si precipitates.

In this section it is first discussed how the resistivity behaviour as shown in Figs. 3.2 and 3.5 can be interpreted. Secondly we will discuss the effects of stacking faults and Si in solid solution on the resistivity of the C49 phase. Note that contributions to the resistivity due to grain boundary and surface scattering can be excluded because the typical scattering lengths associated with grain boundaries (1.2 μm) and film surfaces (180 nm) exceed the effective mean free path (3.6 nm) by orders of magnitude.

The differences in slope of the cooling curves for the resistivity in Fig. 3.2 indicate a phonon contribution or temperature dependent part which is dependent on the anneal treatment, and consequently we do not expect Mathiessen's rule to hold for the high resistivity samples. Instead, Fig. 3.2 clearly shows that after crystallization the resistivity behaviour changes very gradually from 'Mooij like behaviour' [Moo73] to 'Mathiessen like behaviour'. Mooij proposed that the carrier effective mean free path can not be smaller than the interatomic spacing. The effect of such a minimum in the mean free path is a saturation of the resistivity and can be described phenomenologically in terms of the parallel resistivity model [Gur81,All81]. In that description the resistivity is thought to be composed of two resistivities in parallel: the ideal resistivity (ρ_{id}) which should show 'Mathiessen

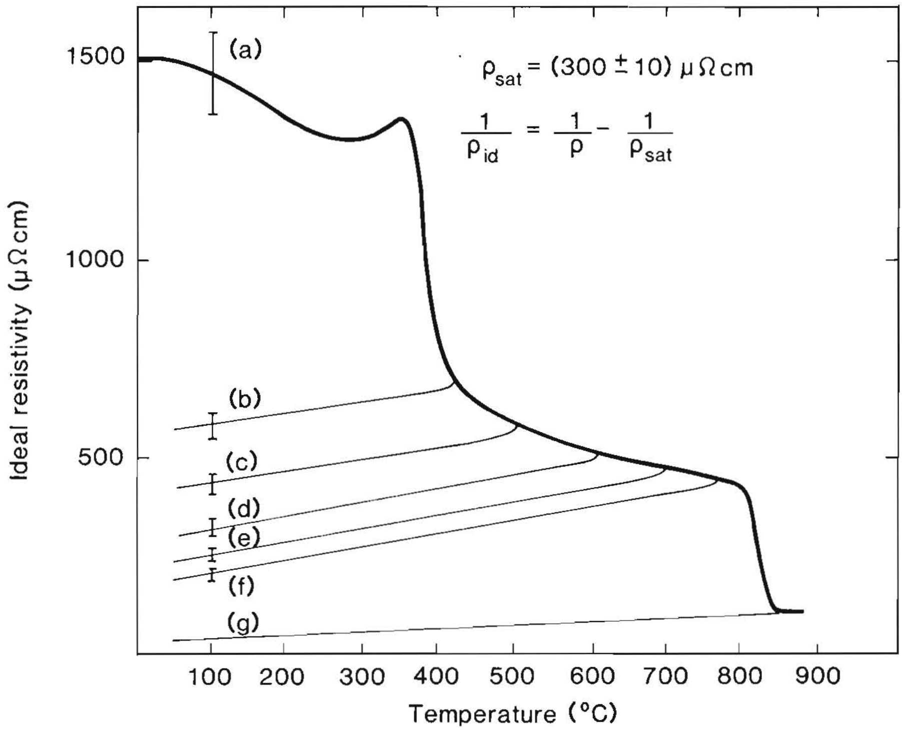

Fig. 3.11. Ideal resistivity versus temperature curves derived from Fig. 3.2 and the parallel resistivity model.

like behaviour' and a constant saturation resistivity (ρ_{sat}) which accounts for deviations of Mathiessen's rule.

The value of the saturation resistivity is correlated to material parameters by Mott [Mot74]. For a spherical Fermi surface and one conduction electron per atom he finds for the saturation resistivity $\rho_{sat} = \hbar a/0.33e^2$. Substituting for 'a' the Ti - Si interatomic spacing in the C49 phase (about 0.27 nm) yields $\rho_{sat} = 340\ \mu\Omega cm$. If the curves in Fig. 3.2 are corrected for the contribution of such a parallel resistivity one may obtain the ideal resistivity curves presented in Fig. 3.11 with $\rho_{sat} = (300 \pm 10)\ \mu\Omega$cm. With the latter value of the saturation resistivity it was possible to equalize the slopes of the cooling curves for samples (b) through (f) in Fig. 3.11.

The resistivity behaviour of our $TiSi_2$ samples is thus interpreted in terms of the parallel resistivity model. The ideal resistivity is found to behave according to Mathiessen's law, and can be described by a temperature independent defect contribution and the temperature dependent phonon contribution. After correction for the saturation effect the phonon contribution in the ideal resistivity is the same for all samples, represented by a slope of (0.31 ± 0.02) $\mu\Omega$cm/K. If the data obtained for C49 $TiSi_2$ prepared from diffusion couples reported in the work of Hensel et al. [Hen86,Hen87b] are also corrected for the saturation effect with the same value of ρ_{sat} one arrives at a slope of 0.27 $\mu\Omega$cm/K. Hence, after taking account of the saturation effect in the resistivity by the parallel resistor model the slope of the temperature resisitivity curves is nearly the same for material prepared from diffusion couples and co-sputtered material. Note that a saturation effect with a similar value of the saturation resistivity has also been used to explain the resistivity behaviour in some other silicides with fairly high room temperature resistivities, for example VSi_2 [Nav86a], $TaSi_2$ [Nav87] and $NbSi_2$ [Nav86c].

We will now turn our attention to the differences in resistivity of various C49 $TiSi_2$ samples. Considering the above discussion these differences in resistivity are expected to reflect differences in defect concentrations. Rather than discussing our results in terms of the ideal resistivities and the parallel resistivity model we will discuss our results in terms of measured resistivities, as this is more commonly done in the literature on the resistivity of silicides. Presenting our discussion in terms of measured resistivities, uncorrected for the saturation effect, greatly facilitates a direct comparison with similar resitivity effects in other silicides.

Fig. 3.12 records stacking fault densities and room temperature resistivities for our samples (b) to (f) and a similar co-sputtered sample which was annealed during an extended period of time above the crystallization temperature but below the transition temperature to the C54 phase. The figure also includes the data of Reader et al. [Rea87b].

Let us first consider the resistivity of the sample which is thought to be the least defective and hence has the lowest resistivity, i.e. C49 $TiSi_2$ prepared from a Ti - Si diffusion couple. Room temperature resistivities in the range of 50 - 70 $\mu\Omega$cm are reported for the material prepared from Ti - Si diffusion couples [Rea87b,Hen86,Hen87b]. Hensel et al. [Hen86,Hen87b] determined the temperature dependent part of the resistivity for such layers to be about 33 $\mu\Omega$cm. If one assumes the same temperature dependent part to be present in the resistivity of other C49 $TiSi_2$ samples too, the mentioned range of room temperature resistivities corresponds to a defect contribution in the range of 20 - 40 $\mu\Omega$cm.

Material grown from diffusion couples has a stacking fault density which is an order of magnitude smaller than that for material prepared from co-sputtered samples (see Fig. 3.8 and Reader et al. [Rea87b]) and it is not expected that the stacking faults can explain the high residual resistivity (see further for an estimate of the resistivity contribution per stacking fault). It was argued in the previous section that the material grown from

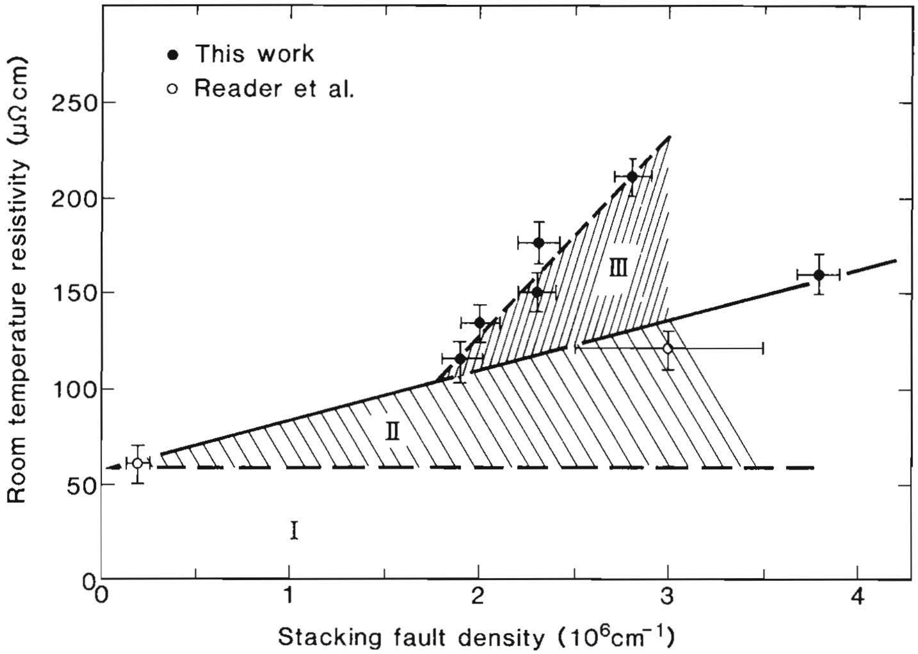

Fig. 3.12. Room temperature resistivity versus stacking fault density for various C49 $TiSi_2$ samples. The solid points near the dotted line correspond to the samples (b) to (f). The open points are taken from the work of Reader et al. [Rea87b]. The solid point in the far right of the figure is obtained from a sample which was annealed during 60 h at 440 °C. Three different contributions to the resistivity are considered, indicated by the shading and the Roman numbers. (I): saturated solid solution of Si in C49 $TiSi_2$ and phonons; (II): stacking faults; (III): super-saturated solid solution of Si in C49 $TiSi_2$.

diffusion couples will contain an excess of Si as compared to the composition of $TiSi_2$ because of a possibly substantial solid solubility of Si in the C49 phase. The Si in solid solution may be accomodated by point defects which act as scattering centers for the charge carriers, thus increasing the materials residual resitivity.

The effect of point defects on the resistivity of silicides is well documented in the case of the isostructural silicides $NiSi_2$ and $CoSi_2$ [Hen84] [Sor82]. Although the temperature dependent part of the resistivity is the same for both materials, $NiSi_2$ shows a much higher residual resistivity than $CoSi_2$. Hensel et al. [Hen84] concluded that the high resistivity of $NiSi_2$ is due to a high density of point defects, probably antisite defects or small deviations from the exact 1 : 2 stoichiometry. The effect of point defects on the residual resistivity of $NiSi_2$ (about 20 $\mu\Omega$cm) is of similar magnitude as the defect contribution to the resistivity of the C49 $TiSi_2$ phase prepared from diffusion couples (20 - 40 $\mu\Omega$cm). In analogy with the $NiSi_2$ case we tend to attribute the high residual resistivity of the C49 phase prepared from diffusion couples to a high density of point defects, which may be related to a deviation of stoichiometry.

It would be interesting to compare the point defect contribution to the resistivity for silicides to that for other conductors. For that purpose we need to know the actual amount of Si in the solid solution and something about the character of the point defects in order to evaluate their concentration. A rough estimate for the solubility limit of Si in C49 $TiSi_2$ can be obtained with the results for our co-sputtered samples. For that purpose we will assume that the precipitation reaction is completed for the C49 samples annealed in the higher temperature regime. In that situation the silicide is a saturated solid solution of Si. The amount of dissolved Si in sample (f) is just equal to the difference between the actual excess of Si as derived from Rutherford backscattering spectrometry $(11 \pm 7) * 10^{16}$ Si/cm^2 (or 8 ± 5 %) and the amount which had precipitated $(1.9 \pm 0.7) * 10^{16}$ Si/cm^2 (1.4 ± 0.5 %). Subtracting these Si quantities yields for the amount of Si in solid solution a value of $(9 \pm 7) * 10^{16}$ Si/cm^2 (7 ± 5 %).

Considering the tendency of the disilicides to form a continuous Si network [Now54a,Gol67], it is reasonable to assume that the dissolved Si is accomodated by vacancies in the Ti sublattice. In that case two substitutional Si atoms yield one Ti vacancy.The amount of Ti atoms as was found with Rutherford backscattering is $(42 \pm 3) * 10^{16}$ Ti/cm^2. The above figures combine to a vacancy concentration on the Ti sublattice of (10 ± 7) % in the saturated solid solution. If these vacancies are responsible for the residual resistivity of C49 $TiSi_2$ (20 - 40 $\mu\Omega$cm), one derives a contribution of (3 ± 2) $\mu\Omega$cm for each percent of vacancies. For comparison, copper shows a resistivity increase of 1.5 $\mu\Omega$cm for each percent of vacancies and 10 $\mu\Omega$cm for each percent of interstitials [Bla57]. For impurity scattering, values ranging from 0.6 to 10 $\mu\Omega$cm for each percent of impurity are reported, depending on the valence of matrix and impurity [Zim62].

We will now turn our attention to the resistivity effects in the material prepared from co-sputtered thin films (see again Fig. 3.12). If a crystallized co-sputtered C49 $TiSi_2$ thin film is annealed at a sufficiently high temperature during a sufficiently long period of time (metastable) equilibrium between Si and a saturated solid solution of Si in C49 $TiSi_2$ will be established. For C49 $TiSi_2$ samples in which the precipitation reaction is essentially complete, the resistivity is composed of the resistivity of the saturated solid solution and the contribution due to stacking faults. The solid line (Fig. 3.12) is thought to depict the relation between resistivity and stacking fault density. Only the lowest resistivities obtained for a certain material contribute to the straight solid line, because only in the samples with the lowest resistivities can the precipitation reaction be considered as complete. For the resistivity per stacking fault one derives from the slope of the straight solid line a value of $(2.5 \pm 0.5) * 10^{-11}$ Ωcm^2. For $MoSi_2$ it has recently been found [Omm88] that the resistivity contribution per stacking fault is about $2.7 * 10^{-11} \Omega cm^2$. In recent papers Krontiras et al. [Kro87] and Badoz et al. [Bad87] found a temperature independent resistivity contribution of about 100 $\mu\Omega$cm in WSi_2 due to a stacking fault density of about $5 * 10^6$/cm. The value for the resistivity contribution per stacking fault which was derived for C49 $TiSi_2$ from Fig. 3.12 is thus of the same magnitude as the values for $MoSi_2$ and WSi_2. However, the resistivity contribution per stacking fault in silicides is quite large compared to that in pure metals. For example, Howie [How60] derived a value of 10^{-12} Ωcm^2 for copper.

When we apply the same procedure to determine the resistivity contribution per stacking fault for our samples (b) to (f) (see Fig. 3.2 and the dashed line in Fig. 3.12) we arrive at a value of about $10 * 10^{-11}$ Ωcm^2, i.e. a value which is about three to four times larger than the values found most commonly in silicides. It is therefore expected that the slow decrease in resistivity after crystallization is not only due to the decreasing stacking fault density. A second process which occurred after crystallization was the diffusion of excess Si out of the super-saturated solution, forming precipitates. This leads to a decreasing density of point defects in the C49 $TiSi_2$ layer which would account for the decrease in resistivity. As we did before we will assume that the Si in the super-saturated solid solution is accomodated by forming Ti vacancies. The dissolved Si just after crystallization (for example in sample (b)) amounts $(11 \pm 7) * 10^{16}$ Si/cm^2 as was found from Rutherford backscattering. This would lead to a Ti vacancy concentration of (13 ± 10) %. The resistivity effect supposedly due to these vacancies is (from Fig. 3.12) (100 ± 20) $\mu\Omega$cm, which is the total resistivity of sample (b) minus the stacking fault and phonon contribution. The resistivity contribution due to vacancies can thus be evaluated as (7 ± 4) $\mu\Omega$cm for each percent of vacancies and is not significantly different from the earlier derived value of (3 ± 2) $\mu\Omega$cm.

Note that the inaccuracies in the above numbers are rather large. This is mainly caused by the sample to sample variation in Si content and the limited accuracy of the actual excess of Si as determined from Rutherford backscattering spectrometry. From Fig. 3.12 it can be concluded that the resistivity effect of the decreasing concentration of Si in solid solution is probably of similar magnitude as the effect due to the annealing of stacking faults. When the precipitation reaction is complete, the remaining resistivity is the sum of the resistivity of a saturated solid solution of Si in C49 $TiSi_2$ and the contribution due to stacking faults.

3.4.3 Hall Effect

The Hall coefficient in the co-sputtered samples was found to change sign upon crystallization (Fig. 3.10). If samples were annealed at temperatures ranging from 490 °C to 755 °C the Hall coefficient was found to have a nearly constant value of $-(3.0 \pm 0.3) * 10^{-4}$ cm^3/C. Reader et al. [Rea87b] reported for the Hall coefficient in C49 $TiSi_2$ prepared from a diffusion couple a value of $-2.8 * 10^{-4}$ cm^3/C, which agrees with the Hall coefficient in the present co-sputtered samples.

Note that in a one-band conduction model a simple relation between the Hall coefficient, the resistivity and the Hall mobility exists. In that situation only two parameters are used to describe the electrical conduction mechanism. In a multi-band structure such a simple relation does not exist because different carriers may have different mobilities. The non-constant Hall coefficient in the low temperature regime of Fig. 3.10 (i.e. just after crystallization) suggests that a single band conduction model is not applicable in the C49 phase. Many researchers [Bad87,Omm88,Nav87,Woe84] [Vri88] report a change of sign of the Hall coefficient with temperature which indicates that a single band model is unacceptable in silicides. Instead, many silicides are found to behave as compensated metal conductors [Bad87]. Hence it appears impossible to characterize electrical conduction in silicides from Hall effect and resistivity measurements alone.

3.5 Conclusions

We have investigated the crystallization of amorphous Ti - Si alloy thin films with a composition slightly Si–rich as compared to the disilicide. As appears to be the case with many silicides, a precipitous drop in resistivity, which is associated with a polymorphous crystallization reaction is followed by a much more gradual decrease in resistivity with higher annealing temperatures. The nature of this gradual decrease in resistivity has been investigated in detail with transmission electron microscopy, secondary electron microscopy, X-ray diffraction and Hall effect measurements.

We have found that crystalline C49 $TiSi_2$ samples annealed at different temperatures can show resistivities ranging from 210 $\mu\Omega$cm just after crystallization to 100 $\mu\Omega$cm just before the transformation to the C54 $TiSi_2$ phase. The slow resistivity decrease is directly related to a decrease in stacking fault density from $2.8 * 10^6$/cm to $1.9 * 10^6$/cm and an increase in Si precipitation.

Resistivity measurements performed *in-situ* as a function of temperature in the regime above room temperature were conveniently described with the parallel resistivity model. In this model a physical minimum for the carrier mean free path in heavily disordered systems is associated with a saturation value in the resistivity. For the C49 phase the value of the saturation resistivity was about 300 $\mu\Omega$cm.

The amount of Si present in the form of precipitates in the C49 $TiSi_2$ phase was always much smaller than the actual excess of Si as measured with RBS. After recrystallization to the C54 polytype all Si had precipitated on the surface of the sample. We therefore concluded that the solid solubility of Si in the C49 phase may be substantial. The dissolved Si is most probably accomodated by the creation of Ti vacancies or Si atoms substituted on the Ti sublattice. Precipitation of Si caused the point defect concentration in the crystalline material to decrease.

The slow resistivity decrease after crystallization was found to be related to both the decreasing stacking fault density and the decreasing density of point defects in the crystalline material. The residual resistivity of the C49 $TiSi_2$ phase remains high even if the stacking fault contribution is negligible. The high residual resistivity was attributed to the presence of point defects. The resistivity per stacking fault was found to be similar to that in other silicides ($2.5 * 10^{-11}$ Ωcm^2). The point defect contribution was found to be a few $\mu\Omega$cm for each percent of point defects.

The Hall effect is practically constant in the regime of the slow resistivity decrease. Besides that, after correction of the resistivities for the above mentioned saturation effect, the slope of the temperature - resistivity curves was found to be independent of the defect concentration in the silicide. The effect of stacking faults and point defects then is probably only to decrease the mobility or the mean free path of the carriers. Hall coefficients and resistivity alone appeared to be insufficient to describe electrical conduction in silicides.

At higher temperatures (about 800 ^oC) the C49 $TiSi_2$ phase recrystallizes into the C54 $TiSi_2$ phase. The resistivity of the latter phase was always low (about 18 $\mu\Omega$cm) regardless of the crystalline quality of the C49 $TiSi_2$ material from which it was prepared. The reproducably low resistivity of the C54 polytype is probably correlated to the elimination of all stacking faults and the precipitation of the larger part, if not all, of the excess Si during the phase transformation This contrasts the behaviour of the resistivities in $MoSi_2$ and WSi_2 where stacking faults are introduced during the hexagonal - tetragonal phase transformation and can only be annealed out at much higher temperatures [Omm88].

Bibliography

[All81] H. Wiesmann, M.Gurvitch, H. Lutz, A. Ghosh, B. Schwartz, M. Strongin, P.B. Allen and J.W. Halley, Phys. Rev. Lett. **38**, 4815 (1981).

[Bla57] F.J. Blatt et al. Phys. Rev. **108**, 285 (1957).

[Bad87] P.A. Badoz, E. Rosencher, J. Torres and G. Fishman, J. Appl. Phys. **62** 890 (1987).

[Bey85] R. Beyers and R. Sinclair, J. Appl. Phys. **57**, 5240 (1985).

[Cho83] T.P. Chow and A.J. Steckl, IEEE Trans. Electron Devices **ED30**, 1480 (1983).

[Cot56] P.G. Cotter, J.A. Kohn and R.A. Potter, J. Am. Cer. Soc. **39** 11 (1956).

[Cro79] B.L. Crowder and S. Zirinsky, IEEE Trans. Electron Devices **ED26**, 369 (1979).

[Gol67] H.J. Goldschmidt in 'Interstitial Alloys' (Butterworths, London 1967).

[Gur81] M. Gurvitch, Phys. Rev. **B24**, 7404 (1981).

[Hen84] J.C. Hensel, R.T. Tung, J.M. Poate and F.C. Unterwald, Appl. Phys. Lett. **44**, 913 (1984).

[Hen86] J.C. Hensel, J.M. Vandenberg, L.F. Mattheis, F.C. Unterwald and A. Maury, Mat. Res. Soc. Symp. Proc. **77**, 737 (1986) (Materials Research Society, Pittsburgh).

[Hen87b] J.C. Hensel, J.M. Vandenberg, F.C. Unterwald and A. Mauri, Appl. Phys. Lett. **51**, 1100 (1987).

[Heu82] F.M. d'Heurle in 'VLSI Science and Technology', ed. by C. Dell'Oca and W.M. Bullis, p. 194 (Electrochemical Soc., Pennington 1982).

[Heu86] F.M. d'Heurle, F.K. LeGoues, R. Joshi and I. Suni, Appl. Phys. Lett. **48**, 332 (1986).

[Hou86] H.J.W. van Houtum and I.J.M.M. Raaijmakers, Mater. Res. Soc. Symp. Proc. **54**, 37 (1986).

[Hou87] H.J.W. van Houtum, I.J.M.M. Raaijmakers and T.J.M. Menting J. Appl. Phys. **61**, 3116 (1987).

[How60] A. Howie, Phil. Mag. **5**, 251 (1960).

[Kem82] M.J.H. Kemper and P.H. Oosting, J. Appl. Phys. **53**, 6214 (1982).

[Kro87] C. Krontiras, I. Suni, F.M. d'Heurle, F.K. LeGoues and R. Joshi, J. Phys. F: Met. Phys. **17**, 1953 (1987).

[Kui85] A.E.T. Kuiper, G.J.C. van der Ligt, W.M. van de Wijgert, M.F.C. Willemsen and F.H.P.M. Habraken, J. Vac. Sci. Technol. **B3**, 830 (1985).

[Lav39] F. Laves and H.J. Wallbaum, Z. Kristallogr. **101**, 78 (1939).

[Mas87] Th.B. Massalsky, J.L. Murray, L.H. Benett and H. Baker, eds., 'Binary Alloy Phase Diagrams' **2** (Am. Soc. Metals., Metals Park, Ohio 1986).

[Mur83] S.P. Murarka, 'Silicides for VLSI Applications' (Ac. Press, New York, 1983).

[Moc78] T. Mochizuki, K. Shibata, T. Inoue, K. Ohuchi, Japan J. Appl. Phys. **17** Suppl. 1, 37, 1978.

[Moo73] J.H. Mooij, Phys. Stat. Sol. (a) **17**, 521 (1973).

[Mot74] N.F. Mott in 'Metal Insulator Transitions' (Taylor and Francis, London 1974).

[Nav85a] F. Nava, T. Tien and K.N. Tu, J. Appl. Phys. **57**, 2018 (1985).

[Nav85b] F. Nava, G. Ottaviani and G. Riontino, Materials Lett. **3**, 311 (1985).

[Nav86b] F. Nava, B.Z. Weiss, K.N. Tu, D.A. Smith and P.A. Psaras, J. Appl. Phys. **60**, 2445 (1986).

[Nav86a] F. Nava, P.A. Psaras, H. Takai, K.N. Tu, S. Valeri and O. Bisi, J. Mater. Res. **1**, 327 (1986).

[Nav86c] F. Nava, O. Bisi and K.N. Tu, Phys. Rev. **B34**, 6143 (1986).

[Nav87] F. Nava, K.N. Tu, E. Mazzega, W. Michelini and G. Queirolo, J. Appl. Phys. **61**, 1085 (1987).

[Nic83] M.A. Nicolet and S.S. Lau, in VLSI Electronics **6**, edited by N.G. Einspruch (Academic, New York, 1983).

[Now54a] H. Nowotny and E. Parthé, Planseeber. Pulvermet. **2**, 34 (1954).

[Omm88] A.H. van Ommen, A.H. Reader and J.W.C. de Vries, 96 - 7818 JAP, accepted for publication in J. Appl. Phys.

[Raa87c] I.J.M.M. Raaijmakers, A.H. Reader and H.J.W. van Houtum, J. Appl. Phys. **61**, 2527 (1987).

[Raa87d] I.J.M.M. Raaijmakers, A.H. Reader and H.J.W. van Houtum, Proc. European Workshop on Refr. Metals and Silicides, published in : le Vide, les Couches Minces **42**, 75 (1987).

[Rea87a] A.H. Reader, I.J.M.M. Raaijmakers and H.J.W. van Houtum, proc. Microsc. Semicond. Mater. conf., Oxford (1987);

[Rea87b] A.H. Reader, A.H. van Ommen and H.J.W. van Houtum, Mater. Res. Soc. Symp. Proc. **92**, 177 (1987) (Materials Research Society, Pittsburgh).

[Sor82]	Y. Sorimachi, H. Ishiwara, H. Yamamoto and S. Furukuwa, Jap. J. Appl. Phys. **21**, 752 (1982).
[Tay61]	A. Taylor in 'X-ray Metallography' (Wiley, New York 1961).
[Tie83]	T. Tien, G. Ottaviani and K.N. Tu, J. Appl. Phys. **54**, 7047 (1983).
[Tho87]	R.D. Thompson, H. Takai, P.A. Psaras and K.N. Tu, J. Appl. Phys. **61**, 540 (1987).
[Vri88]	J.W.C. de Vries and A.H. van Ommen, J. Appl. Phys. **64**, 749 (1988).
[Wei86]	B.Z. Weiss, K.N. Tu and D.A. Smith, Acta Metall. **34**, 1491 (1986).
[Woe84]	P.H. Woerlee, P.M.Th.M. van Attekum, A.A.M. Hoeben, G.A.M. Hurkx and R.A.M. Wolters, Appl. Phys. Lett. **44**, 876 (1984).
[Zim62]	J.M. Ziman in 'Electrons and Phonons' ed. by N.F. Mott, E.C. Bullard and D.H. Wilkinson (Clarendon Press, Oxford 1962).

Chapter 4

Crystallization Kinetics in Ti - Si Alloys

4.1 Introduction

Microstructural changes in silicides upon thermal treatment are studied quite extensively during the last decade [Heu82,Mur83,Cho83] because of the possible application of silicides in state-of-the-art and future integrated circuits. The electrical characteristics of silicides range all the way from those of metallic conductors to those of semiconductors [Mur83,Nic83] and one of the technologically most important properties of a silicide is probably its resistivity. Changes in the microstructure of a particular silicide are strongly reflected in changes in the resistivity of that silicide. Besides that, resistivity is a property which is easily measured in a variety of ambients (vacuum, high temperatures etc.). The facts that resistivity is so conveniently measured and that it is very sensitive to the microstructure suggest that the evolution of the resistivity with thermal treatment may be used as a tool to characterize the phase transformations and the development of the microstructure in a silicide.

A great deal of papers report studies on the crystallization reactions in co-deposited silicides with the aid of *in-situ* resistivity measurements [Wei86,Tho87,Nav85,Nav85a,Nav85b,Nav86a,Nav86b,Tie83]. Resistivity values measured during crystallization are used to derive the crystallized or transformed fraction as a function of time by a simple linear interpolation between the initial and final values of the resistivities. The so determined transformed fraction is fitted to the (Johnson–Mehl–)Avrami equation [Joh86,Avr39,Avr40,Avr41]. The obtained results (usually the Avrami exponent n and a sort of effective activation energy) are then related to a particular crystallization mechanisms. The measurement of such a macroscopic property as the resistivity (or similarly an optical constant or the heat released) during the crystallization process is rather simple. Unfortunately, the physical meaning of the obtained parameters for the microscopy of the process is not clear because the effects of the nucleation and growth of many different crystallites are combined in the temporal evolution of only one parameter. More detailed knowledge on the microscopicy of such crystallization reactions may be obtained with, for example, ***in-situ*** annealing in a transmission electron microscope (TEM) [Raa87a,Raa87b,Wei86] (see chapter 2).

In the previous chapters the phase transformations in Ti - Si alloys were characterized by ***in-situ*** TEM, ***in-situ*** resistivity measurements and X - ray diffraction (XRD). In the formation of the low resistivity C54 $TiSi_2$ phase from co-sputtered material three different stages could be identified, each of which was associated with a characteristic change in the resistivity. The first sharp drop in resistivity at temperatures of about 300 ^oC could be associated with the crystallization of the amorphous alloy to the C49 $TiSi_2$ phase [Cot56,Hou86]. This crystallization reaction was found to take place via (random) nucleation and growth of crystallites in the amorphous matrix. The gradual decrease of the resistivity just after crystallization was found to be due to the annealing of stacking faults and point defects. Finally the second sharp drop in resistivity at temperatures of about 800 ^oC could be associated with the C49 - C54 polymorphous phase transition [Lav39].

The present investigation seeks to combine the knowledge gathered in the microstructural studies (chapters 2 and 3 respectively) with measurements of the kinetics of the changes in resistivity. In section 4.2.1 a critical discussion on the interpretation of resistivity measurements in terms of Avrami kinetics will be presented. Rather than starting from the physically unrealistic assumption that the resistivity of a binary random mixture is linear in its composition we will define two extreme ways of interpreting such resistivity measurements. Under certain conditions these extremes appear not to yield drastically different results and the kinetic parameters of the Avrami equation may be obtained with only a small systematic error. The kinetics of the different processes will be derived from ***in-situ*** resistivity measurements during isothermal anneals (section 4.4.1). Where ever possible, a physical meaning will be attached to the effective activation energies for the total process as obtained from the ***in-situ*** resistivity measurements, and to the activation energies for nucleation or growth obtained from the ***in-situ*** TEM investigations (chapter 2). The significance of nucleation phenomena in the various phase transformations will be addressed.

The kinetic parameters are of course dependent on the composition of the starting material. In order to arrive at a complete picture of the crystallization reactions in the Ti - Si system it is of interest to determine the composition dependence of the kinetic parameters. Therefore, section 4.4.2 reports measurements of the crystallization temperature of various Ti - Si alloy thin films in a wide composition range (20 at. % Si to 89 at. % Si). The pertinent absence of conformities between the thermal stability (or crystallization temperature) of the amorphous alloy and certain characteristic features in the phase diagram (like deep eutectics) will be discussed. The measured composition dependence of the crystallization temperature has some consequences for the interpretation of the observation that an amorphous silicide can be grown from Ti - Si diffusion couples [Hol87,Raa88a,Raa88b], which will also be discussed.

4.2 Reaction Kinetics and Resistivity Measurements

4.2.1 General

An alloy which is in a metastable state α (for example the amorphous state if a crystallization reaction is considered) may transform to a state β in order to decrease its Gibbs free energy. Such a transformation usually requires two steps [Chr81]: *(i)* the formation of super-critical β nuclei in the α matrix and *(ii)* the subsequent growth of these β regions. In an *in-situ* transmission electron microscopy (TEM) heating experiment (see chapter 2) one is able to distinguish between these two processes. Thus separate data for the temperature dependence of the nucleation and growth rate may be obtained. In order to characterize a phase transformation it is sometimes more practical or convenient to measure some macroscopic property of the material during the transformation (like the resistivity or some optical constant). Unfortunately, the changes in such a macroscopic property during the transformation depend in a less direct way on the nucleation and growth rates of individual β regions.

In this section it is described firstly how the nucleation and growth rates of separate β regions in an α matrix determine the transformed fraction as a function of time and temperature. Secondly, the relation between the transformed fraction and the resistivities of the initial (α), partially transformed, and final (β) state will be addressed. In bulk samples a transformation usually occurs by nucleation and growth in three dimensions. In our thin film samples it appeared that the film thickness (50 - 200 nm) is small compared to a typical dimension of a growing β region (1 - 5 μm). Although initially the β regions are small compared to the thickness of the film and are growing in three dimensions, the major part of the transformation occurs by two-dimensional growth of β nuclei. Therefore, all equations will be presented in their two dimensional form.

4.2.2 Avrami Kinetics

Let us suppose that the formation of super-critical nuclei of material β in a matrix consisting of material α occurs at a nucleation rate J ($\mathrm{m}^{-2}\mathrm{s}^{-1}$). At this stage it is irrelevant whether heterogeneous nucleation on surfaces or defects or homogeneous nucleation within the material is the dominant mechanism. Let us further assume that the linear growth rate Γ (ms^{-1}) is isotropic. In the initial stages of transformation the β regions will be well separated and show negligable overlap. In the limit of small t, the transformed fraction ξ after a time t is simply given by the integral:

$$\lim_{t \to 0} \xi = \int_{\tau=0}^{t} \pi \Gamma^2 (t - \tau)^2 \, J \, d\tau \equiv \xi_0 \tag{4.1}$$

In later stages of the transformation process the β regions will impinge mutually. This geometrical impingement problem is well known and was analyzed by Johnson et al. [Joh86] and Avrami [Avr39,Avr40,Avr41]. Avrami identified the integral in Eq. 4.1 with the so-called extended transformed fraction ξ_0. The extended transformed fraction has to be corrected for the multiply counted β regions to yield the actual transformed fraction ξ. The extended transformed fraction ξ_0 is related to the actual transformed fraction ξ with the differential equation:

$$\frac{d\xi}{d\xi_0} = 1 - \xi \tag{4.2}$$

Combination of Eq. 4.1 and 4.2 yields for the actual transformed fraction ξ after correction for mutual impingement:

$$\xi = 1 - exp[- \int_{\tau=0}^{t} \pi \Gamma^2 (t - \tau)^2 \, J \, d\tau] \tag{4.3}$$

The integral in the exponential form can only be evaluated if additional assumptions on the growth rate and the nucleation rate as a function of time are made. Avrami generalized Eq. 4.3 to:

$$\xi = 1 - exp[-\kappa . t^n] \tag{4.4}$$

where κ and n are time independent constants for a specific transformation. In the remainder of the text Eqs. 4.3 and 4.4 will be referred to as the Avrami equation and the generalized Avrami equation respectively. From the form of Eq. 4.4 it can be seen that a plot of $ln[-ln(1 - \xi)]$ versus

$ln(t)$ yields a straight line with a slope equal to n. The value of n relates to the 'mode' of transformation. For example, in the simplest case one may assume two dimensional growth with a constant growth rate from preexisting (quenched-in) nuclei. In that case the nucleation rate would formally be described by a delta function peaked at $t = 0$ and, by evaluating the integral in the Avrami equation, one finds that the value of n equals 2. Another simple case is that of a constant nucleation rate and a constant growth rate. The latter case would correspond to a value of n of 3. A more detailed list of n-values for several processes is listed in the literature, for example in the monograph of Christian [Chr81].

The temperature dependence of the (steady state) nucleation and growth rates occurring in the integral of Eq. 4.1 and Eq. 4.3 is frequently described in the form of a simple Arrhenius type relation [Gre85,Kos81,Ran81,Hei81]. for the (steady state) nucleation rate:

$$J = J_0 exp[-\frac{E_n}{kT}] \tag{4.5}$$

and for the growth rate:

$$\Gamma = \Gamma_0 exp[-\frac{E_g}{kT}] \tag{4.6}$$

where E_n and E_g denote the activation energy for the nucleation and growth process respectively. J_0 and Γ_0 are preexponential factors which depend in detail on the particular nucleation and growth process involved. The Arrhenius type behaviour of the nucleation and growth rate is also reflected in the temperature dependence of the 'rate constant' κ, and in many cases κ also behaves according to an Arrhenius temperature dependence with an effective activation energy E_κ^{eff}. The effective activation energy E_κ^{eff} for the total transformation process may be calculated by evaluating the integral in the Avrami equation (Eq. 4.3). In the simple case of a constant nucleation and growth rate one finds for the effective activation energy from Eqs. 4.3, 4.5 and 4.6:

$$E_\kappa^{eff} = 2E_g + E_n = n.E_\tau^{eff} \tag{4.7}$$

For other cases similar relations are easily derived. It is frequently more convenient to plot a characteristic transformation time, for example the time τ_c needed to transform a fraction $\xi = 1 - e^{-1}$ (about 63.2 %) of the sample. (This time just corresponds to the time where the product κt^n reaches a value of 1). If κ shows Arrhenius type behaviour, the reciprocal of the characteristic time τ_c will also show Arrhenius type behaviour, but the effective activation energy will differ from that derived from κ by a factor

$1/n$ and is thus a sort of weighted average of the activation energies for nucleation and growth. More detailed treatments on the effective activation energy of reactions which can be described by an Avrami type equation are described in literature [Ran81,Ran80].

The above shows that by measurements of the total transformed fraction as a function of time (e.g. by resistivity measurements or differential scanning calorimetry) one cannot separate the contributions to the activation energy which are due to the nucleation and growth process. Although the measurement of a macroscopic property is experimentally simpler than for example *in-situ* electron microscopy experiments the physical meaning of the derived activation energies may be somewhat blurred.

4.2.3 Transformed Fraction and Resistivity

While interpreting resistivity measurements during crystallization or other solid state phase transformations many authors tacitly assume that a simple linear relation exists between the transformed fraction and the resistivity of the partially transformed sample [Tho87,Nav85,Nav85a,Nav85b,Nav86a] [Nav86b,Tie83]. Weiss et al. [Wei86] attempted to check such a resistivity - composition relation by correlating resistivity measurements with estimates of the fraction transformed from transmission electron microscopy (TEM) micrographs. They report that the electrical *conductivity* is linear in the fraction transformed upto a fraction of 35 %. A problem we have is that Weiss et al. used a linear interpolation of the *resistivity* to interpret their data in the remainder of their paper. In the following it will become clear that linearity in conductivity and resistivity in fact are the two most extreme situations of a resistivity - transformed fraction relationship.

In this section the validity and the extremes of relations between the transformed fraction ξ and a macroscopic property of the partially transformed binary mixture will be investigated. For that purpose we will use a fictituous transformation in which the transformed fraction ξ is described by Eq. 4.4 with $n = 3$. The resistivity behaviour of the specimen during the transformation will be calculated under different assumptions of a ξ - ρ relation. The present discussion is focussed on the behaviour of the electrical resistivity of the mixture with composition [Lan52,Lan78], but it may equally well be applied to other macroscopic properties like the dielectric constant [Asp79,Asp82].

An obvious guess to describe the transformed fraction ξ in terms of the resistivities $\rho_{\alpha,\beta}$ (or conductivities $\sigma_{\alpha,\beta}$) of the pure materials α and β is a simple linear interpolation, viz:

$$\rho = (1 - \xi_\rho)\rho_\alpha + \xi_\rho \rho_\beta \tag{4.8}$$

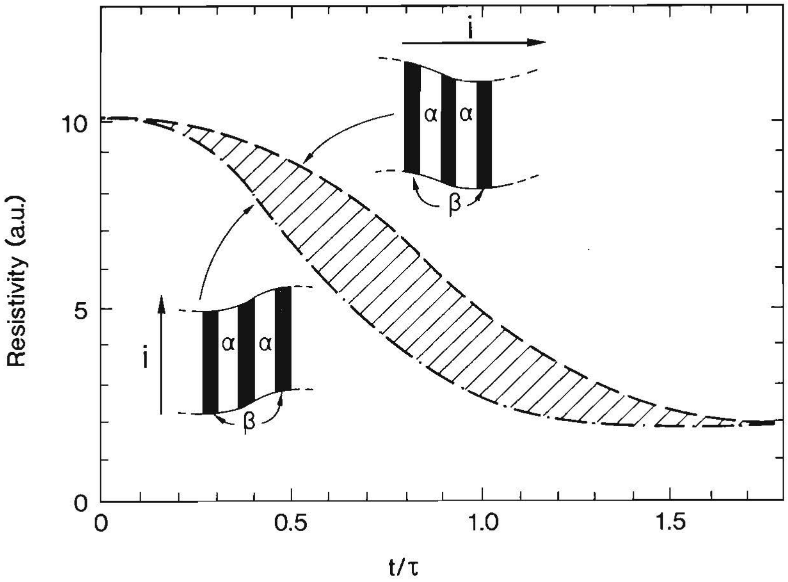

Fig. 4.1. Resistivity as a function of reduced time (t/τ_c) for two extreme microstructures. Regardless of the samples actual microstructure, its resistivity always is in between the two limiting cases (shaded region). This figure was calculated with the aid of the Avrami equation with n = 3 and a resistivity change from 10 (arbitrary) units to 2 units.

where the index ρ attached to the symbol for the transformed fraction (ξ) indicates that the fraction ξ_ρ has been derived under the assumption of linearity in resistivity. The above relation would describe the series resistivity of a sample consisting of separate layers of α and β material and is thus an upperlimit for the resistivity of the mixture (see Fig. 4.1). The obvious alternative guess describes the parallel resistivity of such a layered sample, viz:

$$\rho^{-1} = \sigma = (1 - \xi_\sigma)\rho_\alpha^{-1} + \xi_\sigma\rho_\beta^{-1} \tag{4.9}$$

where the index σ indicates that the transformed fraction ξ_σ is assumed to behave linear in the conductivity. The latter situation is a lower limit of the resistivity of the binary mixture (see Fig. 4.1). The actual situation will not correspond to either of the above mentioned cases, but the resistivity will always assume a value in between the two extremes, indicated by the shaded area in Fig. 4.1.

Solving the Eqs. 4.8 and 4.9 for ξ_ρ and ξ_σ and comparing the two transformed fractions shows that they are related according to:

$$\xi_\rho = \frac{\rho}{\rho_\beta}\xi_\sigma \tag{4.10}$$

The difference between ξ_ρ and ξ_σ is smaller the smaller the difference in resistivity of the pure phases α and β. This implies that for transformations during which the resistivity changes are small, it is not critical what specific approach one uses to determine the transformed fraction from the resistivities. However for transformations which result in large resistivity changes, say a factor of 2 or larger, the value of the resistivity of the partially transformed binary mixture will depend in detail on how the β phase is dispersed in the α matrix. Unfortunately such microstructural properties of the sample are not often known a priori.

More elaborate treatments to interpolate in a reasonable way between the extreme situations are described in literature. For example the Bruggeman [Bru35] effective medium approximation is very often used to describe the resistivity of a binary mixture as a function of composition [Lan52,Lan78,Lac86]. The present section is not intended to review and evaluate all composition - resistivity relations which are described in literature. Instead, an indication will be given of the magnitude of the systematic errors in the kinetic parameters which can be expected if an erroneous resistivity - composition relation is assumed.

Let us first assume that the samples resistivity as a function of composition during transformation is best described by a set of resistors in parallel (Eq. 4.9). Furthermore let us assume that the actual transformed fraction (ξ_σ) as a function of time is indeed governed by the generalized Avrami equation (Eq. 4.4). As an example we will again take $n = 3$ in the present calculations, but this is by no means a restriction to the generality of the discussion. Under the above assumptions one may calculate σ and $\rho = \sigma^{-1}$ as a function of reduced time (t/τ_c). If we now use the calculated resistivity path as a function of reduced time as a fictitious measured resistivity path, and determine the fraction transformed (ξ_ρ) under the other extreme assumption of resistors in series (Eq. 4.8), ξ_ρ can generally not be described with an Avrami type equation.

The result of this exercise is depicted in a graph of $ln[-ln(1-\xi)]$ versus $ln(t)$ in Fig. 4.2. The result is calculated for $\rho_\alpha = 10$ and $\rho_\alpha/\rho_\beta = 10, 5$ and 2. In the limit of $\rho_\alpha/\rho_\beta \rightarrow 1$ the curves ξ_σ and ξ_ρ as a function of reduced time are the same. For values of ρ_α and ρ_β substantially different from unity large deviations from a straight line are observed (Fig. 4.2). If a sort of 'best fit' straight line is estimated through the curves in the region of interest (say between 1 % and 99 % transformation) values of n result which are significantly different from the model value ($n = 3$).

The above discussion illustrates that significant deviations may occur if wrong assumptions are used to determine the transformed fraction from the resistivity especially if the relative change in resistivity during the transformation is large. In practice it is convenient to determine the transformed fractions starting from *both* extreme assumptions, i.e. ξ_ρ from Eq. 4.8 *and* ξ_σ form Eq. 4.9. Both these quantities are then plotted in a graph of $ln[-ln(1-\xi)]$ versus $ln(t)$) and one chooses the best approach simply by judging which model yields transformed fractions which are best described by a single straight line. The differences in slope are representative for possible systematic errors in the value of n.

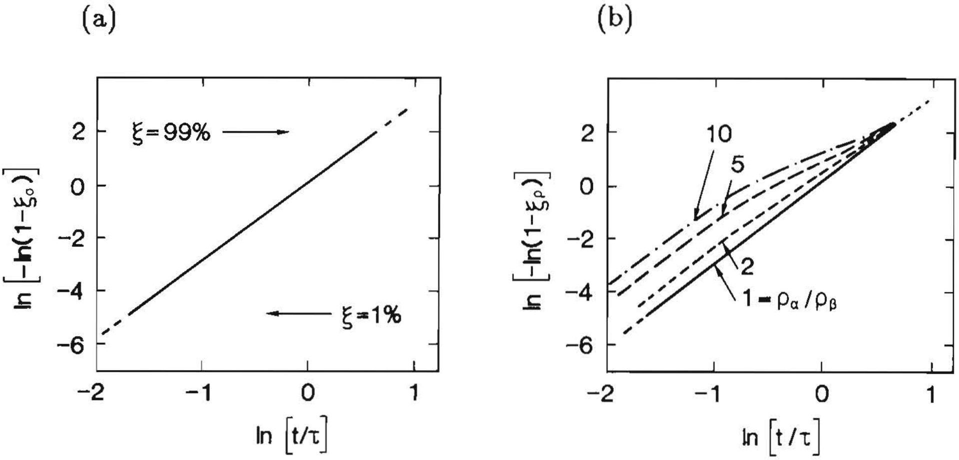

Fig. 4.2. The effect of erroneous assumptions in the transformed fraction - resistivity relation on the measured kinetic parameters. (a): $ln[ln-(1-\xi_\sigma)]$ as a function of the logarithm of the reduced time t/τ. Practical transformed fraction detection limits are indicated (about 1 % and 99 %). (b): Starting from data depicted in (a), the transformed fraction has been calculated under the assumption of linearity in resistivity, i.e. according to Eq. 4.8. The largest deviations from the Avrami equation are observed for large changes in resistivity (ρ_α/ρ_β) during transformation.

4.3 Experimental

Different layers of a Ti - Si alloy were deposited on thermally oxidized silicon wafers. The details of the deposition of these films were described previously (see chapter 2). The composition of the alloy thin films was derived from Rutherford backscattering spectrometry.

The amorphous thin films were annealed in high vacuum. The resistivity of the thin film was measured *in-situ* during the anneal as described earlier in chapter 3. Isothermal anneals at temperatures in the range of 250 °C to 850 °C and ramped (rate 0.1 °C/s) temperature - resistivity curves were recorded. Before and after annealing the crystalline phases in the samples were identified with an X-ray diffractometer with a conventional 2Θ geometry and CuKα radiation.

4.4 Results and Discussions

4.4.1 Kinetic Aspects

Kinetic measurements were performed on samples with a layer thickness of about 200 nm and a composition somewhat Si–rich compared to that of the disilicide (Ti/Si = 0.44 ± 0.04 or 69 ± 2 at. % Si). Three different stages can be distinguished during the formation of the final equilibrium C54 $TiSi_2$ phase from the nearly stoichiometric amorphous starting material (see Fig. 3.2): *(i)* a fast drop in resistivity associated with the crystallization of the amorphous alloy; *(ii)* a gradual decrease in resistivity just after crystallization due to the annealing of stacking faults and point defects and *(iii)* a second sharp drop in resistivity associated with the C49 - C54 polymorphous phase transition.

In the following the kinetics of the above mentioned processes will be investigated. For that purpose, the resistivity of the samples was measured during isothermal anneals. As discussed before, the resistivity or the conductivity of the sample was used as a linear measure of the crystallized fraction. Assuming that the transformations obey the Avrami equation the Avrami exponent n was determined from a plot of $ln(-ln(1-\xi))$ versus $ln(t)$. The effective activation energy (E_{τ}^{eff}) was determined under the assumption of Arrhenius type behaviour of the characteristic time τ_c. The next figures depict the kinetics of the various transitions occurring in the Ti - Si system. Fig. 4.3 shows the Arrhenius type behaviour of τ_c for the three different reactions. The subsequent three figures (Fig. 4.4 to Fig. 4.6) show results for the crystallization, precipitation and C49 - C54 phase transformation processes respectively, in terms of the generalized Avrami equation (Eq. 4.4).

(i) Crystallization

The kinetics of the crystallization reaction at temperatures of about 250 °C are depicted in Fig. 4.4. In Fig. 4.4a the two limiting cases of the resistivity - transformed fraction relation are outlined. The magnitude of the drop in resistivity during the crystallization process is only 15 % of the original value. As expected, no large differences are found for the upper and lower limit of ξ. The Avrami equation appears to give a remarkable good description of reality.

In the whole investigated temperature range the Avrami exponent n (from the slope of the solid lines) is found to be near the value of 3, indicating a constant nucleation rate and a twodimensional growth process. This result is consistent with the results presented in chapter 2. There it was shown that the amorphous thin films crystallize by a (random) nucleation and growth mechanism. The grain diameter was found to be much larger than the film thickness so that the dimension of growth is 2.

The characteristic time τ_c is recorded as a function of reciprocal temper-

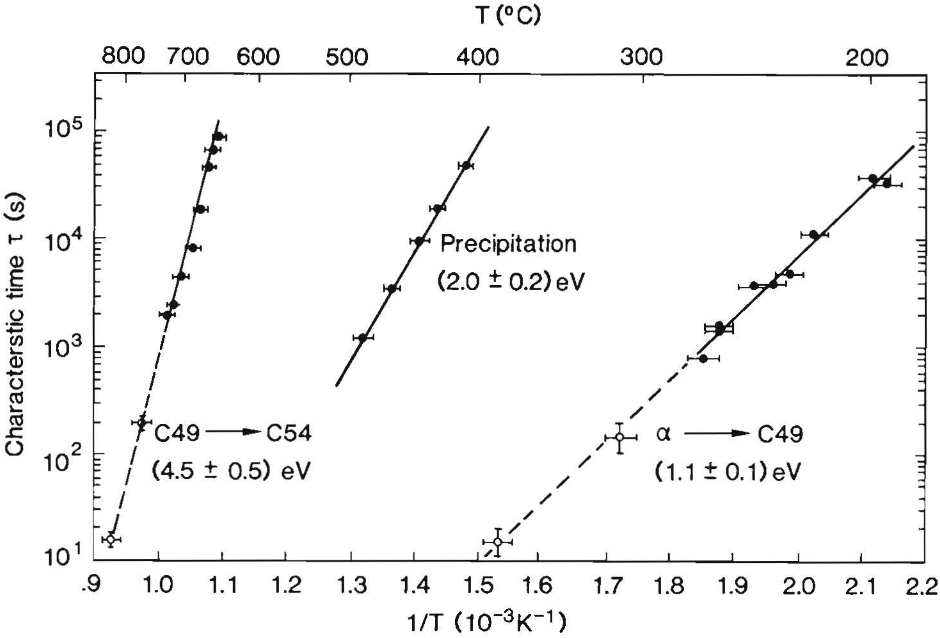

Fig. 4.3. Arrhenius plot of the characteristic time for $1 - 1/e$ transformation. Solid dots are from isothermal anneal treatments, while open dots are derived from ramped anneal treatments. The three curves depict from left to right the C49 - C54 transformation, the precipitation and the crystallization reaction respectively. Effective activation energies are indicated in the figure.

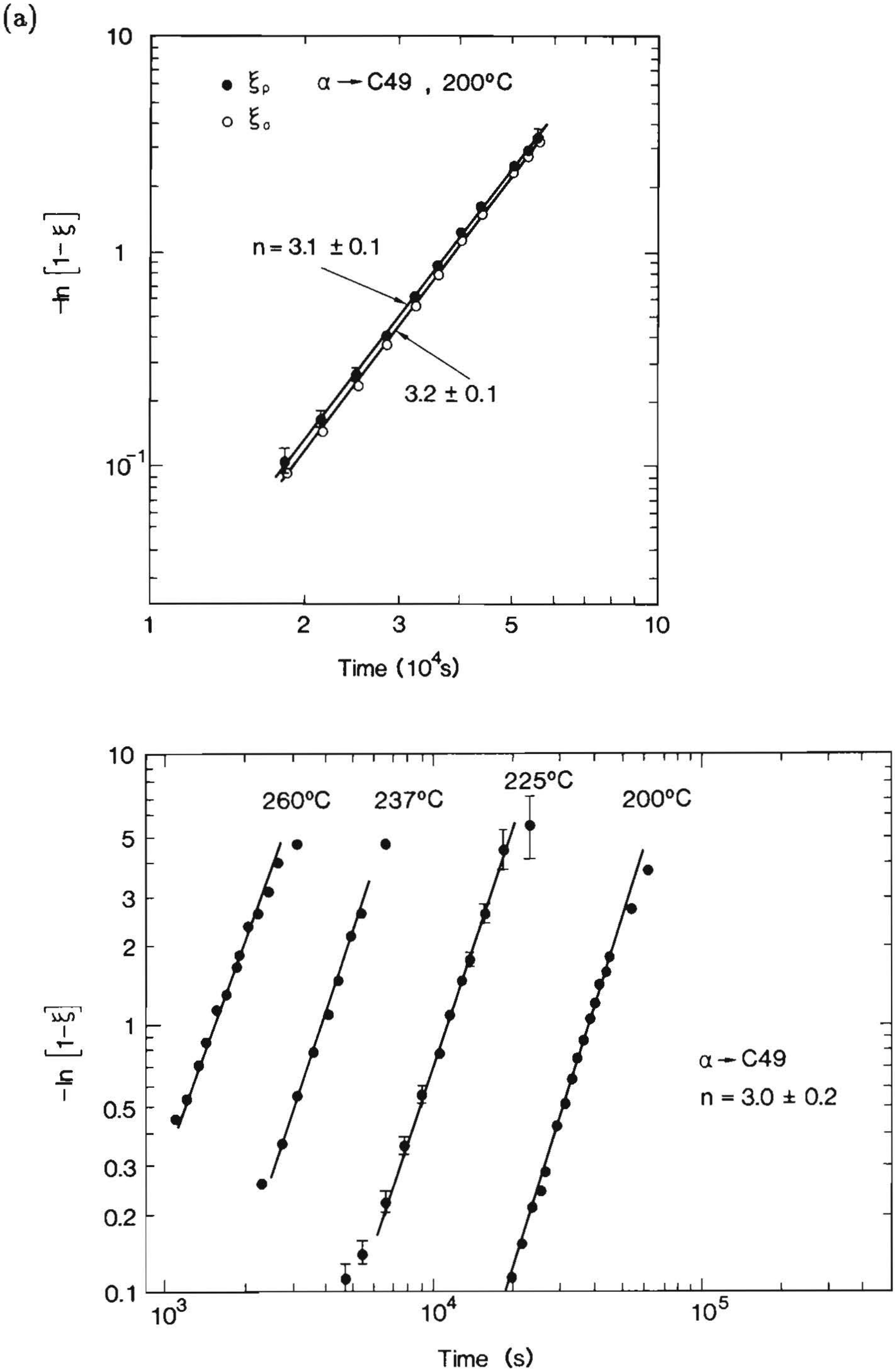

Fig. 4.4. Kinetics of the crystallization reaction according to the Avrami equation. (a) Transformed fractions according to the two extreme approaches (see text) (b) Transformed fractions calculated from Eq. 4.8.

ature in Fig. 4.3. The slope of the straight lines in this figure is a weighted average between the activation energy for growth and that for nucleation (see Eq. 4.7). For the total crystallization process we find an effective activation energy (E_T^{eff}) of (1.1 ± 0.1) eV. Let us now calculate the effective activation energy E_T^{eff} with the independent values for E_n and E_g as determined from the *in-situ* TEM experiments described in chapter 2, and the experimentally obtained value of n (3.0 ± 0.1). From the results presented in chapter 2 we find for the activation energy for the growth rate of crystals (see Fig. 2.7): $E_g = (1.2 \pm 0.1)$ eV. As a rough estimate for the activation energy of nucleation we obtained a value of $E_n = (2.4 \pm 0.6)$ eV. From Eq. 4.7 we find for the effective activation energy E_T^{eff} a value of (1.6 ± 0.3) eV, which appears to be somewhat higher than the value obtained from the present experiments: (1.1 ± 0.1) eV. The difference is probably caused by differences in experimental circumstances. Note that the experiments reported in chapter 2 were carried out on Ti - Si alloy thin films supported by a relatively thin and flexible Si_3N_4 membrane, while the present experiments were carried out on the same thin films, but now supported by a rigid oxidized Si substrate.

A similar study was undertaken by Thompson et al. [Tho87]. They reported an Avrami exponent of (1.8 ± 0.3) for the crystallization reaction, which is much smaller than the Avrami exponent which was found in the present samples (3.0 ± 0.2). Low values of the Avrami exponent are frequently indicative of nucleation saturation in an early stage of the reaction or growth from preexisting (quenched) nuclei. Thompson et al. [Tho87] reported an effective activation energy of 1.5 eV, a value which is somewhat larger than the value found in the present work. According to the results presented in Fig. 4.8 (see further) deviations of $TiSi_2$ stoichiometry may lead to a larger activation energy for crystallization. In their TEM micrographs one observes that the grains of their completely crystallized thin film are more like the eutectically formed crystallites in our Si–rich ($\alpha Ti_{23}Si_{77}$) samples (see Fig. 2.6a) than they resemble the polymorphically grown crystals in our $\alpha Ti_{31}Si_{69}$ alloy. Therefore the larger activation energy as found by Thompson may be caused by small deviations from the $TiSi_2$ stoichiometry in their samples.

(ii) Precipitation

It was shown in chapter 3 that the resistivity of the C49 $TiSi_2$ phase slowly decreases upon annealing at higher temperatures and during longer periods of times. The resistivity decrease was associated with the annealing of stacking faults and point defects and resulted in an increasing Si precipitation at the surface of the sample. It is of interest to investigate the kinetics

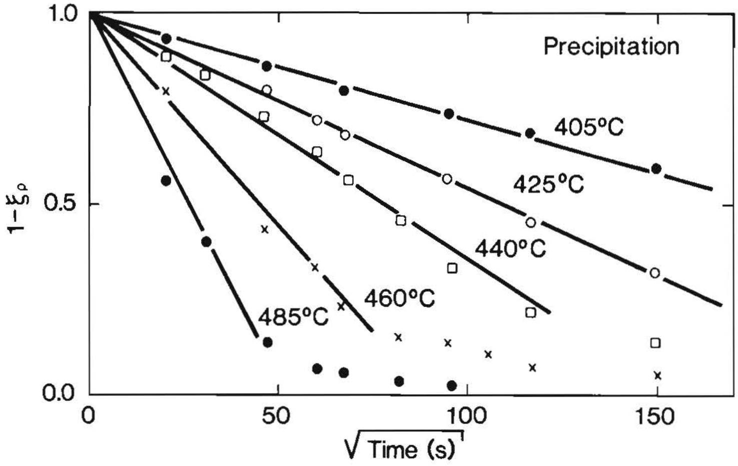

Fig. 4.5. Kinetics of the precipitation reaction. A linear decrease of 1 - ξ_p with square root of anneal time is found, indicating a diffusion controlled precipitation reaction.

of this reaction and to determine which activated process plays a role in the precipitation reaction.

The precipitation reaction differs from the crystallization process in that it corresponds to excess Si diffusing to the surface of the thin film. This will result in a decreasing solute concentration (in addition to the decreasing stacking fault density) in the silicide, which changes the resisitivity of the matrix as a whole. The boundary conditions for many precipitation problems [Chr81] tend to be of such complexity that the diffusion equation cannot be solved exactly. Furthermore, in this work the average resistivity of the sample is measured. Gradients in the resistivity, associated with solute concentration gradients, are not noticed so that experimental results can only be interpreted semiquantitatively.

We define a dimensionless super-saturation δ by:

$$\delta = \frac{c - c^{\infty}}{c^0 - c^{\infty}} \tag{4.11}$$

where c represents the concentration of solute and c^0 and c^{∞} the concentration of solute in the matrix at the start and at the end of the reaction respectively. In the case of a homogeneous concentration of solute c, and if a linear relation between resistivity and solute concentration is valid, it can easily be derived that the dimensionless super-saturation δ corresponds to $1 - \xi_\rho$ where ξ_ρ has been defined in Eq. 4.8.

In Fig. 4.5 we show the above defined super-saturation versus the square root of the anneal time. In the entire temperature range the square root time dependence suggests that the temporal evolution of the above defined super-saturation δ can be described by a solution of the non-stationary diffusion equation. The absolute value of the slope of the straight lines in Fig. 4.5 then is related to an effective diffusion coefficient. One can define a characteristic time τ_c like in the previous section. From Fig. 4.3 one obtains for the effective activation energy in τ_c a value of (2.0 ± 0.2) eV.

If diffusion of Si through crystalline C49 $TiSi_2$ is the dominant basic process during the precipitation reaction the value of the activation energy of the process would be that of the activation energy for Si diffusion through crystalline $TiSi_2$. In growth experiments of the C49 $TiSi_2$ phase in Ti - Si diffusion couples (where it has been established that Si diffusion is rate limiting [Mae86,Mae87,Bag80] (see also chapter 5) one finds values of the activation energy of about 1.8 - 2.2 eV [Hun83] (see chapter 5), so indeed near the activation energy of the precipitation reaction.

(iii) C49 - C54 Transformation

In the temperature range from 650 °C to 850 °C the alloy thin films transform from the C49 $TiSi_2$ phase to the stable C54 $TiSi_2$ phase. This transformation is associated with a second precipitous drop in resistivity from about 100 $\mu\Omega$cm to about 18 $\mu\Omega$cm. In Fig. 4.6 the transformed fraction as calculated from the observed resistivity values is plotted versus anneal time. Fig. 4.6a shows the differences between the two extreme situations, parallel or series resistivities. The drop in resistivity is quite large in the case of this polymorphous phase transformation, and consequently the differences observed are larger than those observed in the crystallization reaction (see Fig. 4.4). A comparison of the deviations of the two extreme approaches with a straight line (least square fit) in the insert of Fig. 4.6a shows that the best approach is to determine the transformed fraction from a linear interpolation between the initial and final values of the resistivity. If a linear conductivity-composition relation is assumed significant deviations of the fit to the Avrami equation are observed in the central region of the transformation ($10\% < \xi < 90\%$). In the very start and at the very end of the transformation deviations from the straight line are observed. The values of ξ derived from a linear interpolation in resistivity seem to fit the straight line better in the lower transformed fraction regime, while values of ξ derived from a linear interpolation in conductivity fit the straight line better in the higher transformed fraction regime. Depending on which of the two extreme approaches we use, a value of 2.8 or 3.1 is found for the Avrami exponent.

Fig. 4.6b shows the transformed fraction (as derived from a linear interpolation in resistivity) versus anneal time at different temperatures. The

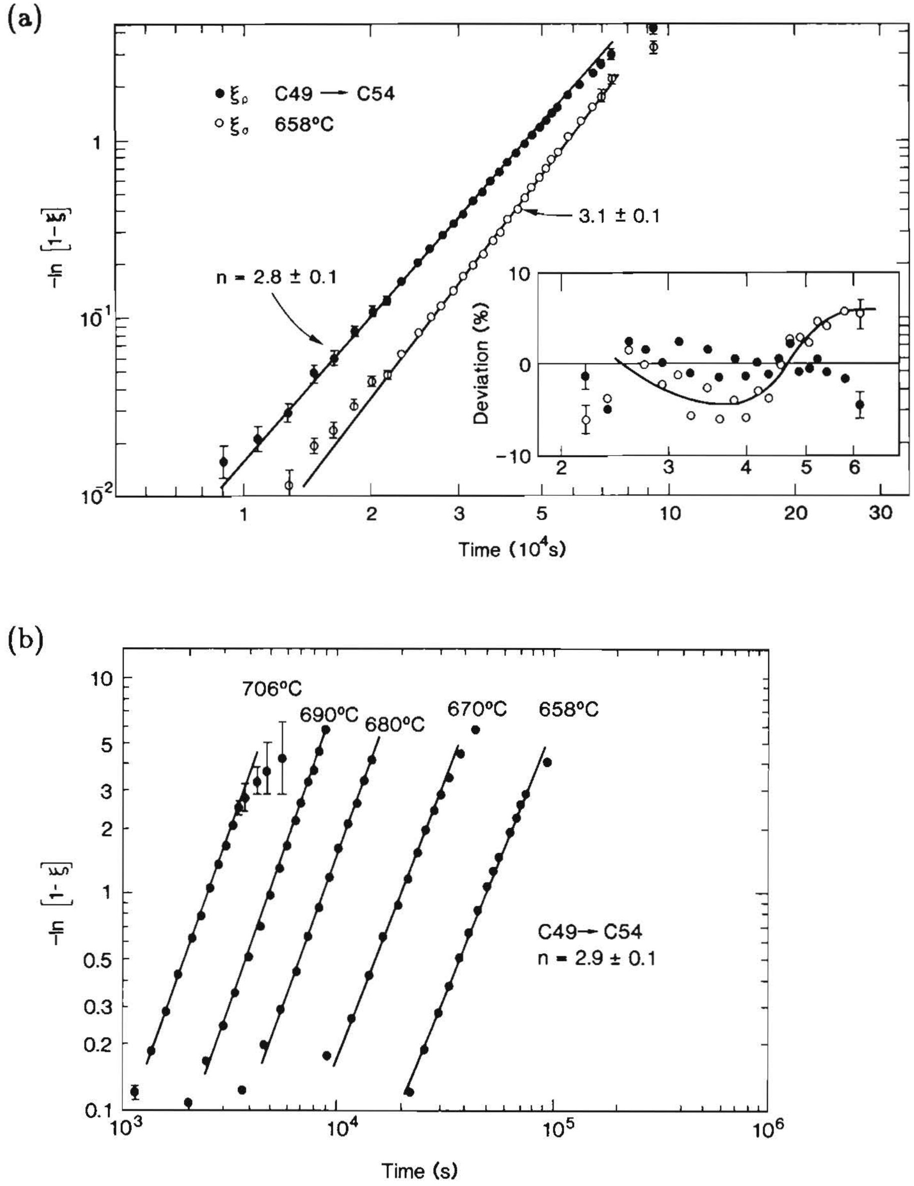

Fig. 4.6. Kinetics of the C49 - C54 transformation reaction according to the Avrami equation. (a) Transformed fractions according to the two extreme approaches (see text) (b) Transformed fractions calculated from Eq. 4.8.

slopes of the straight lines correspond to an Avrami exponent of (2.9 ± 0.1). Grain sizes are observed to be larger in the C54 phase than in the C49 phase, being much larger than the thickness of the thin film. Again, the observed value of the Avrami exponent is consistent with two dimensional growth and a constant nucleation rate.

The activation energy for the transformation can be derived from the straight line in the high temperature region of Fig. 4.3. The effective activation energy is found to be very large: (4.5 ± 0.8) eV which agrees well with the value of 4.4 eV reported by Thompson et al. [Tho87]. The reduced activation energy (E^{eff}/kT_m, where T_m the melt temperature) is very large (about 30) compared to typical reduced activation energies for self-diffusion in close packed metals (18 ± 3. [Ash80]). This is an indication that nucleation plays a profound role in the process.

The participation of critical nuclei in the nucleation process is usually described by a Boltzmann factor containing the energy of formation of a critical nucleus. The nucleation rate can be written as in Eq. 2.4, i.e. as a product of the Boltzmann factor and a factor containing the activation energy for growth of the critical nucleus. The effective activation energy of the total reaction was shown to be equal to a weighted average of the activation energies for nucleation and growth (Eq. 4.7). Thus the contribution of the formation energy of a critical nucleus (contained in the Boltzmann factor as E_c) to the total activation energy for nucleation (E_n) may enlarge the effective activation energy (E_T^{eff}) for the total transformation to the observed values. Unfortunately it was not possible to actually see growing C54 crystals in the crystalline C49 matrix during *in-situ* annealing in a TEM.

In classical nucleation theory the critical radius r$_c$ of a spherical nucleus of β material in an α matrix can be expressed as [Heu88,Chr81]:

$$r_c = \frac{2\,\gamma_{\alpha,\beta}}{G^v_{\alpha,\beta}} \tag{4.12}$$

where $\gamma_{\alpha,\beta}$ is the (isotropic) interfacial energy between tha α and β phases and $G^v_{\alpha,\beta}$ is the free energy change of the phase transformation per unit volume. The energy of formation of such a nucleus of critical size can be written as:

$$G_c = \frac{16\pi\gamma^3_{\alpha,\beta}}{3\,(G^v_{\alpha,\beta})^2} \tag{4.13}$$

In principle the radius and formation energy of a critical nucleus can be calculated from the above equations. However, the interfacial energies and the difference in volume free energy between the C54 and C49 TiSi$_2$ polytypes are not known. Furthermore, there are other factors which influence the nucleation behaviour in these thin solid film reactions, notably mechanical strain and the presence of surfaces, interfaces and grain boundaries.

A rough estimate of the change in free energy upon transformation ($G^v_{\alpha,\beta}$) may be obtained from the following. Firstly, because of the chemical and structural similarity of the polytypes of $TiSi_2$ [Hen86,Hen87b,Hou86] (see chapter1) the enthalpy change for the phase transition is probably only a fraction of the heat of crystallization (0.11 eV/atom [Kem82,Raa86]), i.e. of the order of 0.01 eV/atom. Secondly, from Kaufmans data [Kau79] one may obtain estimates of structural contributions to the free energy of formation. For example, the free energy difference between a hypothetical body centered cubic and a hexagonal close packed alloy of $TiSi_2$ stoichiometry is only about 0.05 eV/atom. Thirdly, it is not known at present whether the C49 phase is a metastable phase or rather a low temperature modification of the C54 phase. If the C49 phase is a low temperature phase the free energy difference is principally zero at the transformation temperature. From the above arguments it is concluded that an upper limit for the free energy change in the C49 - C54 transformation is at most 0.05 eV/atom ($6 * 10^8$ J/m^3).

A quantitative estimate for the interfacial energy between the two $TiSi_2$ polytypes is even more difficult to obtain. It is observed that at temperatures just slightly above the transformation temperature to the C54 phase the $TiSi_2$ film shows effects of grain boundary grooving [Hov88](see for example Fig. 3.9), which may indicate a rather high surface energy of the C54 phase. Surface energies of free solid surfaces are reported to be in the range of 0.5 to 2 J/m^2 [Mur75]. Interphase boundaries tend to have free energies near to that of high angle grain boundaries in pure metals, for which a value near 1/3 of the value for the free surface is an acceptable average [Mur75]. Thus, an estimate of the interfacial energy of the C54 phase in the C49 matrix is about 0.3 J/m^2.

Inserting the above estimates in Eq. 4.12 yields for the radius of a critical nucleus an approximate lower limit of 1 nm. An estimate for the free energy of such a critical nucleus based on Eq. 4.13 is 25 eV. This number has only qualitative meaning: the nucleation barrier can never be surmounted by the thermal motion of the atoms. Consequently, since nucleation of the C54 phase is observed to take place at reasonable temperatures, the actual nucleation mechanism can not be a homogeneous one (as is assumed in the derivation of the above equations) but rather will be heterogeneous at surfaces, grain boundaries or interfaces. The very low values of $G^v_{\alpha,\beta}$ will cause the net volume free energy gain of a critical nucleus to be very sensitive to strain in the C49 $TiSi_2$ phase [Chr81]. This is corroborated by observations that the C49 - C54 transformation temperature depends on film thickness [Hou86] and grain size [Hou87].

In conclusion, since the radius and free energy of a critical nucleus are probably extremely large, the nucleation process must be very important in the C49 - C54 polymorphous phase transformation. Large changes in the transformation temperature may be brought about by only small variations in the effective activation energy. These small variations in the activation energy can be caused by mechanical strain and the actual state of interfaces and surfaces in the silicide thin films.

4.4.2 Composition Dependence of Crystallization Temperature

In order to investigate the crystallization temperature of Ti - Si alloy thin films, Ti - Si alloys of different compositions (20 to 89 at. % Si derived from Rutherford backscattering spectrometry (RBS)) were deposited on thermally oxidized (600 nm) Si substrates. An estimate of the geometrical thickness of the alloy thin films can be derived from the RBS spectra if assumptions are made on the Ti and Si molar volumes in the alloy thin film. Assuming the bulk molar volume for Ti ($V_m^{Ti} = 18 * 10^{-24}$ cm^3) and for Si the molar volume in its 'metallic' form ($V_m^{Si} = 12 * 10^{-24}$ cm^3) a thickness of about 70 nm was calculated. The thickness of the films varied somewhat ($\pm$ 20 nm) with composition, the Ti–rich films being thicker than the Si–rich films. Within the films impurities like C and O were not present above the RBS and Auger detection limit which was estimated to be about 0.5 at. %. Some argon was incorporated in the thin films during the deposition process in the films with a large Si content (maximum about 3 at. % for the Si–richest film). All as-deposited thin films were found to be amorphous according to X-Ray diffraction.

The above described alloy thin films were heated in vacuum with a constant heating rate of 0.1 °C/s. Resistivity-temperature curves similar to those presented earlier in Fig. 3.2 and characterized by one or sometimes two sudden drops in resistivity were obtained. It was shown in chapter 3 that for the stoichiometric $TiSi_2$ alloy the sudden drop in resistivity at about 300 °C is associated with crystallization. For the other alloys, X-ray diffraction of as-deposited samples and samples annealed at temperatures just beyond such a precipitous drop in resistivity confirmed that crystallization had occurred. The temperature at which the resistivity reaches a value intermediate between that of the amorphous and that of the crystalline state is identified as the crystallization temperature of the alloy. The crystallization temperature was measured at a heating rate of 0.1 °C/s in these experiments.

The phases in the samples just after crystallization were identified with the aid of X-ray diffraction. Some representative examples of diagrams from

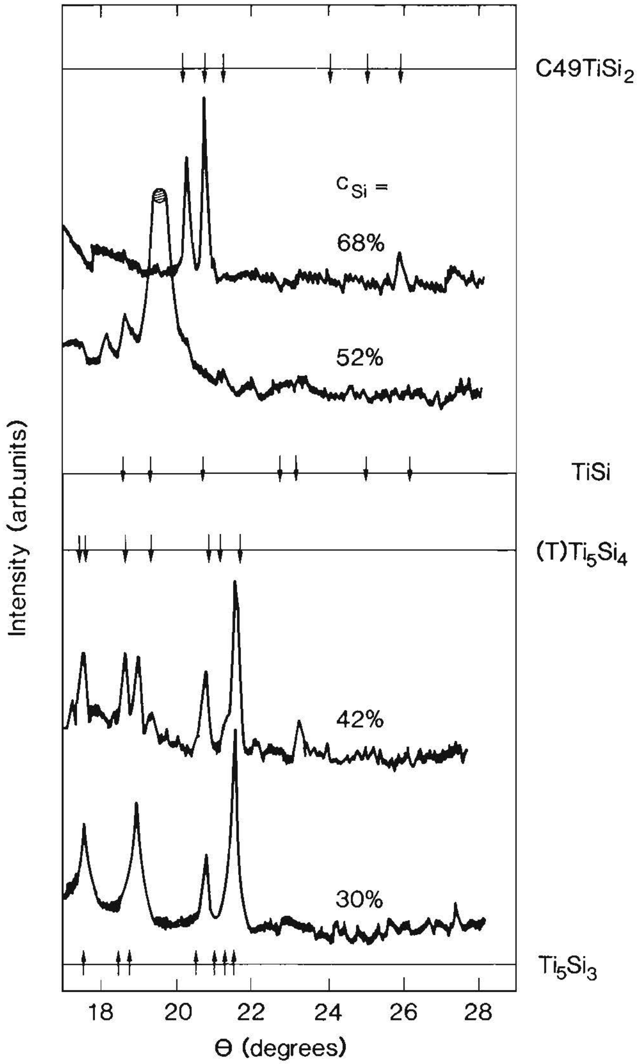

Fig. 4.7. X-ray diffraction analyses of some representative samples annealed at a temperature just above the crystallization temperature. The crystalline phase in the Si–rich samples (top curve) can be identified as C49 TiSi$_2$. Unambiguous phase identification is not possible in the central part of the Ti - Si system. Note the single very strong diffraction (extending off scale) in the 52 at. % Si sample.

our crystallized alloys are shown in Fig. 4.7. In the $TiSi_2$ - Si two-phase region (top part of the figure) all reflections are found to originate from the C49 $TiSi_2$ phase [Cot56,Hou86] or polycrystalline Si. In the intermediate composition range unique identification of the constituting phases of the crystalline material is difficult, if not impossible. For example, the diffraction pattern after crystallization of an alloy containing 52 at.% Si exhibits a single very strong reflection at a d-value of (0.2305 ± 0.001) nm corresponding to a θ value of about (19.5 ± 0.1) degrees. A similar reflection was observed by Maex [Mae88] in a co-sputtered 'Ti_3Si_4' alloy. Maex argues that this single peak does not originate from a stable silicide but originates from yet another metastable phase in the Ti - Si system. The high number of stable phases and the likely presence of metastable phases in the central region of the Ti - Si binary system, the similarity of the diffraction patterns of these phases, and the highly textured nature of the crystallized thin films make an unambiguous phase identification nearly impossible for thin film samples with compositions in the range of 30 to 65 at. % Si. The main conclusion from our X-ray diffraction work is that just after the drop in resistivity the sample has crystallized. Thus, it seems justified to associate the drop in resistivity with a crystallization reaction.

In Fig. 4.8 the measured crystallization temperatures for thin films on SiO_2 are presented. Also shown is the equilibrium phase diagram [Mas87] in the bottom part of the figure. The crystallization temperature of amorphous Si was derived from crystallization experiments on pure sputtered Si layers on SiO_2 [Raa88c] so that the curve can be extrapolated to the crystallization temperature of amorphous Si. The most salient feature of Fig.4.8 is the sharp minimum in the crystallization temperature at the stoichiometric composition of $TiSi_2$. While the crystallization temperature of an alloy close to stoichiometry is just below 300 °C, the crystallization temperature reaches values of 500 °C and higher for Ti–rich alloys. Crystallization temperatures on the Ti–rich side of the $TiSi_2$ stoichiometry are observed to rise more rapidly with composition than they do on the Si–rich side. Note that the measured values of the crystallization temperature agree closely with those measured by other investigators. The values also agree with the results derived from the *in-situ* TEM work (chapter 2) from which the crystallization temperature was taken as the temperature for which the growth speed of separate crystallites reaches an appreciable value, say 10^{-9} ms^{-1}. In the upper part of the figure the measured activation energies from section 2.3.2, section 4.4.1 and Maex et al. [Mae88] are shown. In these Ti - Si alloys the dip in crystallization temperature is associated with a sharp minimum in the activation energy as is evidenced by the upper curve in Fig. 4.8.

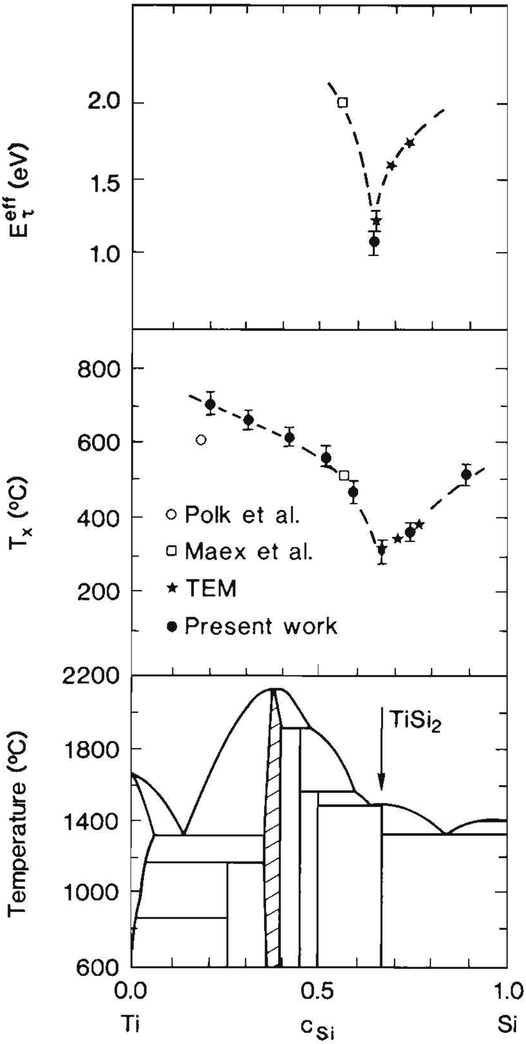

Fig. 4.8. Activation energies for crystallization (upper diagram) and temperatures for crystallization (middle diagram). Solid dots: this work; squares: Maex et al. [Mae88]; asterisks: derived from *in-situ* TEM anneals (see text); open circle: Polk et al. [Pol78] The bottom part of the figure shows the equilibrium phase diagram of the Ti - Si system.

The stability of the amorphous alloy appears not to be related to prominent features in the phase diagram. Although the crystallization temperature is depressed near the composition of the compound phase $TiSi_2$, such a depression is not measured near to that of the other equilibrium compounds occurring in the phase diagram. Alloys with a composition near to that of a deep eutectic are frequently thought to be the most stable amorphous alloys [Hor80,Wal76]. This is also not reflected in Fig. 4.8: although in the Ti - Si binary system two deep eutectics are present no evidence for enhanced stability or enhanced crystallization temperatures is found in the neighbourhood of the Si–rich eutectic.

In a recent paper Buschow [Bus84] demonstrates similar effects in Zr-based binary amorphous alloys. The thermal stability of the tested alloys (as characterized by their crystallization temperature) shows no conformity with features in the phase diagram. For these Zr-based alloys not even a correlation between the activation energy and the crystallization temperature could be found. (In Fig. 4.8 both the activation energy and the crystallization temperature show a minimum for alloy compositions near that of $TiSi_2$.)

Predicted crystallization temperatures of amorphous alloys are derived from models which are based on a kinetic approach: crystallization occurs once the viscosity of the amorphous solid reaches some critical value [Bus80,Bus82]. This implies that the crystallization temperature is proportional to the activation energy needed to move the constituent atoms in the amorphous alloy. One expects that this activation energy varies smoothly with composition. This contrasts the present observations of the the sharp dip in crystallization temperature and activation energy near the composition of $TiSi_2$ in Fig. 4.8.

Deviations of the Buschow model are expected if there exists a crystallization path via a simple metastable crystalline solid solution with a free energy lower than that of the amorphous phase [Mie88]. The results presented in chapter 2 show that the mode of crystallization is polymorphous for the alloys with a composition close to that of the disilicide while it is eutectic for the Si–richer alloys and the Ti–rich alloy. Sofar only alloys with a composition close to that of the $TiSi_2$ stoichiometry were found to crystallize polymorphically. This would suggest that the pronounced minimum in crystallization temperature and activation energy near compositions of the disilicide may be due to the presence of an easy crystallization path leading to the C49 $TiSi_2$ solid solution. This was corroborated with the results of chapter3, where it was argued that the C49 $TiSi_2$ phase has a phase field of substantial width. Thus there exists a reasonable range of compositions for which the free energy of the crystalline solid solution is lower than that of the amorphous phase, thus allowing for a diffusionless transformation from the amorphous to the crystalline solid solution.

Ti–rich alloys were remarkably resistant to crystallization; even down to Si concentrations of 20 at. %. This is in agreement with work of Polk et al. [Pol78] and Suryanarayana et al. [Sur80] The latter investigators even succeeded in preparing amorphous alloys with only 15 at. % Si. The crystallization temperatures of Ti–rich alloys are even higher than the normal growth temperatures of *crystalline* silicides in diffusion couples [Hun83,Mur83] (see chapter 5). The fact that the crystallization temperature is higher than the growth temperature suggests that the mobility of Ti (required for crystallization) is much smaller than the mobility of Si (required for compound growth) Note that this is just one of the conditions which is necessary to form an amorphous phase in a diffusion couple [Bar87,Sar86,Bar86].

4.5 Conclusions

In this chapter, a detailed treatment of the kinetics of the different phase transformations in Ti - Si alloys of various compositions is reported. In this and many other investigations resistivity measurements are used to characterize a certain phase transformation in terms of Avrami kinetics. The assumption that the transformed fraction during a crystallization reaction is linear in the resistivity of the sample has been discussed. We presented an analyses of the systematic errors in kinetic parameters (like the Avrami exponent) if such a linear relation is not valid.

The various reactions to prepare the equilibrium C54 $TiSi_2$ polytype from an initially amorphous co-sputtered alloy were studied. The crystallization reaction to the C49 polytype of $TiSi_2$ is described remarkably well by a constant nucleation and growth rate of crystals in the amorphous matrix, which is in accordance with an earlier study by us employing *in-situ* annealing in an electron microscope. In later stages of the reaction or at higher temperatures an excess of Si, present as a solute in the Si–rich samples, is eliminated from the crystalline silicide by a diffusion controlled precipitation process, probably diffusion of Si through the crystalline C49 material. This process causes the room temperature resistivity to decrease with about a factor of 2. The final stage of the process is characterized by a constant nucleation and growth rate of C54 material in the C49 $TiSi_2$ matrix and a high activation energy of about 4.5 eV, indicating that nucleation is difficult. A model calculation starting from the classical nucleation theory supported this point of view. It was argued that thin film interfaces, grain boundaries and surfaces are responsible for small changes in the formation energy of a critical nucleus which leads to appreciable changes in C49 - C54 transformation temperature.

The composition dependence of certain kinetic parameters was addressed too. The crystallization temperature and the effective activation energy for crystallization of Ti - Si alloys with a composition in the range of 20 to 89 at. % Si was measured with the aid of ***in-situ*** resistivity measurements. Characteristic features of the equilibrium phase diagram are not reflected in the composition dependence of the crystallization temperature. The most stable amorphous alloy is not necessarily that with a composition close to the lowest eutectic in the equilibrium phase diagram. A minimum in the crystallization temperature and activation energy was found for alloys with compositions close to that of the disilicide. It was suggested that the suppression of the crystallization temperature and the associated minimum in the effective activation energy for the crystallization reaction is caused by the presence of a relatively easy diffusionless crystallization path.

Ti–rich alloys with a Si concentration smaller than about 60 at. % are found to be fairly stable in their amorphous state. The crystallization temperature (ranging from about 500 °C to about 700 °C) is in the same range or even larger than the temperatures which are normally quoted for growth of crystalline silicides in diffusion couples (about 500 °C). This fact is a necessary condition to be able to explain the observation that it is possible to grow an amorphous phase in a Ti - Si diffusion couple at slightly lower temperatures (about 400 °C). The growth of such an amorphous phase starting from crystalline materials will be treated in the next chapter.

Bibliography

[Ash80] M.F. Ashby, Acta Metall. **28**, 1085 (1980).

[Asp79] D.E. Aspnes, J.B. Theeten and F. Hottier, Phys. Rev. **20**, 3292 (1979).

[Asp82] D.E. Aspnes, Thin Solid Films **89**, 249 (1982).

[Avr39] M. Avrami, J. Chem. Phys. **7**, 1103 (1939).

[Avr40] M. Avrami, J. Chem. Phys. **8**, 212 (1940).

[Avr41] M. Avrami, J. Chem. Phys. **9**, 177 (1941).

[Bag80] J.E. Baglin, F.M. d'Heurle, W. Hammer and C.S. Petersson, Nucl. Instr. Methods **168**, 491 (1980).

[Bar85] J.C. Barbour, F.W. Saris, M. Nastasi and J.W. Mayer, Phys. Rev. **32**, 1363 (1985).

[Bar87] J.C. Barbour, R. de Reus, A.W. Denier van der Gon and F.W. Saris, J. Mater. Res. **2**, 168 (1987).

[Bru35] D.A.G. Bruggeman, Ann. Phys. (Leipzig) **24**, 636 (1935).

[Bus80] K.H.J. Buschow and N.M. Beekmans, Solid State Commun. **35**, 233 (1980).

[Bus82] K.H.J. Buschow, Solid State Commun. **43**, 171 (1982).

[Bus84] K.H.J. Buschow, J. Phys. F: Met. Phys. **14**, 593 (1984).

[Cho83] T.P. Chow and A.J. Steckl, IEEE Trans. Electron Devices **ED30**, 1480 (1983).

[Cot56] P.G. Cotter, J.A. Kohn and R.A. Potter, J. Am. Cer. Soc. **39** 11 (1956).

[Chr81] J.W. Christian, The Theory of Transformations in Metals and Alloys, 2nd ed. Part I (Pergamon, Oxford, 1981).

[Gre85] A.L. Greer, Proc 5Th Int. Conf. Rapidly Quenched Metals, Wúrzburg, Germany, Sept. 1984, ed. by S. Steeb and H. Warlimont, **1**, p 215 (North Holland, Amsterdam 1985).

[Hei81] M. von Heimendahl and G. Kuglstatter, J. Mater. Sci. **16**, 2405 (1981).

[Hen86] J.C. Hensel, J.M. Vandenberg, L.F. Mattheis, F.C. Unterwald and A. Maury, Mat. Res. Soc. Symp. Proc. **77**, 737 (1986) (Materials Research Society, Pittsburgh).

[Hen87b] J.C. Hensel, J.M. Vandenberg, F.C. Unterwald and A. Mauri, Appl. Phys. Lett. **51**, 1100 (1987).

[Heu82] F.M. d'Heurle in 'VLSI Science and Technology',ed. by C. Dell'Oca and W.M. Bullis (Electrochem. Soc., Pennington 1982).

[Heu88] F.M. d'Heurle, J. Mater. Res. **3**, 167 (1988).

[Hol87] K. Holloway and R. Sinclair, J. Appl. Phys. **61**, 1359 (1987).

[Hor80] E. Hornbogen and I. Schmidt, in Liquid and Amorphous Metals, edited by E. L scher and H. Coufal (Sythoff and Noordhoff, Alphen aan den Rijn, The Netherlands, 1980).

[Hou86] H.J.W. van Houtum and I.J.M.M. Raaijmakers, Mater. Res. Soc. Symp. Proc. **54**, 37 (1986).

[Hou87] H.J.W. van Houtum, I.J.M.M. Raaijmakers and T.J.M. Menting J. Appl. Phys. **61**, 3116 (1987).

[Hov88] L.J. Van Den Hove, PhD thesis, University of Leuven (Leuven, Belgium 1988).

[Hun83] L.S. Hung, J. Gyulai, J.W. Mayer, S.S. Lau and M.A. Nicolet, J. Appl. Phys. **54**, 5076 (1983).

[Joh39] W.A. Johnson and R.F. Mehl, Trans. Am. Inst. Min. (Metall.) Engrs. **135**, 416 (1939).

[Kau79] L. Kaufman, CALPHAD **3**, 45 (1979).

[Kem82] M.J.H. Kemper and P.H. Oosting, J. Appl. Phys. **53**, 6214 (1982).

[Kos81] U. Kóster and U. Herold in 'Glassy Metals I, Ionic Transport, Electronic Transport and Crystallization', ed. by H.J. Gúntherodt and H. Beck, p. 225 (Springer Verlag, Berlin 1981).

[Lac86] D.S. McLachlan, J. Phys. C: Solid Stat Phys. **19**, 1339 (1986).

[Lan52] R. Landauer, J. Appl. Phys. **23**, 779 (1952).

[Lan78] R. Landauer, Proc. of the First Conf. on the Electrical and Optical Prop. of Inhomogeneous Media, Columbus OH, 7 - 9 sept. (1977), AIP Conf. Proc. **40**, 2 (1978).

[Lav39] F. Laves and H.J. Wallbaum, Z. Kristallogr. **101**, 78 (1939).

[Mae86] K. Maex, R.F. de Keersmaecker, M. van Rossum, W.F. van der Weg and G. Krooshof, proc. conf. Ion Beam Mixing and Modification of Materials, Catania (Italy) (1986).

[Mae87] K. Maex, R.F. de Keersmaecker, M. van Rossum, W.F. van der Weg and G. Krooshof, Proc. Workshop on Refr. Metals and Silicides Aussois (France) 1987, published in: le Vide, les Couches Minces **42**, 141 (1987).

[Mae88] K. Maex, PhD thesis, University of Leuven (Leuven, Belgium 1988).

[Mas87] Th.B. Massalsky, J.L. Murray, L.H. Benett and H. Baker, eds., 'Binary Alloy Phase Diagrams' **2** (Am. Soc. Metals., Metals Park, Ohio 1986).

[Mie88] A.R. Miedema and A.K. Niessen, to be published, J. Jap. Met. Soc. (1988).

[Mur83] S.P. Murarka, 'Silicides for VLSI Applications' (Ac. Press, New York, 1983).

[Mur75] L.E. Murr, 'Interfacial Phenomena in Metals and Alloys' (Addison-Wesley Publ. Comp., Reading, Ma 1975).

[Nav85] F. Nava, G. Ottaviani and G. Riontino, Mater. Lett. **3**, 311 (1985).

[Nav85a] F. Nava, T. Tien and K.N. Tu, J. Appl. Phys. **57**, 2018 (1985).

[Nav85b] F. Nava, G. Ottaviani and G. Riontino, Materials Lett. **3**, 311 (1985).

[Nav86a] F. Nava, P.A. Psaras, H. Takai, K.N. Tu, S. Valeri and O. Bisi, J. Mater. Res. **1**, 327 (1986).

[Nav86b] F. Nava, B.Z. Weiss, K.N. Tu, D.A. Smith and P.A. Psaras, J. Appl. Phys. **60**, 2445 (1986).

[Nic83] M.A. Nicolet and S.S. Lau, in VLSI Electronics,**6**, edited by N.G. Einspruch (Academic, New York, 1983) .

[Pol78] D.E. Polk, A. Calka and B.C. Giessen, Acta Metallurgica **26**, 1097 (1978).

[Raa86] The heat of crystallization of a $TiSi_2$ alloy was measured by differential scanning calorymetry. It was found to be (11 ± 2) kJ/mol (unpublished result 1986).

[Raa87a] I.J.M.M. Raaijmakers, A.H. Reader and H.J.W. van Houtum, J. Appl. Phys. **61**, 2527 (1987).

[Raa87b] I.J.M.M. Raaijmakers, A.H. Reader and H.J.W. van Houtum, Proc. European Workshop on Refr. Metals and Silicides, Published in : le Vide, les Couches Minces **42**, 75 (1987).

[Raa88a] I.J.M.M. Raaijmakers, A.H. Reader and P.H. Oosting, J. Appl. Phys. **63**, 2790 (1988)

[Raa88b] I.J.M.M. Raaijmakers, P.H.Oosting and A.H. Reader, Mater. Res. Soc. Symp. Proc. XX, xxx (1988) (Materials Research Society Pittsburgh).

[Raa88c] The same amorphous Si layers on SiO_2 were heated with a constant heating rate (0.1 K/s) in a vacuum furnace while monitoring the desorption of argon with a mass spectrometer. The single desorption peak at 550 ^oC was associated with crystallization of the Si layer. (unpublished result.)

[Ran80] S. Ranganathan, J.C. Claus, R.S. Tiwari and M. von Heimendahl, Proc. Conf. Metallic Glasses, Budapest (1980), Vol. **2**, p 327 (1980).

[Ran81] S. Ranganathan and M. von Heimendahl, J. Mater. Sci. **16**, 2401 (1981).

[Sar86] F.W. Saris, L.S. Hung, M. Nastasi and J.W. Mayer, Mater. Res. Soc Symp. Proc. **54**, 81 (1986).

[Sur80] C. Suryanarayana, A. Inoue and T. Masumoto, J. Mat. Sci. **15**, 1993 (1980).

[Tie83] T. Tien, G. Ottaviani and K.N. Tu, J. Appl. Phys. **54**, 7047 (1983).

[Tho87] R.D. Thompson, H. Takai, P.A. Psaras and K.N. Tu, J. Appl. Phys. **61**, 540 (1987).

[Wal76] R.M. Walser and R.W. Bene, Appl. Phys. Lett. **28**, 624 (1976).

[Wei86] B.Z. Weiss, K.N. Tu and D.A. Smith, Acta Metall. **34**, 1491 (1986).

Chapter 5

Reactions in Titanium Silicon Thin Film Diffusion Couples

5.1 Introduction

5.1.1 General

The reaction of Ti thin films with Si is studied extensively because of the application of $TiSi_2$ as a low resistivity and high temperature resistant material in integrated circuits. Both the reaction of Ti with crystalline Si (self aligned ohmic contacts [Mur83] or Schottky barrier diodes [Rho80]) and the reaction of Ti with sputter-deposited Si layers (local 'strap' interconnection [Jon87,Won87,Hou88]) are of importance.

There also exists a considerable scientific interest in reactions in metal - Si thin film diffusion couples. Whereas in a bulk diffusion couple (typical dimensions exceeding 10 μm) all phases as predicted by the equilibrium phase diagram are generally present, in a thin film diffusion couple (thickness smaller than 1 μm) only one or two phases are usually found. These phases might also be of a metastable nature and thus are not necessarily present in the equilibrium phasediagram. Attempts to predict which phase or phases actually will be found are formulated more or less successful in semi-empirical rules for first phase nucleation [Wal76,Ben87,Ron83,Pre84] or solutions of the diffusion equation with the appropiate boundary conditions [Gos82,Wil86,Geg80].

In the next section is presented a comprehensive review of the relevant literature on the reactions occurring in the Ti - Si system. The evident ambiguities and questions lead to the formulation of the purpose of the investigations described in this chapter.

5.1.2 Reactions between Si and Ti layers: a review

When the crystalline phases in a thin film diffusion couple after reaction are to be identified one relies on X-ray or electron diffraction. In the not so distant past, such phase identification led to the conclusion that metal rich crystalline phases like Ti_5Si_3, Ti_5Si_4 or TiSi were present in considerable amounts [Liu79,Mur80,Ber84,Kik87,Ost83]. It is now known that $TiSi_2$ shows polytypism and may crystallize in two slightly different crystal structures. These structures are commonly referred to as the C49 $TiSi_2$ phase ($ZrSi_2$ structure [Cot56]) and the C54 $TiSi_2$ phase ($TiSi_2$ structure [Lav39]). As has been pointed out by Beyers et al. [Bey85], most of the reflexes which were originally assigned to metal rich phases really originated from the C49 $TiSi_2$ phase. It is suspected that the lattice constants as determined by Cotter et al. [Cot56] are obtained from material which was contaminated with Al and hence are slightly different for uncontaminated C49 $TiSi_2$ material. The lattice constants for pure C49 $TiSi_2$ were determined by Beyers et al. [Bey85] and more accurate by van Houtum et al. [Hou86].

It is generally agreed upon that at temperatures in excess of about 500 °C the C49 polytype of $TiSi_2$ is the main growing phase in Ti - Si thin film diffusion couples [Hun83,Hou86,Aum85,Bey85,Hen87,Iye85]. Although most reported diffraction patterns can now be indexed correctly, depending on anneal treatment a minor amount of the monosilicide is sometimes found to be present [Hou86,Hun83,Bey85]. The TiSi phase is however always reported to be taken over by the faster growing C49 phase in later stages of reaction. At higher temperatures the C49 polytype transforms to the equilibrium C54 polytype of $TiSi_2$. The temperature at which this occurs is reported to depend on impurities [Bey85], film thickness [Hou86] and grain size [Hou87].

Ti and Si show reactivity at temperatures well below those required for silicide growth [But84,Rub86,Nem85,Loe85,Idz86] Deposition of Ti on atomically clean Si at room temperature is reported to result in a measurable reaction. Van Loenen et al. [Loe85] concluded from channeling and blocking medium energy ion scattering that deposition of Ti at room temperature did result in intermixing of the first two to three monolayers of deposited material. The resulting compound had a composition of about 50 at. % Si, i.e. close to that of the monosilicide.

Butz et al. [But84] reported extended intermixing of Ti deposited on clean Si at temperatures as low as 300 °C. Rubloff et al. [Rub86] point out that the rate of the low temperature reaction as described by Butz et al. is much too large to be associated with normal interfacial silicide formation. It was suggested that the high reactivity at low temperatures is due to grain boundary diffusion and local silicide formation at grain boundaries. Nemanich et al. [Nem85] concluded from Raman spectroscopy that Ti and crystalline Si start to intermix at temperatures of about 400 °C. No silicides were formed at these low temperatures as was concluded from the absence of silicide Raman peaks. Idzerda et al. [Idz86] showed that intermixing of Ti and Si starts after heating to about 250 °C. Stoichiometric silicide layers were obtained at temperatures around 400 °C.

Recently Holloway et al. [Hol87] reported on the character and the amount of intermixing at low temperatures. Holloway et al. described the interactions during rapid thermal annealing in thin (5 nm) sputter-deposited Ti - Si multilayers. The average composition of their multilayers was either 40 at. % Si or 60 at. % Si, i.e. symmetrical around the composition of the monosilicide. Although significant inter-diffusion occurred over distances of the order of 5 nm at low temperatures (455 °C) crystalline silicides only nucleated at temperatures in excess of 500 °C. They concluded that the growth of crystalline silicides was preceeded by the formation of an amorphous alloy of approximately equiatomic composition.

Maex et al [Mae88,Mae86,Mae87] reported the sequence of phase formation in Ti - crystalline Si binary diffusion couples during ion beam mixing with 260 keV Xe^+ ions. It was found that ion beam mixing at substrate temperatures in the range of 100 °C to 300 °C induced the formation of an amorphous phase of approximate composition Si/Ti = 4/3. Implantation at higher temperatures caused the formation of crystalline material, first with the Ti_3Si_4 stoichiometry and at higher temperatures with the stoichiometry of TiSi (about 400 °C) and $TiSi_2$ (between 450 °C and 500 °C)

The growth kinetics of Ti silicides is investigated systematically by several authors. Reproducible results were first reported by Hung et al. [Hun83]. Diffusion controlled growth of the disilicide is found if the reaction takes place between Ti and evaporated (amorphous) Si in the temperature range from 475 °C to 550 °C. It appeared that the reaction between Ti and crystalline Si required higher growth temperatures and could not be reproduced easily. These effects were attributed to impurities at the Ti - crystalline Si interface. Aumann et al. [Aum85] conclude that diffusion controlled growth of $TiSi_2$ occurs upto temperatures of 650 °C.

It is the commonly accepted view that during the diffusion controlled growth of $TiSi_2$ the main diffusing species is the Si atom [Chu74]. Maex [Mae88] recently performed marker experiments under conditions of ion beam mixing in the temperature regime from 100 °C to 300 °C. Xe and W markers were used. Diffusion controlled growth of an amorphous silicide with approximate equiatomic composition was reported. Maex concluded that in this lower temperature range Si is the main moving species too. From these studies we expect that in the entire relevant temperature range (100 °C to 650 °C) Si will be the main moving species during silicide formation.

It is known that typical wet-chemical cleaning procedures [Hen72,Tau85] leave C and O on the Si surface in the monolayer regime. If the cleaning procedure incorporates an HF dip etch to remove the native oxide, F may be present in the submonolayer regime [Ker72,Raa88c]. Several investigators addressed the effect of impurities on the reactions between Ti and Si. A detailed study on the effect of interfacial impurities on Ti - Si reactions was reported by Taubenblatt [Tau85,Tau82,Tau86]. Studies undertaken at other institutes [Rub86,Lir85,Hun80] are in essential agreement with the work of Taubenblatt. An important result of these studies is that neither C [Tau82] nor O [Tau86] impede the growth of Ti silicides. Upon room temperature deposition of Ti, the Ti breaks the Si - C or Si - O bonds to form a Ti - C or Ti - O solid solution. C and O both are soluble and mobile in Ti at fairly low temperatures i.e. much below the temperature at which an interfacial silicide is formed over reasonable distances [Hou86]. Thus a clean interface between Ti and Si is always present before silicide formation starts, although the Ti itself may be contaminated. Of course the above statement is not valid for severely contaminated surfaces which may result from careless cleaning procedures. It is for example reported [Tau82] that as little as 0.5 nm Si_3C_4 may completely inhibit the reaction between Ti and Si. The effects of such severe interface contamination will not be discussed.

It is reported by several investigators [Hou86,Ber84,Mer84] that C and O are 'snow-ploughed' by the advancing reaction front into the unreacted Ti layer. As long as the concentration of the impurities is below the solubility limit the reaction rate is found to be about equal to the rate in uncontaminated samples. This is consistent with diffusion through the silicide being the rate limiting step during growth of the disilicide phase. Apparently common impurities like C and O do not have a large effect on the rate of reaction and one is tempted to reconsider the conclusion of Hung et al. [Hun83] that the presence of these impurities at the Si - Ti interface was the primary cause of the bad reproducability and higher reaction temperatures in the case of the reaction of Ti with crystalline Si.

5.1.3 Purpose of this Study

The above described results from literature are all evident of a considerable low temperature reactivity in the Ti - Si system. Differences in the reaction of Ti with amorphous or crystalline Si are reported for which a solid explanation is still sought. Ion beam mixing of Ti on crystalline Si and the reaction of Ti with amorphous Si is reported to result in the growth of an amorphous alloy. Upon thermal reaction of Ti with crystalline Si it is not clear what the first reaction product consists of and at what temperature it is formed. In this chapter, investigations on the reactions in thin film Si - Ti diffusion couples are reported. The objectives of our work are two fold.

Firstly, we intend to study the growth of an amorphous Ti - Si phase in fairly thick sputter-deposited Ti and αSi layers. Rather than using very thin multilayers [Hol87] a three layer Si - Ti - Si stack is used which contains excess Si as compared to the disilicide. The growth kinetics and the composition of the amorphous silicide will be investigated. We will show that an amorphous silicide may be grown to fairly large thicknesses even without the use of ion beam mixing.

Secondly, we will compare the reactions occurring in Ti - amorphous Si and those in Ti - crystalline Si diffusion couples. An explanation for the ambiguities and bad reproducibility reported in literature will be sought.

5.2 Experimental

The reactions between amorphous Si and polycrystalline Ti were studied with the layer structure defined in Fig. 5.1a. 100 mm diameter Si(100) wafers were thermally oxidized to form 50 nm of SiO_2. The layer stack always comprized of a Ti layer of thickness d embedded between two Si layers of approximate thickness $1.5 * d$. The ratio of the thicknesses of the Si and Ti layers (1.5) was chosen such as to have an excess of deposited Si compared to the composition of the disilicide. After complete reaction of the Ti layer with the Si layers to the disilicide (with supposedly equal reaction rates on both Ti - Si interfaces) a layer of Si of approximate thickness $0.4 * d$ would be left on both sides of the silicide layer.

The reactions between Ti and mono-crystalline Si were investigated by means of the layer structures defined in Figs. 5.1b and c. Samples shown in Fig. 5.1b consisted of Ti layer of nominal thickness 20 nm, covered with a 60 nm sputter-deposited αSi layer. Similar to samples (a), the ratio of Ti and Si thickness was chosen such as to have excess Si in the deposited layer. In samples (c) no capping layer is present.

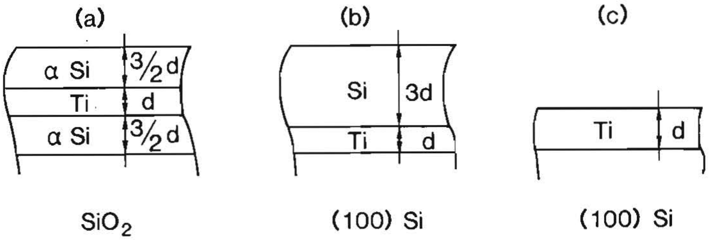

Fig. 5.1. Layer structures used to investigate Ti - Si reactions. αSi denotes a sputter-deposited (amorphous) Si layer. Reference will be made to different samples by their Ti thickness '*d*' and the structure: (a) trilayer samples; (b) bilayer samples and (c) single layer samples.

The last step in the cleaning procedure before Ti deposition on crystalline Si consisted of a dip etch in 1 % HF/H_2O solution followed by rinsing in de-ionized water and spin drying in N_2. It has been shown [Tau85,Hen72,Hun80] that this procedure leaves about equal amounts of C and O upto a total of 0.5 to 1.5 * 10^{15} at./cm^2. F is present in the submonolayer regime [Ker72]. Estimates from secondary ion mass spectroscopy measurements on a Ti/Si interface show a maximum of about 0.01 monolayer of F [Raa88c]. To remove these residual surface impurities some wafers were sputter-etched *in-situ* before Ti deposition. In our deposition system this procedure leads to amorphization of a thin (2 - 3 nm) surface layer and implantation of some Ar (typically in the range of 5 * 10^{14} cm^2) [Bos87].

Ti and Si layers were deposited in a load locked turbomolecular pumped RF diode sputtering system (Perkin Elmer 4400). The vacuum chamber was equipped with a Meissner trap. The base pressure was in the low 10^{-5} Pa range; the working gas pressure (Ar) during sputtering was 0.7 Pa. The substrates were not intentionally heated before or during deposition; the substrate temperature was estimated not to exceed 60 °C. Ti and Si layers were deposited sequentially without breaking the vacuum.

Samples were annealed in a turbo-molecular pumped high vacuum furnace with a base pressure in the 10^{-5} Pa range. Temperatures were in the range of 300 °C to 650 °C, the anneal time ranged from 1 h to 56 h. In addition to these furnace anneals, some samples were *in-situ* annealed in a Philips EM300 Transmission Electron Microscope (TEM), equipped with a W-filament heated hot stage. For these experiments a trilayer stack like in Fig. 5.1 was deposited on specially prepared electron transparent Si_3N_4 substrates [Jac86] (see Fig. 2.1) allowing direct plan view observation of the films in the TEM without additional sample processing during annealing

[Raa87a,Raa87b] (see chapter 2).

The actual thickness of the deposited layers was measured with Rutherford Backscattering Spectrometry (RBS) and cross-sectional transmission electron microscopy (TEM). Reactions between the Si/Ti layers were analyzed with RBS, Auger Electron Spectroscopy (AES) combined with sputter-depth profiling, X-ray diffraction (XRD) and cross-sectional TEM.

Rutherford backscattering spectra were measured with an incident 2 MeV He ion beam and (usually) a scattering angle of 170^o. The angle of incidence was set according to the desired depth resolution and is indicated in the RBS spectra where ever relevant. The backscatterred spectra were simulated with the RUMP simulation program [Doo85].

Auger analysis was done with a PHI 600 Scanning Auger Microprobe. The 3 keV, 1 μA primary electron beam was rastered over a 0.01 mm^2 area. Sputter-depth profiling was performed with a 3 keV Ar^+ ion beam rastered over a 2 mm^2 area, the current density being about 80 $\mu A/cm^2$. Electron and ion beam were 30^o and 55^o off normal to the sample surface respectively.

X-ray diffraction analysis was performed in a conventional 2Θ diffractometer (Philips) equipped with a $CuK\alpha$ source. In order to obtain cross-sectional TEM specimens standard preparation techniques, including ion milling, were used. Specimens were observed in a Philips EM400 microscope, operating at 120 kV.

5.3 Results and Discussion: Ti - amorphous Si

5.3.1 As-deposited Layers

The thicknesses of the layers used in the trilayer stacks (Fig. 5.1a) as measured with cross-sectional transmission electron microscopy (TEM) and Rutherford backscattering spectrometry (RBS) are listed in Table 5.1. In the remainder of this section we will refer to specific samples with their nominal Ti layer thickness as defined in the first column of Table 5.1. The thickness determined from the RBS data are systematically smaller than those determined from TEM micrographs. This is so because the RBS thickness is calculated assuming bulk molar volumes for Ti ($17.6 * 10^{-24}$ cm^3) and diamond Si ($20 * 10^{-24}$ cm^3) which is not true for thin films deposited at low substrate temperatures. The overall composition of our trilayer stacks as determined by RBS is between Ti/Si = 1/2.4 and Ti/Si = 1/2.9, dependent on the type of sample, but excess deposited Si is always present as compared the composition of the disilicide.

X-Ray diffraction (XRD) of the as-deposited samples showed a strong Ti (002) reflection. Cross-sectional TEM revealed columnar grains. So it can be concluded that the Ti layer is polycrystalline, strongly textured with the {001} planes parallel to the substrate surface. The Si layers were found to be amorphous according to XRD and TEM. The amorphous Si layers will hereafter be denoted with αSi layers. Impurity analyses with AES showed the concentration of C and O to be below the detection limit of the Auger system, which is estimated to be about 0.5 at. %. Moreover, Auger depth profiling showed no significant amounts of C and O on the Ti - αSi interfaces (see for example the Auger depth profiles discussed in the next section).

samples	**Si thickness (nm)**		**Ti thickness (nm)**	
	TEM	RBS	TEM	RBS
15 nm	...	20 ± 3	...	15 ± 2
20 nm	36 ± 2	30 ± 3	23 ± 1	21 ± 1
60 nm	...	98 ± 8	...	58 ± 3
100 nm	...	130 ± 10	110 ± 10	100 ± 5

Table 5.1: Layer thicknesses of the trilayer samples measured with TEM or RBS. The Si thickness is that of a single layer of Si.

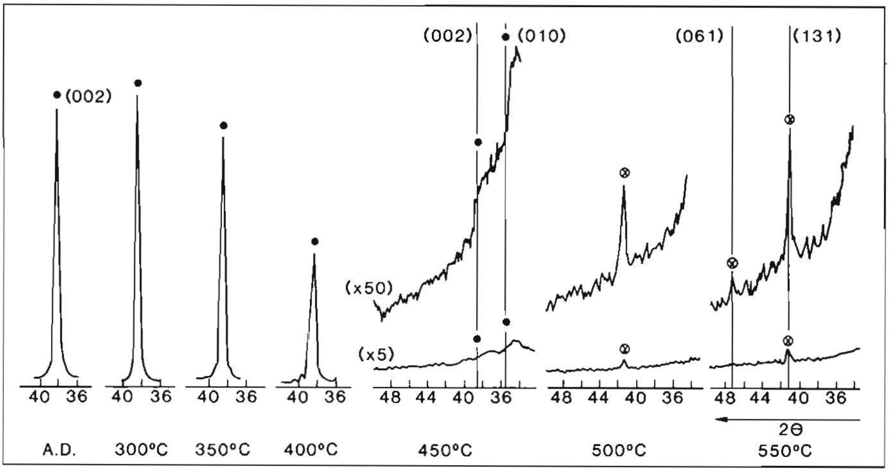

Fig. 5.2. XRD patterns of the 20 nm samples annealed at different temperatures. Solid dots: Ti reflection, crossed circles: C49 $TiSi_2$ reflection. Note the strong decrease of Ti diffraction intensity with anneal temperature and the near absence of crystalline Ti and crystalline C49 $TiSi_2$ in the sample annealed at a temperature of 450 °C.

5.3.2 Reaction of Ti and αSi Layers

The reactions in the αSi - Ti - αSi stacks were first studied with XRD. The 20 nm samples (see Table 5.1) were annealed during 1 h at temperatures ranging from 300 °C to 550°C. The relevant results are recorded in Fig. 5.2. The Ti(002) reflection drastically decreased in intensity after 1 h anneals at temperatures exceeding 350 °C. After a 450 °C, 1 h anneal the initially strong Ti(002) reflection has almost completely vanished. Apparently, large amounts of the poly-crystalline Ti layer were consumed to form a layer which is disordered according to XRD. We observed that the remnants of the Ti reflections after a 450 °C anneal shifted to larger interplanar spacings, possibly caused by Si incorporation in the Ti lattice. It is also noted that considerable broadening of the reflections occurs. Annealing the layers at higher temperatures ($\geq$ 500 °C) caused the nucleation of C49 disilicide as follows from the appearance of the (131) and (061) reflections of the C49 $TiSi_2$ phase [Bey85,Hou86].

The results obtained by *in-situ* TEM annealing of the 15 nm sample (see Table 5.1) are consistent with the XRD results. Fig. 5.3 shows bright field (BF) micrographs and selective area electron diffraction (SAD) patterns taken at different temperatures. The BF micrograph of the as-deposited sample (Fig. 5.3a) shows diffraction rings from polycrystalline Ti in the

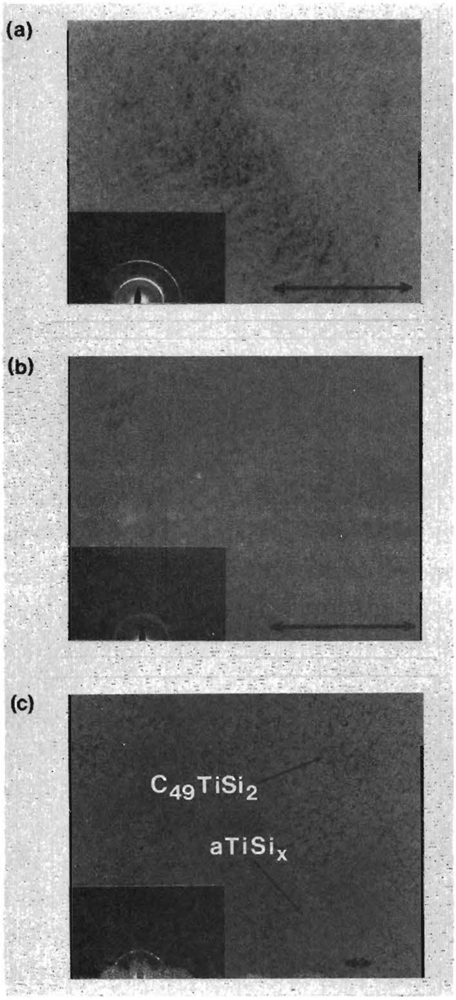

Fig. 5.3. Bright field micrographs and selective area diffraction patterns obtained while heating the 15 nm sample in situ in a TEM. (a) As deposited; (b) 450 °C; (c) 550°C. The disappearance of Ti crystalline material and the growth of amorphous material is evident from the BF micrograph and the SAD pattern of the 450 °C sample (b). C49 $TiSi_2$ crystallites nucleate and grow in the amorphous material at temperatures of approximately 500-550 °C. The arrows correspond to a length of 1 μm.

selective area diffraction pattern. Diffuse bands originating from the αSi layers are also seen in the SAD pattern. The bright field micrograph contains a black speckled contrast which is due to Ti crystallites. At 450 °C (Fig. 5.3b) the poly crystalline Ti has disappeared as indicated by the disappearance of the black contrast in the bright field micrograph and the diffraction rings in the selective area diffraction pattern. Instead, the pattern now shows diffuse diffraction bands indicative of the formation of amorphous material. The 'interplanar spacings' calculated from the diameters of the diffuse bands agree with the values quoted by Holloway et al. [Hol87]: 0.22, 0.15 and 0.12 nm respectively and they cannot be attributed to Ti or any known Ti - Si compound. Of these bands the one corresponding to the spacing of 0.22 nm is clearly visible in the diffraction pattern of Fig. 5.3, the other ones are very weak. Further heating of the sample induced the formation of crystalline material at approximately 530 °C (Fig. 5.3c). The selective area diffraction pattern in this figure indicates the presence of C49 $TiSi_2$ [Bey85,Hou86].

A more detailed study on the inter-diffusion of the Ti - Si layers was performed by Auger Electron Spectroscopy (AES) combined with sputter-depth profiling and cross-sectional TEM. Fig. 5.4 shows AES depth profiles of the Si_{LMM} (91 eV), the Ti_{LMM} (386 eV, Ti_I) and the O_{KLL} (510 eV) peak to peak intensities for the 20 nm samples, as-deposited and annealed at 400 °C, 450 °C and 500 °C respectively. The corresponding TEM cross-section micrographs are shown in Fig. 5.5. The shape of the Si profile in the as-deposited sample (Fig. 5.4a) suggests a Ti - Si interaction limited to a thickness of approximately 2.5 nm. This is also evident from the TEM cross-section in Fig. 5.5a. The reaction of Ti and αSi in the as-deposited sample may be caused by energetic heavy particle bombardment during sputter-deposition (like Ar ions which are accelerated over the substrate dark space [Cha80]). A similar limited reaction was also reported by Holloway et al. [Hol87] in their sputter-deposited multilayers but not by Brasen et al. [Bra86] who prepared similar multilayers by evaporation.

After a 1 h anneal at 400 °C shoulders develop in the Si and Ti profile (Fig. 5.4b) indicating a more extensive inter-diffusion. This is also seen from the TEM micrograph in Fig. 5.5b. Ti - Si alloyed layers of approximately 8 nm thickness are found on both Ti - αSi interfaces. The planar growth of the reacted layers indicates that transport of one of the reactants through the growing layer is the rate limiting process. In Fig. 5.5b no bright field contrast is observed within the formed compound. Additionally, selective area diffraction patterns show diffuse rings as in Fig. 5.3b. Both of these observations are consistent with the X-ray diffraction results and the *in-situ* TEM heating experiments which showed that the reacted layers are

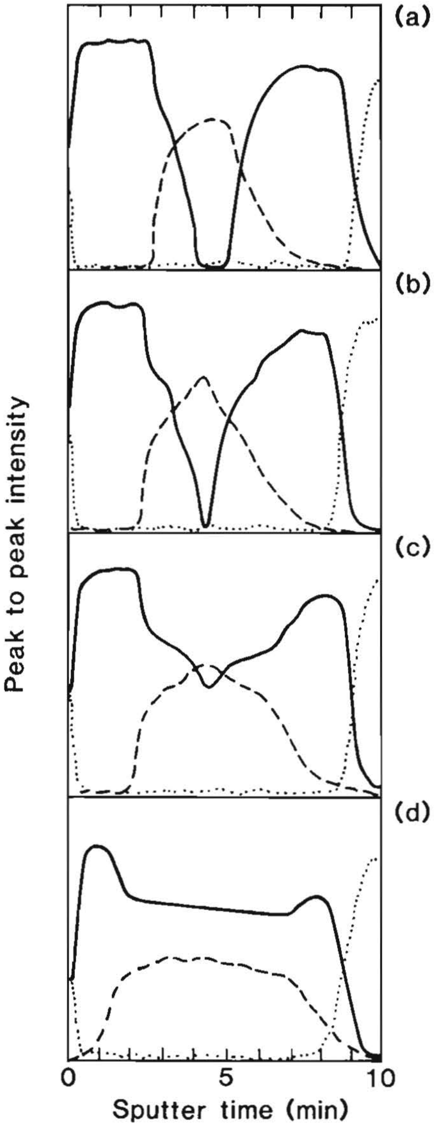

Fig. 5.4. AES depth profiles of the 20 nm samples annealed during 1 h at different temperatures: (a) as-deposited; (b) 400 °C; (c) 450 °C;(d) 500°C. (Solid lines: Si; dashed lines: Ti; dotted lines: O.)

amorphous. After a 450 °C, 1 h anneal (Fig. 5.4c and Fig. 5.5c) the Ti layer is nearly completely consumed to form an amorphous Ti - Si (αTiSi$_x$) alloy. Some remnants of crystalline material are present in the center of the trilayer stack alloy. (We will denote the formed layer with αTiSi$_x$ because the composition is not known yet.)

Increasing the anneal temperature to 500 °C causes a crystalline compound to nucleate at the top αSi - αTiSi$_x$ interface (Fig. 5.5d). At the lower αSi - αTiSi$_x$ interface some amorphous alloy is still present. The crystalline phase was identified from a selective area diffraction pattern as the C49 polytype of $TiSi_2$. The Auger depth profile (Fig. 5.4d) shows that Si is now present throughout the entire layer. After anneals at higher temperatures (550 °C) all Ti was consumed to form the C49 disilicide.

From the relatively flat Auger profiles after anneals at 500 °C (Fig. 5.4d) and 550 °C (not shown) the stoichiometry of the crystalline reacted layers is easily obtained. (The determination of the composition of the amorphous phase will be addressed in detail in section 5.3.4, the Auger spectrometer was calibrated as described in that section.) One derives for the composition in the crystalline reacted layers: $TiSi_{1.8 \pm 0.1}$ or (64 ± 2) at.% Si for the (500 °C) annealed sample and $TiSi_{1.9 \pm 0.1}$ or (66 ± 2) at.% Si for the 550 °C annealed sample. Although the composition of the sample annealed at 550 °C is close to that of the disilicide, the sample annealed at 500 °C is somewhat richer in Ti, possibly due to the presence of a minor amount of Ti-rich material or a slight deviation from stoichiometry of the C49 $TiSi_2$

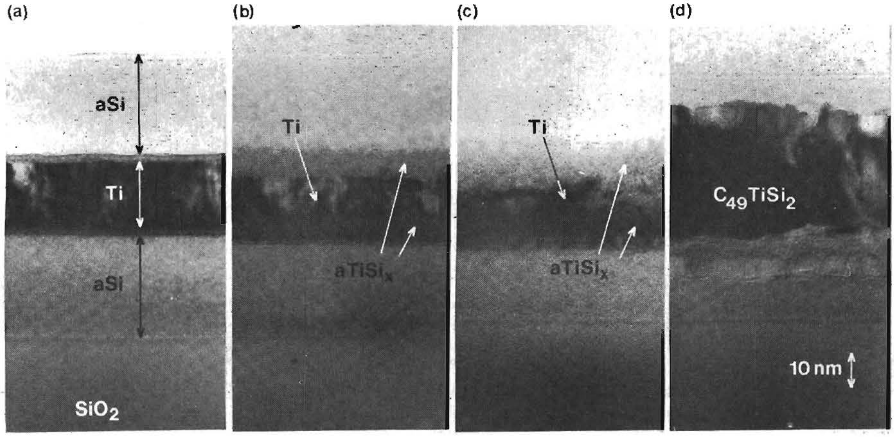

Fig. 5.5. TEM cross-section micrographs of 20 nm samples annealed during 1 h at different temperatures: (a) as-deposited; (b) 400 °C; (c) 450 °C; (d) 500 °C (see also Fig. 5.4). Note the Kirkendall voids on both αSi-αTiSi$_x$ interfaces.

phase, see chapter 3. Similar results were obtained if a different analyses using TEM cross-section micrographs was applied (see section 5.3.4)

At this point note the void like contrast along the αSi - αTiSi$_x$ interfaces in Fig. 5.5b, c and d. It can be observed that the contrast (or 'greyness') in between the voids is much more similar to the contrast of the amorphous silicide than to that of the αSi, therefore we conclude that the voids are actually situated with in the amorphous silicide layer. It is known [New86,Sch85,Joh86] that the growth of amorphous layers by solid state reaction from crystalline materials is usually accompanied by the growth of Kirkendall voids at the interface between the fast moving species and the amorphous phase. Therefore we suggest (as did Holloway et al. [Hol87]) that the observed contrast along the αSi - αTiSi$_x$ interface are Kirkendall voids.

Kirkendall voids are formed during the growth of a binary alloy when ever there is a large difference in diffusion flux of the two constituents due to a chemical concentration gradient. In our case, Si is the dominant moving species [Mae88] and the flux of Si atoms cannot be balanced by an opposite flux of Ti atoms. In the case of a vacancy diffusion mechanism, conservation of lattice sites requires a vacancy flux to compensate for the Si flux. Note that the definition of 'vacancy' or 'lattice site' in an amorphous alloy is a little bit vague. For our purpose the definition of a 'vacancy' in an amorphous alloy as a hole of the size of the smallest (Si) atom (as defined by Buschow [Bus81,Bus82] in his study on the crystallization of amorphous alloys) will do. In a crystalline solid, surfaces, dislocations and grain boundaries may act as possible sinks for the vacancy flux [Bar52]. In an amorphous alloy no extended defects are present, and 'vacancies' can only be eliminated at an interface or surface.

We observed Kirkendall voids within the αTiSi$_x$ alloy at the Si - αTiSi$_x$ interface. The Si layer is observed to remain amorphous after the anneal at 550 ^{o}C which implies that the mobility of 'vacancies' in the αSi layer is much smaller than their mobility in the αTiSi$_x$ layer at this temperature, otherwise the Si would crystallize [Bus81,Bus82]. The 'vacancies' thus can not reach the surface of the sample or the αSi - SiO$_2$ interface and a super-saturation of 'vacancies' near the αSi - αTiSi$_x$ interface results. This super-saturation can be decreased by the nucleation and growth of voids. Although Si must be mobile in the amorphous alloy to grow it to the observed dimensions, the amorphous alloy does not crystallize because crystallization requires motion of both Ti and Si atoms [Bar87,Sar86,Bar86]

The nucleation and growth of voids at the Si - TiSi$_x$ interface is of paramount importance in technology. We observed a loss of adhesion between thicker (100 nm) Ti and αSi layers which were annealed for long times

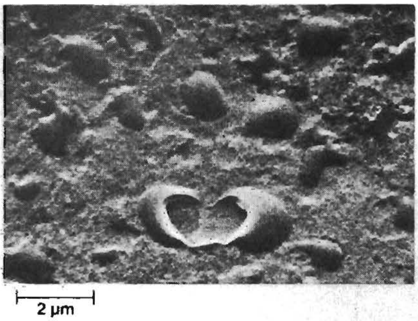

Fig. 5.6. SEM micrograph of a 40 nm Ti/70 nm αSi diffusion couple on an oxidized Si substrate, annealed at 650 °C during about 10 min. showing typical 'blister' like defects.

at temperatures exceeding 400 °. This loss of adhesion may be caused by a coalescence of the voids to a continuous layer. It is thought that the occurrence of the typical morphological defects which are usually observed after the reaction between αSi and Ti (so-called 'blisters' [Hou88]) are related to the nucleation and growth of these voids and the presence of entrapped gasses in the sputter-deposited layers. Fig. 5.6 shows a scanning electron microscopy (SEM) micrograph of such defects on a reacted Ti/αSi diffusion couple. After deposition the present Si layers contain a few at. % Ar. It was found with Rutherford backscattering spectrometry (not shown) that after reaction at 450 °C the argon was forced out of the silicide phase and had concentrated at the αSi - αTiSi$_x$ interfaces, i.e. at the location of the voids. The argon concentration in the unreacted Si did not change upon anneal at these temperatures. Starting from the assumptions that the as-deposited αSi layer contains a conservative 1 at. % Ar, and that after reaction this argon is concentrated in the voids as an ideal gas one may calculate that during reaction the pressure in the voids may rise to enormously high values (exceeding a few 100 bar). These high pressures may be able to lift or break the remainder of the Si capping layer.

5.3.3 The Growth Kinetics of Amorphous Silicide

We will now describe the dependence of the amorphous silicide thickness on anneal time. Two questions are dealt with in this section. Firstly, is the growth of αTiSi$_x$ controlled by diffusion of Si through the growing amorphous layer (as was found by Maex et al. [Mae87] during ion beam mixing of Ti layers on Si)? Secondly, is there a limit to the thickness of amorphous silicide which can be grown or does it (in principle) keep growing until all Ti or Si is consumed?

In order to answer the above questions the growth kinetics were inves-

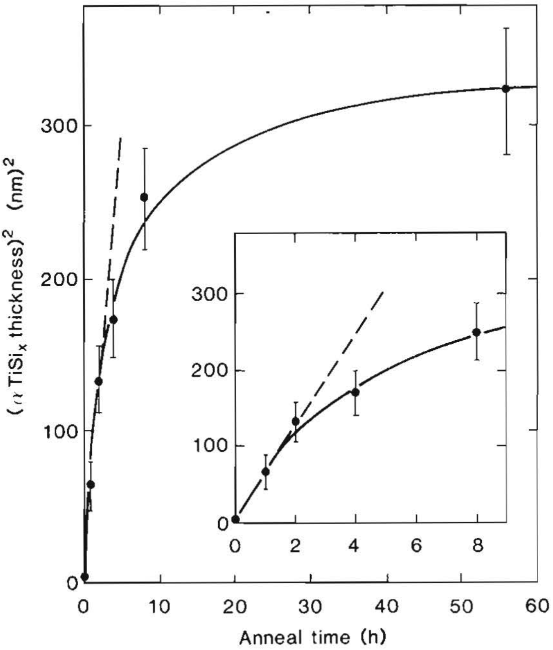

Fig. 5.7. The squared silicide thickness (averaged thickness from the layers formed at the upper and lower αSi - Ti interfaces) as a function of anneal time at 400 °C. The inserted figure is a magnification of the first part of the curve. After long anneal times saturation occurs.

tiged with the aid of isothermal anneals at 400 °C. The resulting amorphous layer thickness was measured from TEM cross-sectional micrographs. As was discussed in the previous section, the Kirkendall voids were thought to be part of the silicide layer. Accordingly, the silicide layer was assumed to extend from the Ti - αTiSi$_x$ interface just to the centre of the row of voids.

In Fig. 5.7 the square of the amorphous silicide layer thickness (the average of the αTiSi$_x$ thicknesses on both Ti - αSi interfaces) is depicted as a function of anneal time at 400 °C for the 20 nm samples. From this figure it seems that although the initial stages of growth may be controlled by diffusion (up to 2 h anneal time, dashed line in Fig. 5.7), the data points for the longer anneals show large deviations from such simple diffusion limited behaviour.

Several arguments are in favor of diffusion controlled growth in the initial stages of reaction. Firstly, it was observed that the compound layer shows very planar interfaces. This points to a rate controlling process which decreases with increasing thickness. Secondly, from the data presented in

Fig. 5.7 one may derive an effective chemical inter-diffusion coefficient from the simple relation $\tilde{D} = 1/2\ x^2/t$. In the initial stages of the reaction one derives a value of $(0.9 \pm 0.3) * 10^{-16}$ cm^2/s from the slope of the dashed line. It is known that the C49 $TiSi_2$ phase grows by diffusion of (mainly) Si in the temperature range of 475 °C to 650 °C [Hun83,Aum85,Mae88]. Hung et al. [Hun83] measured the effective inter-diffusion coefficient for the growth of the C49 $TiSi_2$ phase from Ti and αSi. Extrapolating their data measured between 475 °C and 575 °C down to 400 °C yields a value of about 10^{-16} cm^2/s. The observation that a simple extrapolation from the growth rate of crystalline C49 $TiSi_2$ explains the growth rate of the present amorphous silicide suggests that the same process is rate limiting in both cases: diffusion of Si through the compound layer.

The suppression of the growth rate in the later stages of the reaction is not caused by the limited Ti layer thickness in our 20 nm samples, Some experiments were also performed on much thicker αSi - Ti - αSi layers (the 60 and 100 nm samples, refer to Table 5.1). It appeared that in these thicker layer samples, the amorphous silicide thickness was equal to those in the thin layer samples. For example, if a 100 nm sample was annealed at 400 °C for 56h a layer of (18 ± 3) nm amorphous silicide was present on each interface. This compares to the value of (18 ± 1) nm as was found for the 20 nm layer sample after the same anneal procedure.

The suppression in growth rate causes the amorphous phase thickness to be limited to a depth of approximately 18 nm on each of the Ti - αSi interfaces at a temperature of 400 °C. The question now arizes why the growth of amorphous alloy virtually stops at this thickness? Earlier we noted that the growth of amorphous alloy was accompagnied by excessive Kirkendall void formation at the αSi - $\alpha TiSi_x$ interfaces. It appeared that together with the progression in the growth of the $\alpha TiSi_x$ layers the voids grew larger. Newcomb and Tu [New86] found similar voids in Ni - Zr diffusion couples. They proposed that these voids ultimately will reduce interfacial contact and effectively cut off the Ni supply. We believe that similar arguments will apply to our Ti - Si diffusion couples, the voids at the αSi - $\alpha TiSi_x$ interfaces cutting of the Si supply and thereby limiting the thickness of the amorphous layer which can be grown.

5.3.4 The Stoichiometry of the Amorphous Alloy

The poor definition of the plateaus in Fig. 5.4 suggests that the composition of the reacted amorphous layers is not constant over the depth of the layers but varies from Si–rich at the Si - $TiSi_x$ interface to Ti–rich at the $TiSi_x$ - Si interface. In principle, depth resolved Si concentration profiles may be obtained from Auger depth profiles after calibration of the spectrometer. The method is however very susceptable to erroneous interpretation due to sputter-induced artefacts. A quick and more absolute estimate of composition may be obtained from TEM micrographs (for example those from Fig. 5.5). The amount of Si and Ti consumed to form the amorphous alloy can be determined from thickness measurements if the thickness of the as-deposited layers is also measured. Although this method yields a reliable and absolute measure of the composition of the amorphous alloy, only the *average* composition of the entire $\alpha TiSi_x$ layer can be obtained and any composition gradients (which are likely to be present, see further) are not detected. In this section we will firstly determine the average composition of the reacted layer from TEM micrographs. Secondly we will attempt to show that large composition gradients are present in the amorphous alloy from Auger depth profiles.

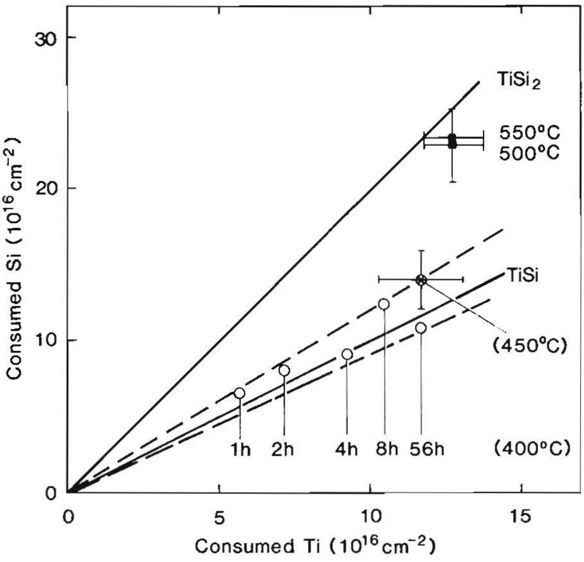

Fig. 5.8. The number of consumed Si atoms versus the number of consumed Ti atoms per unit area as determined from thickness measurements from TEM micrographs.

To determine the numbers of Ti and Si atoms consumed, the atomic volumes of Ti and Si are assumed to be equal to the bulk atomic volumes. This is generally not true for thin films deposited at low temperatures. Since both the Si and the Ti density were found to be lower than their bulk values (Table 5.1), the effect of a smaller density in the Ti thin film will at least partly cancel with the smaller densities in the Si thin films when calculating the composition of the alloy. Thus the error in the composition due to smaller densities of material in thin films is expected to be small. The occurrence of Kirkendall voids at the αSi - αTiSi$_x$ interface was the main source of error in the thickness measurements of the αSi layers. As was discussed before, the contrast or greyness in between the voids was much more similar to the contrast of the amorphous silicide than to that of the αSi. Therefore the αSi layer thickness was determined as if the voids are part of the amorphous silicide layer.

Fig. 5.8 shows a plot of consumed Ti versus consumed Si, obtained with thicknesses determined from TEM micrographs and bulk molar volumes. The straight solid lines denote the compositions of TiSi and TiSi$_2$ respectively. For the samples annealed at 400 ^{o}C during 1 h up to 56h, and 450 ^{o}C during 1 h, the average composition of the formed alloy is close to equiatomic. Increasing the anneal temperature to 500 ^{o}C and 550 ^{o}C moves the composition of the reacted layer to that of TiSi$_2$. This is consistent with the fact that after a 1 h anneal at 500 ^{o}C the disilicide has nucleated; the reaction layer now almost solely comprizes of C49 TiSi$_2$ (see Fig. 5.5d). After a 1 h anneal at 550 ^{o}C the entire reacted layer consists of crystalline TiSi$_2$.

We concluded that the average composition of the amorphous alloy which is formed in all samples annealed at temperatures of 400 ^{o}C and 450 ^{o}C is close to equiatomic. In order to determine the upper and lower bound of the average composition the αTiSi$_x$ alloy we draw the dashed straight lines in Fig. 5.8. All calculated compositions for the amorphous alloy fall within the area defined by those two lines. From the slope of these lines one determines the average Si concentration in the amorphous alloy to be in the range $0.47 \leq c_{Si} \leq 0.55$.

The Auger profiles (Fig. 5.4) suggest that the amorphous alloy can not be described by a single depth independent composition. Depth resolved Si concentrations may be derived from Auger measurements. Samples consisting of tri-layer stacks of different thicknesses (Ti thickness d = 20 nm, 60 nm and 100 nm) were annealed at 400 ^{o}C for different periods of time. Fig. 5.9 shows the Auger intensity ratio Y_{Si}/Y_{TiII} as a function of sputter time for samples annealed at 400 ^{o}C during 1 h. The Si$_{LMM}$ (91 eV) and the Ti$_{LMM}$ (410 eV, Ti$_{II}$) Auger transition were used. Only the reacted region at the upper Si - Ti interface is shown. To facilitate comparison of the profiles of the samples with different layer thicknesses the sputter time axis was shifted until the centers of the reacted regions coincided. It is immediately apparent from the curves in Fig. 5.9 that within the present measurement accuracy the reacted regions are of the same width and composition. The curves in Fig. 2 show two clear inflexions which are most probably associated with the Si - silicide and the silicide - Ti interface. The slope of the steep parts of the curves (outside the two inflexions) are representative for the depth resolution of our measurement (approximately 4 nm). The gradually decreasing intensity ratio between the two inflexions is probably representative for the decreasing Si concentration with increasing depth in the reacted amorphous layer. The intensity ratio changes from $Y_{Si}/Y_{TiII} = 2.0 \pm 0.2$ at the Si - silicide interface to 0.45 ± 0.1 at the silicide - Ti interface.

Fig. 5.10 shows depth profiles similar to those in the previous figure (Fig. 5.9) for the 60 nm sample annealed during different periods of time at a temperature of 400 °C. The composition boundaries appear to be nearly unaffected by the layer thickness of the amorphous alloy. Some flattening of the profiles is observed after long anneals. This is consistent with the fact that when the Si supply is choked off by the Kirkendall voids the alloy

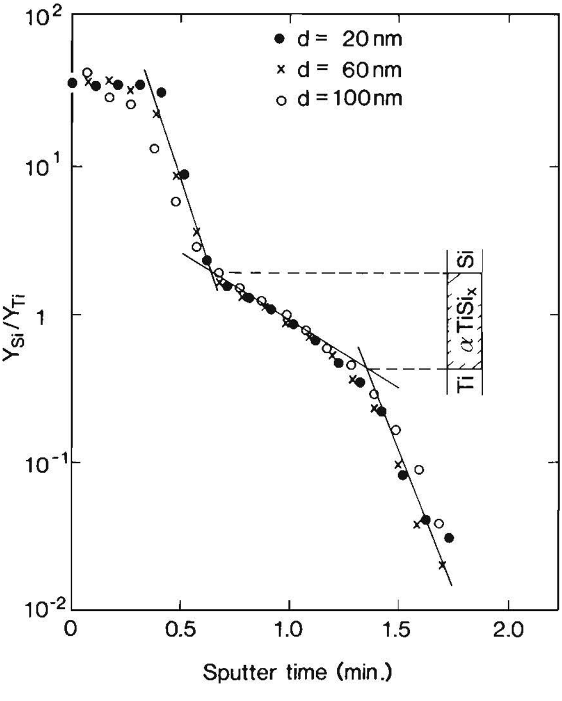

Fig. 5.9. Auger intensity ratio Y_{Si}/Y_{TiII} at the reacted interface as a function of sputter time after an anneal at 400 °C during 1 h. Results for three different Ti thicknesses are shown. The thickness of the amorphous alloy is about 8 nm and supposedly extends over a range of intensity ratios as indicated by the shaded bar.

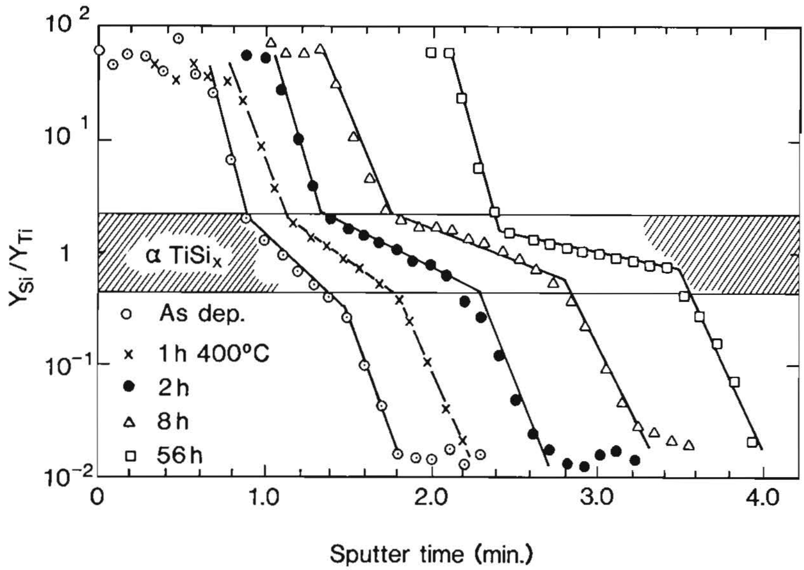

Fig. 5.10. Auger intensity ratio Y_{Si}/Y_{TiII} at the reacted interface of the 60 nm sample as a function of sputter time and after different anneal times at 400 °C. Curves have been shifted horizontally for clarity. The amorphous alloy extends over the intensity ratios indicated by the shaded bar. It is observed that no significant changes in the vertical position of the bends in the curves are observed upto 8 h anneal time.

stops growing and accordingly the Si concentration will eventually level off at a constant value.

In order to relate the measured Auger intensity ratio's to the actual composition of the amorphous alloy, we calibrated the Auger spectrometer. For that purpose samples consisting of co-sputtered thin films and bulk samples [Kem82] of different composition were used. The composition of these samples was measured with Rutherford backscattering spectrometry. The Si/Ti Auger intensity ratio was measured under the same conditions as those under which the diffusion couples had been measured, including the ion bombardment used for depth profiling. In Fig. 5.11 the measured intensity ratio's for the Ti_{LMM} 386 eV (Ti_I) and the Ti_{LMM} 410 eV (Ti_{II}) with the Si_{LMM} 91 eV peak are recorded versus the Si concentration measured with RBS. Using this calibration, the intensity ratios measured at the inflexions of the curves in Fig. 5.9 ($Y_{Si}/Y_{TiII} = 2.0 \pm 0.2$ and $Y_{Si}/Y_{TiII} = 0.45 \pm 0.1$) would correspond to silicon concentrations of $c_{Si} = 0.7 \pm 0.1$ and $c_{Si} = 0.2 \pm 0.1$ respectively.

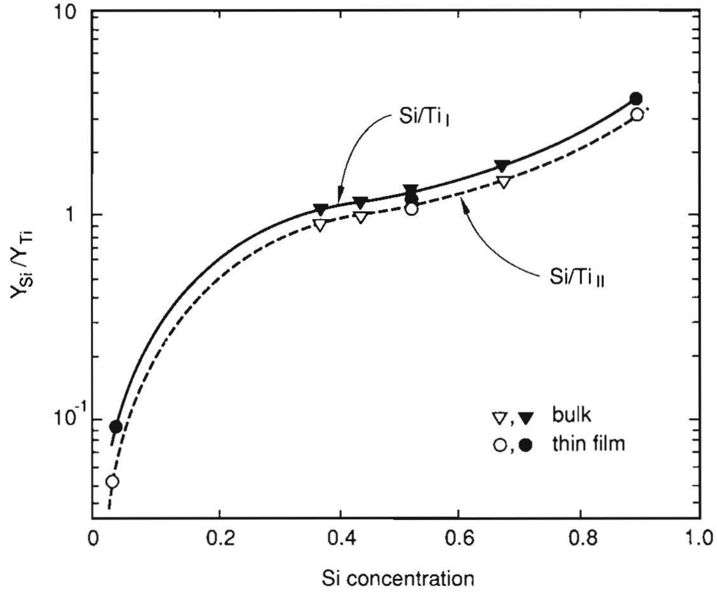

Fig. 5.11. Auger intensity ratios Y_{Si}/Y_{Ti} as a function of Si concentration. Two different Ti Auger peaks were used: the Ti_{LMM} transitions at 386 eV (Ti_I) and 410 eV (Ti_{II}) respectively. For Si the Si_{LMM} (91 eV) peak was used

It is known [Hof80,Cob74] that several sputter-induced artefacts may yield an apparent composition profile while there really is a constant composition in the layer. These effects include for example preferential sputtering, ion beam mixing and ion beam enhanced diffusion or surface segregation in the analyzed region. Although these effects certainly play a role in the above described Auger depth profiles, it is thought that they do not explain the large change in the Auger intensity ratio (with almost a factor of five) from the silicide - Si to the Ti - silicide interface. Moreover, the value of the Auger intensity ratio at the interfaces was found to be independent of the thickness of the amorphous layer. If all artefacts are tacitly neglected the Auger profiles would lead to a concentration ranging from about 20 at. % Si at the Ti - silicide interface to about 70 at. % Si at the silicide - Si interface. The absolute value of the silicon concentration at the interfaces may contain some systematic errors due to the above mentioned sputter-induced artefacts, so that the above numbers have semi-quantitative significance only: a considerable composition gradient exists in the amorphous alloy. Composition gradients were reported also during the growth of a NiZr amorphous alloy from poly-crystalline Ni and Zr thin films [Ros84,Bar86]. In the next section it will be shown that such large composition gradients are also expected from a thermodynamic point of view in the Ti - Si system.

As was mentioned in the introduction, Maex et al. [Mae86,Mae87] were able to obtain amorphous Ti - Si alloys of approximately equiatomic composition by ion beam mixing of Ti deposited on crystalline Si substrates. The roughly equiatomic composition of the αTiSi$_x$ alloy in our samples agrees also with the composition found by Holloway et al. [Hol87]. They derived their composition also from TEM micrographs, but used multilayer samples consisting of much thinner Ti and Si layers. Thus, it is now demonstrated that the growth of this amorphous alloy may also be induced thermally in the Ti - Si system.

5.3.5 Titanium Silicon Free Energy Diagram

We concluded in the previous section that during growth of the amorphous alloy a large composition gradient exists. This composition gradient probably points to a very wide phase field of the amorphous material. It was found from TEM micrographs that the average composition of the alloy was close to equiatomic and from Auger depth profiling that the composition ranges from about 20 at. % to about 70 at. % Si. We will try to explain these phenomena with a free energy diagram of the Ti - Si system. Free energy diagrams are more useful in this case than equilibrium phase diagrams because metastable equilibria are easier elucidated in the free energy diagram.

Gibb's free energy diagrams can be approximately calculated from for example Kaufman's [Kau79,Kau73] compilaton of thermo-chemical data. For the free energy of the amorphous state at low temperatures one usually calculates the free energy of the undercooled liquid. However, the free energy of amorphous solid alloys of elements which show large negative heat of mixing is considerably smaller than that of the undercooled liquid due to chemical short range ordering or structural relaxation of the amorphous state towards the crystalline equilibrium state [Mie88]. As a first approximation we accounted for these effects by adding an extra negative contribution to the free energy of the undercooled liquid. The correction term was taken equal to $4 * c_{Si}(1 - c_{Si})\ \Delta G_{l-\alpha}$, where c_{Si} is the Si concentration in the alloy and $\Delta G_{l-\alpha}$ the free energy contribution due to the above effects at the equiatomic composition. An estimate for the magnitude of $\Delta G_{l-\alpha}$ could be derived from measured heats of crystallization of amorphous Ti - Si alloys [Raa86,Kem82]. The value of $\Delta G_{l-\alpha}$ is estimated to be about 20 kJ/mol. Fig. 5.12 shows the calculated free energy curves of the amorphous, hcp and diamond states, and the minimum of the free energy curves of the equilibrium stoichiometric compounds. The diagram is calculated from the data of Kaufman [Kau79,Kau73] for a temperature of 400 °C. Metastable two phase equilibria are shown as dashed lines in the diagram. From the free energy diagram one derives with the aid of a tangent construction that the phase field of the amorphous alloy extends from about $c_{Si} = 0.3$ to about $c_{Si} = 0.7$ (indicated by the shaded bar).

If there are no reaction barriers present at the interfaces, the situation at these interfaces is close to a metastable equilibrium. In that case the position of the phase boundaries derived from the free energy diagram correspond directly to the composition at the interfaces. On the Ti side of the diagram, metastable equilibrium prevails between the amorphous phase and a super-saturated solid solution of Si in hcp Ti. The shift in the Ti interplanar spacings to larger values as was noted earlier in this chapter from X-ray diffraction analyses (see Fig. 5.2) is thought to be due to the super-saturation of hcp Ti with Si

The width of the calculated phase field is subject to some systematic errors, the largest being the uncertainty in the exact shape and position of the free energy curve of the amorphous phase. Moreover, the composition of the alloy on the Si-rich side was derived using the assumption that metastable equilibrium between *diamond* Si - amorphous silicide exists. Our sputtered Si layers however were *amorphous* and their free energy most certainly is higher than the value for the diamond state. For example, Sinke et al. [Sin88] calculated this free energy difference to be in the

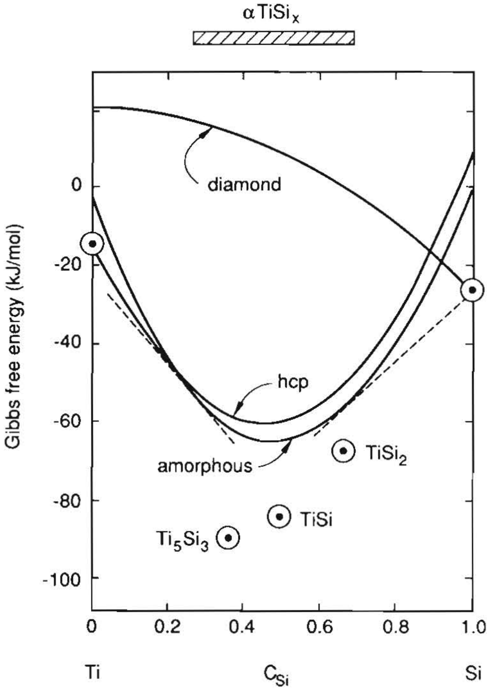

Fig. 5.12. Calculated free energy diagram at a temperature of 400 °C. (hcp = hexagonal close packed.) Metastable two phase equilibria are indicated by the dashed lines. The phase field of the amorphous silicide is indicated by the shaded bar.

range 10 - 18 kJ/mol., dependent on the amount of relaxation. Fan et al. [Fan81] found for their sputter-deposited αSi layers a heat of crystallization of 10 kJ/mol. which would correspond to well-relaxed αSi in terms of Sinke's work. The higher free energy of the amorphous state of Si would shift the composition at the Si–rich side to even higher concentrations of Si. In conclusion, although the exact boundaries of the phase field are rather uncertain, the width of the phase field of the amorphous alloy is expected to be substantial. This is consistent with the experimentally noticed variation in composition with depth.

We would like to note here that the phase field of the amorphous phase is wide enough to contain the composition of several equilibrium compounds. A necessary condition for the growth of an amorphous phase by diffusion is that its crystallization temperature is substantially higher than its growth temperature. In chapter 4 we measured the crystallization temperatures of co-sputtered amorphous alloys of diffrent compositions. Recall that a depression in the crystallization temperatures to temperatures of about 300 ^{o}C was found for samples with compositions close to that of the disilicide. Crystallization temperatures exceeding the growth temperature of the present amorphous alloy (400 ^{o}C - 450 ^{o}C) were found for samples with compositions in the range of $0.2 \leq c_{Si} \leq 0.6$. Consequently, the phase field cannot extend beyond those limits. This sets the Si–rich boundary of the phase field at a Si concentration of about 0.6.

5.4 Results and Discussions: Ti - crystalline Si

5.4.1 Low Temperature Reaction

This section is mainly concerned with the reactions between a polycrystalline Ti layer and a monocrystalline Si substrate occurring at temperatures below 500 ^{o}C. For that purpose we will use the samples with the bilayer and single layer structure depicted in Fig. 5.1b and c respectively.

The bilayer samples with the structure of Fig. 5.1b, consisting of a Si substrate with a sputter-deposited layer of Ti and a sequentially deposited layer of αSi offer the possibility to compare the reaction of the same Ti layer with the crystalline Si (xSi) substrate and the sputter-deposited amorphous Si (αSi) layer. The cleaning procedure of the monocrystalline Si substrates included a 1 minute dip-etch in an aqueous 1 % HF solution to remove the native oxide just before loading the wafers in the deposition system. This procedure is known to leave some O and C on the surface in the monolayer regime [Hen72,Tau85] and a minor amount of F [Ker72,Raa88c]. Thus the crystalline Si - Ti interface is slightly contaminated. The αSi - Ti interface is expected to be more clean since the layers are deposited subsequently in the same vacuum.

Bilayer samples (Fig. 5.1b) with 20 nm Ti and 57 nm αSi layer (derived from Rutherford backscattering spectrometry) were heated in a high vacuum furnace at temperatures between 300 °C and 500 °C during 1 h. The as-deposited and annealed samples were investigated with cross-sectional transmission electron microscopy (TEM), Auger electron spectroscopy (AES) with sputter-depth profiling and Rutherford backscattering spectrometry (RBS) At first we will present and discuss the TEM results presented in Fig. 5.13 and 5.14. After that we turn our attention to the depth resolved compositional data obtained from AES in Fig. 5.15 and RBS in Figs. 5.16 and 5.17.

Fig. 5.13 shows cross-sectional TEM micrographs of the samples annealed at 400 °C and 450 °C for 1 h. The micrographs for the annealed samples in Fig. 5.13a and b show reacted regions at both Ti - Si interfaces and look very much like the micrographs of Fig. 5.5b and c, the main difference being that the bottom αSi layer and the oxidized substrate have now been replaced by an unoxidized monocrystalline Si substrate. The reacted layer at the Ti - αSi interface is a similar amorphous silicide as described in section 5.3.2 (αTiSi$_x$). At the amorphous silicide - αSi interface voids (presumably Kirkendall voids, as was suggested in section 5.3.2) are visible. The thickness of the amorphous layer at the Ti - αSi interface as measured from the TEM micrographs is (7.4 ± 0.7) nm for the 400 °C anneal. This compares well with the amorphous silicide thicknes which can be derived from the micrographs of the trilayer stacks in Fig. 5.5b for the sample annealed at 400 °C ((8 ± 1) nm).

At the Ti - xSi interface a planar reacted layer is formed too. From the absence of bright field contrast in the layer one concludes that the layer is amorphous or possibly microcrystalline. Preliminary diffraction experiments on the reacted layers in the cross-section of the sample annealed at 450 °C were done in the TEM with 'focussed condensor aperture nanodiffraction' [Jay86]. No differences between the diffraction patterns of the reacted layer at the Ti - xSi interface and that at the Ti - αSi were found. In both cases, the diffraction pattern of the reacted layer consisted of diffuse rings without any evidence for the presence of crystalline material with a grain size larger than 2 nm. We will denote the present layer with 'TiSi$_y$' in order to be able to distinguish it from the previously discussed αTiSi$_x$ layer.

The thickness of the compound layer grown at the Ti - xSi interface during a 1h anneal at 400 °C is measured from the TEM micrographs to be (5.9 ± 0.3) nm. The reactions occurring at a crystalline and amorphous Si - Ti interface thus proceed with approximately the same rate in the low temperature regime (below 450 °C). The small thickness difference which

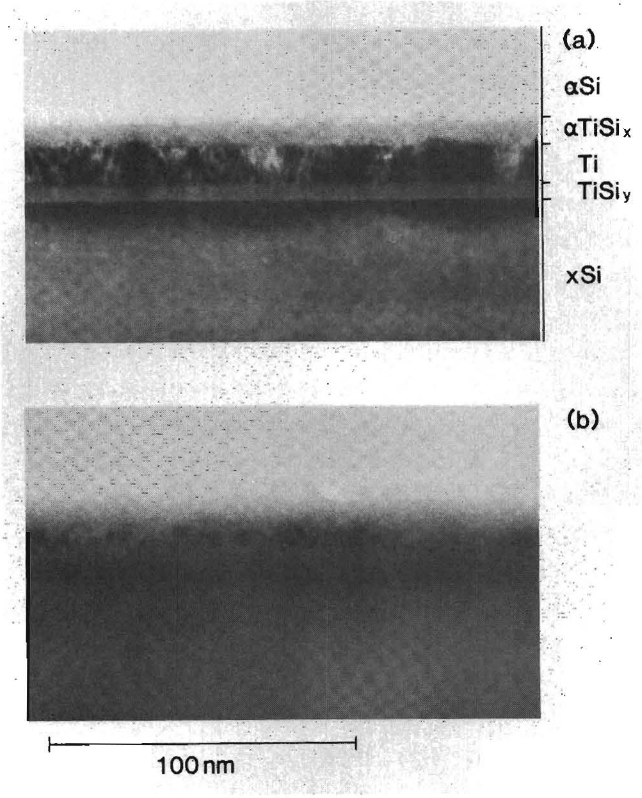

Fig. 5.13. TEM cross-section micrographs of bilayer samples annealed during 1 h at 400 °C (a) and 450 °C (b). The arrow denotes a length of 100 nm.

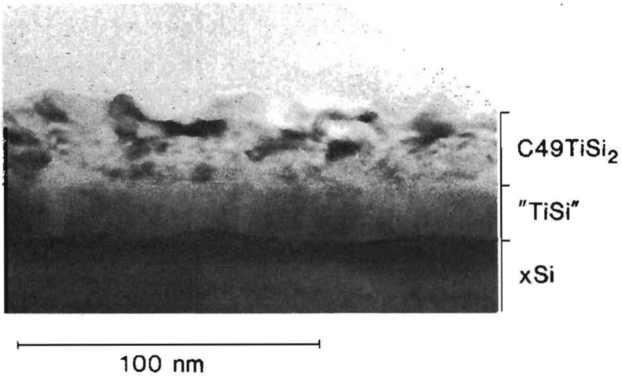

Fig. 5.14. TEM cross-section micrographs of a bilayer sample annealed during 1 h at 500 °C. The arrow denotes a length of 100 nm.

is observed may be ascribed to the presence of interfacial impurities, but it can also be attributed to the presence of a reaction barrier at the xSi - silicide interface (influencing the driving force or concentration gradient) or to differences in the reacted layer itself.

Fig. 5.14 shows a bilayer sample annealed at a temperature of 500 °C during 1 h in vacuum. Although the top layer of unreacted αSi has probably disappeared during the ion milling process, two distinct reacted layers can be distinguished. The fairly course grained crystalline layer in the cross-section next to the αSi layer consists of the C49 $TiSi_2$ phase. (Later we will show that this is consistent with composition measurements from AES and RBS.) The layer which is formed next to the crystalline Si substrate is also found to be crystalline and consists of very fine grains. Sporadically some larger crystallites were noted, in structure similar to the ones in the upper layer. The crystalline structure of the fine grained layer could not be determined, but it was definitely not the C49 $TiSi_2$ phase. We will tentatively denote this crystalline layer with 'TiSi'.

Fig. 5.15 records elemental depth profiles obtained by sputter-depth profiling and AES of the as-deposited (a) and annealed ((b): 400 °C, (c): 450 °C and (d): 500 °C) bilayer samples. After an anneal at 350 °C during 1 h a very slight reaction was noted, but that profile is not shown in Fig. 5.15. Consistent with the results obtained from cross-sectional TEM, after the anneal at 400 °C during 1 h a very distinct reaction had occurred. The slopes of the Si and Ti depth profile from both Ti - Si interfaces degraded, indicating interfacial compound formation. After an anneal at 450 °C during 1 h nearly the entire Ti layer has reacted with the Si substrate and the deposited αSi layer.

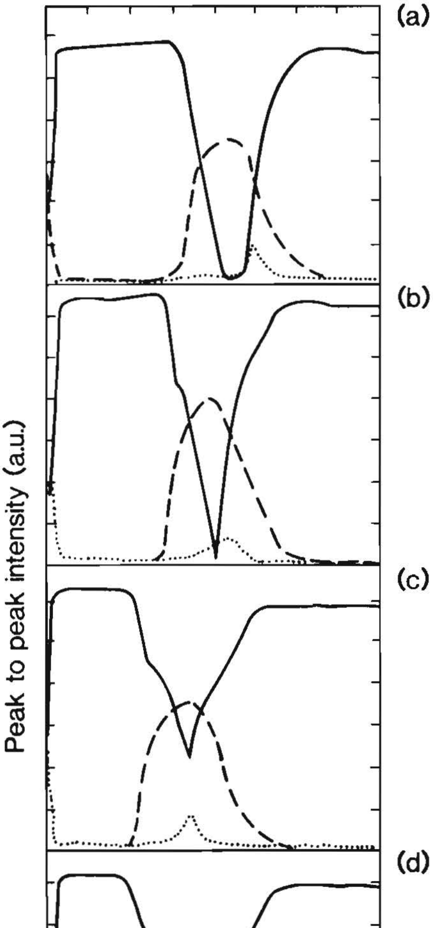

Fig. 5.15. Auger depth profiles of the bilayer samples, as-deposited (a) and annealed during 1 h at 400 °C (b), 450 °C (c), and 500 °C (d). (solid line: Si_{LMM} (91 eV), dashed line: Ti_{LMM} (386 eV, Ti_I), dotted line: O_{KLL} (510 eV).) For the horizontal line pieces marked 'a' and 'b' in Fig. (d) see text.

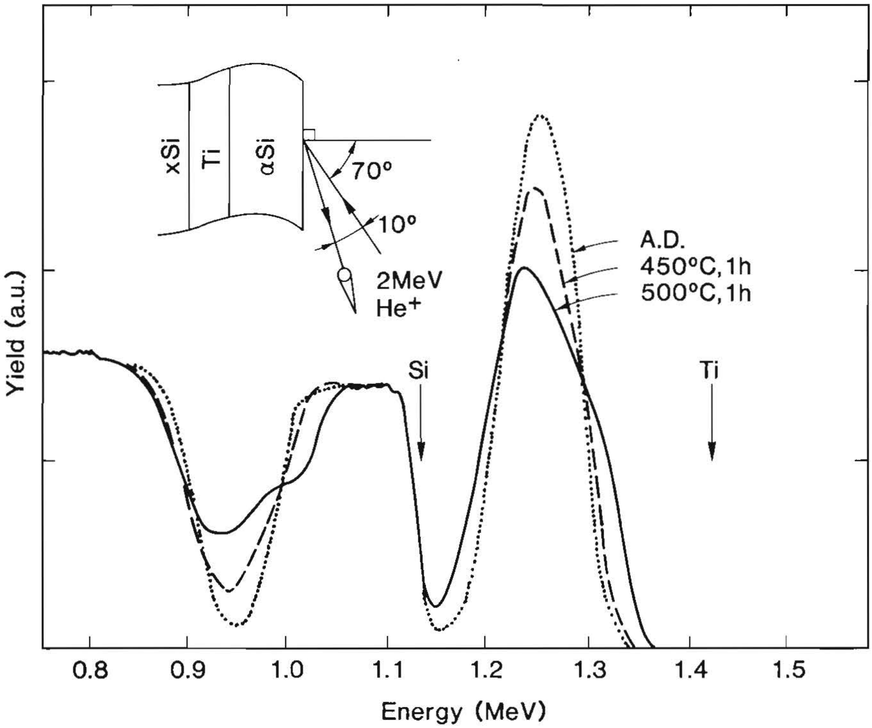

Fig. 5.16. Rutherford backscattering spectra of the as-deposited and annealed bilayer samples. Note the development of a plateau corresponding to the composition of $TiSi_2$ at the Ti - αSi interface and the absence of such a plateau at the Ti - *x*Si interface in the spectrum for the sample annealed at 500 °C.

The present Si substrates were cleaned wet chemically, and some O and C is present on the Ti - *x*Si interface as discussed before. The O profile in Fig. 5.15 evidences that the oxygen which was originally present at the Ti - *x*Si interface has segregated ('snow-ploughed' [Mer84,Ber84,Ben85] to the unreacted central parts of the Ti layer by the advancing silicide reaction front. For clarity the C depth profile is not shown in Fig. 5.15. The magnitude of the interfacial C peak in the depth profile of the as-deposited sample was about the same as that of the O peak. Upon annealing the C impurities were also pushed to the unreacted center of the Ti layer, similar to oxygen.

Fig. 5.16 shows the Rutherford backscattering (RBS) spectra obtained from an as-deposited sample and samples annealed at 450 °C and 500 °C in vacuum during 1 h. In agreement with the TEM and AES results, after the 450 °C anneal a clear reaction can be noted on both interfaces. Simulations of the spectra obtained from samples annealed at 400 °C and 450 °C

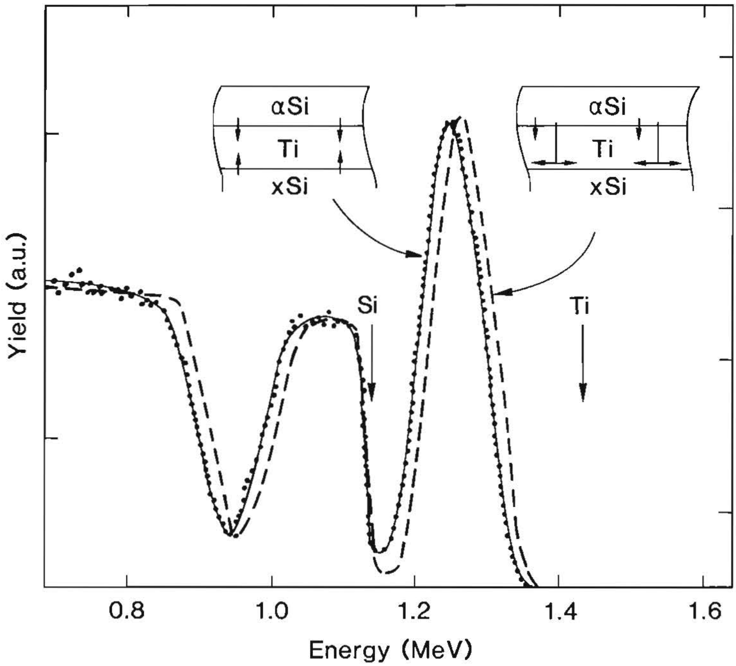

Fig. 5.17. Measured (dots) and simulated backscattering spectra for the bilayer sample annealed at 450 °C. Two simulations are drawn in the figure. The dashed line represents the situation that only the αSi layer delivers Si to the reaction fronts. The solid line represents the situation that both the substrate and the αSi layer participate in the reaction.

suggested a thin layer of monosilicide to be present at both interfaces.

Using Rutherford backscattering it can be shown that the Si needed to form the reacted layer at the *x*Si interface is originating directly from the Si substrate and not from the alternative source: Si from the αSi layer transported through the Ti layer by some kind of fast diffusion mechanism (for example grain boundaries). In order to find out which is the actual source of the Si in the reacted layer next to the *x*Si substrate we simulated RBS spectra corresponding to the two viable alternatives: *(i)* both Si layers grow from Si originating from the toplayer of αSi and *(ii)* the reacted layer next to the *x*Si substrate is formed by reaction with the Si substrate while the reacted layer next to the αSi layer is formed by reaction with that αSi layer. Both simulations are shown together with the measured data in Fig. 5.17. It may be clear from this figure that the simulation according to the second alternative is by far the best fit to the measured spectrum. Similar conclusions were reached for the samples annealed at 400 °C and 500 °C.

From a bilayer sample that was annealed at 500 °C during 1 h the Auger depth profile in Fig. 5.15d results. A clear plateau has developed at the Ti - αSi interface, the formation of which is evident from the RBS data too (Fig. 5.16). A good fit to that part of the spectrum could be obtained by assuming a layer of $TiSi_2$ at the Ti - αSi interface. No clear plateau is visible at the Ti - xSi interface. The limited depth resolution of RBS in the present measuring conditions prevents an unambiguous conclusion on the stoichiometry of the reacted layer at the Ti - xSi interface. A good fit could however be obtained by assuming a TiSi layer at the Ti - xSi interface.

Additional data on the composition of the reacted layers can be derived from the Auger depth profiles. The Ti/Si atomic ratio can be derived from the ratio of the Auger peak to peak intensities measured in the middle of the reacted regions (as indicated in Fig. 5.4d by the straight horizontal line pieces 'a' and 'b') and the calibration described in the previous section (see Fig. 5.11). For the reacted region next to the αSi interface we derive an intensity ratio of $Y_{TiI}/Y_{Si} = 0.61 \pm 0.05$, corresponding to a Si concentration of (66 ± 4) at. %. This value is close to the value of the Si concentration in the disilicide and agrees with the RBS data. Thus the Auger depth profile, the RBS data and the TEM cross-section of the 500 °C annealed sample show the formation of the C49 $TiSi_2$ phase at the Ti - αSi interface.

For the intensity ratio Y_{TiI}/Y_{Si} in the reacted layer at the xSi interface one finds a value of 0.77 ± 0.07, corresponding to a Si concentration of (50 ± 10) at. %. This value of the Si concentration represents the composition of the fine grained reacted layer formed by the reaction of Ti with xSi observed in the cross-section of Fig. 5.14. The composition of the material next to the xSi substrate is thus found to be close to that of the monosilicide and the material is crystalline. In the initial reaction stages of Ti - xSi diffusion couples the orthorombic TiSi [Bru61] phase is frequently observed besides the C49 $TiSi_2$ phase [Bey85,Hou86,Hun83] Therefore the layer discussed here may be the orthorombic monosilicide. Apparently the formation of the disilicide is more difficult in a reaction with xSi than in a reaction with αSi.

If samples are only cleaned with a wet chemical cleaning procedure some monolayers of C and O are present on the surface before Ti deposition. In addition, if a HF dip is included in the cleaning procedure, a minor amount of F may be present. In practice and if needed these residual impurities can be removed by a sputter-etch performed in the same vacuum system where the Ti layer is to be deposited. This paragraph describes the effects of such a sputter-etch on the low temperature reaction of Ti and xSi. For that purpose single layer samples containing a 50 nm Ti layer were annealed at a temperature of 400 °C during 5 h in vacuum and were analyzed with RBS. From previous sections one derives that during such an anneal a Ti -

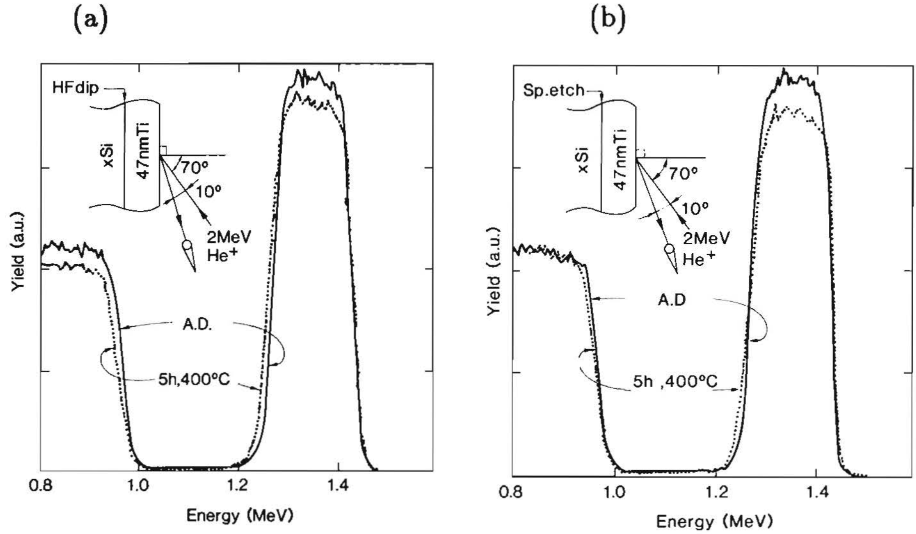

Fig. 5.18. Measured Rutherford backscattering spectra for Ti layers on monocrystalline Si annealed at 400 °C during 5 h. (a) HF dip before inserting the wafer in the deposition system; (b) HF dip and additional *in-situ* sputter-etch to remove resiudual impurities. solid lines: as-deposited, dots: annealed.

αSi interface would react to form about 14 nm of an amorphous silicide of average equiatomic composition (see Fig. 5.7). In Fig. 5.18 the RBS spectra for the as-deposited and annealed sample are shown. Fig. 5.18a shows the results for a wet-chemical clean only whereas Fig. 5.18b shows the results for the sample which was additionally cleaned with an *in-situ* sputter-etch.

For both annealed samples a good fit to the spectra could be obtained by assuming a layer of (15 ± 8) nm TiSi to be present. We observed no significant differences in the spectra for the sputter-etched and non sputter-etched sample after the low temperature anneal. Moreover, the observed layer thickness is similar to that which forms during a similar anneal on a Ti - αSi interface. Apparently, a Ti - xSi interface and a Ti - αSi interface are equally reactive, even if some residual impurities are present at the Ti - xSi interface. This is consistent with earlier work. For example, Taubenblatt et al. [Tau85,Tau82,Tau86] and others [Rub86,Lir85,Abd86] have shown that upon deposition of Ti on a contaminated Si surface the Si - C and Si - O bonds are readily broken, even at room temperature, to form a solid solution of O or C in Ti. Several research groups [Mer84,Ber84,Ben85,Hou86,Aum85] have shown that C and O are readily redistributed in the unreacted Ti layer during the reaction of Ti with Si. The Auger depth profiles for O in Fig. 5.15 are in agreement with these findings.

Summarizing, in reactions of Ti with two different structural forms of Si, namely sputter-deposited (amorphous) and monocrystalline Si, it appears that at temperatures not exceeding 450 °C, the rate for the reaction with xSi is the same as the rate for the reaction with αSi. It was established that in the reaction of Ti with αSi an amorphous silicide formed. The crystalline state of the layer formed from reaction with a crystalline Si substrate remains unclear. From the similarities of the layers in growth rate, composition and bright field contrast in the TEM we tentatively conclude that the layers grown simultaneously from Ti and xSi or αSi are structurally and compositionally the same. At higher temperatures, however, a marked difference in reaction occurs. In the reaction of Ti with *amorphous* Si at a temperature of 500 °C the C49 $TiSi_2$ phase nucleates and grows. When the same Ti layer is reacted with *crystalline* Si at temperatures of 500 °C a crystalline reacted layer of approximately equiatomic composition formed, presumably orthorombic TiSi.

Clues for understanding the differences in reaction of Ti with αSi and xSi are offered by the literature on the formation of the isotypical silicides of the systems Hf - Si and Zr - Si [Mas87] (see chapter 1).

It is known that in the reaction of Hf with xSi at temperatures of about 600 °C the growth of HfSi is diffusion controlled. At higher temperatures (685 °C) the disilicide phase forms, but its growth is controlled by nucleation of the $HfSi_2$ phase in the monosilicide [Zie73]. Similar resultsobservations are reported in the Zr - Si system, the 'nucleation temperature' for the formation of disilicide being somewhat lower (625 °C) [Heu88]. Recently So et al. [So 86] studied the reaction of Hf and evaporated (amorphous) Si. Again, the monosilicide formed first; the growth of $HfSi_2$ from HfSi onαSi is reported to be diffusion controlled, however. A nucleation controlled process for the growth of the disilicide from the monosilicide in the case of reaction of the metal with xSi and a diffusion controlled growth process in the case of reaction with αSi is now reported for many other silicides too, for example $CoSi_2$ [Lin84b], $NiSi_2$ [Lin84c], $CrSi_2$ [Lin86] and $ErSi_{1.7}$ [Lau82]. These observations can be explained by considering the following reactions and their associated free energies ΔG.

$$MSi + xSi \longrightarrow MSi_2$$

$$\Delta G = \Delta G_x \tag{5.1}$$

$$MSi + \alpha Si \longrightarrow MSi_2$$

$$\Delta G = \Delta G_x + \Delta G_{\alpha - x} \tag{5.2}$$

where M stands for a transition metal, and $\Delta G_{\alpha-x}$ is the (negative) free energy of crystallization of αSi. The reaction free energy of the first reaction (with xSi) is usually very small. For example in the case of M = Zr it is only about − 1.5 kJ/mol at room temperature (neglecting entropy effects) [Nic83,Pre78], which is of the order of kT (2.5 kJ/mol at room temperature). The disilicide is thus barely stable with respect to the monosilicide and crystalline Si. For reactions with such low free energy changes, one expects nucleation to play a crucial role in the silicidation process [Heu88], see also chapter 4. The heat of crystallization of amorphous Si is about 10 - 18 kJ/mol, dependent on the amount of relaxation [Sin88,Fan81], so that in forming the disilicide from reaction with αSi the free enthalpy change is much larger than in the reaction of the monosilicide with xSi. Large heats of reaction are associated with low nucleation barriers, consequently leading to lower nucleation temperatures which explains the above results.

The above reasoning for Hf and Zr silicides is directly applicable to the observed reactions in the Ti - Si system. In the case of M = Ti in reaction 5.1, the free enthalpy of reaction to form the equilibrium C54 structure silicide from the monosilicide amounts to − 1.5 kJ/mol [Nic83,Pre78]. The enthalpy of reaction to the C49 polytype is not known, but it can scarcely exceed this value. It is also observed that at low temperatures (upto 450 °C) Ti - αSi interfacial reaction leads to the formation of an amorphous compound with an average composition of the monosilicide. Low temperature reaction of a Ti - xSi interface leads to the formation of a similar compound. In analogy with the reactions in the Zr and Hf systems, the low values of the heat of reaction when forming the disilicide from the monosilicide implies that a nucleation barrier is to be expected in the case of the reaction with crystalline Si but not for the reaction with amorphous Si.

Nucleation difficulties on a monocrystalline substrate may also explain the irreproducible results reported by Hung et al [Hun83] for the Ti - xSi reaction and the inconsistencies observed in literature [Iye85,Aum85,Pic86] [Ben85]. In the next section the reaction of Ti with xSi at conventional growth temperatures (550 °C to 700 °C) will be examined.

5.4.2 High Temperature Reaction

The main objective of the investigations in the present section is to unravel the technologically important question why the reaction on a crystalline Si substrate is so difficult to reproduce [Hun83]

Si substrates with (100) orientation and p-type 20 - 50 Ωcm resistivity were cleaned wet chemically including a dip etch in a 1% aqueous HF solution. For the present experiments the single layer sample structure as defined in Fig.5.1c was used with a Ti layer thickness of about 50 nm or

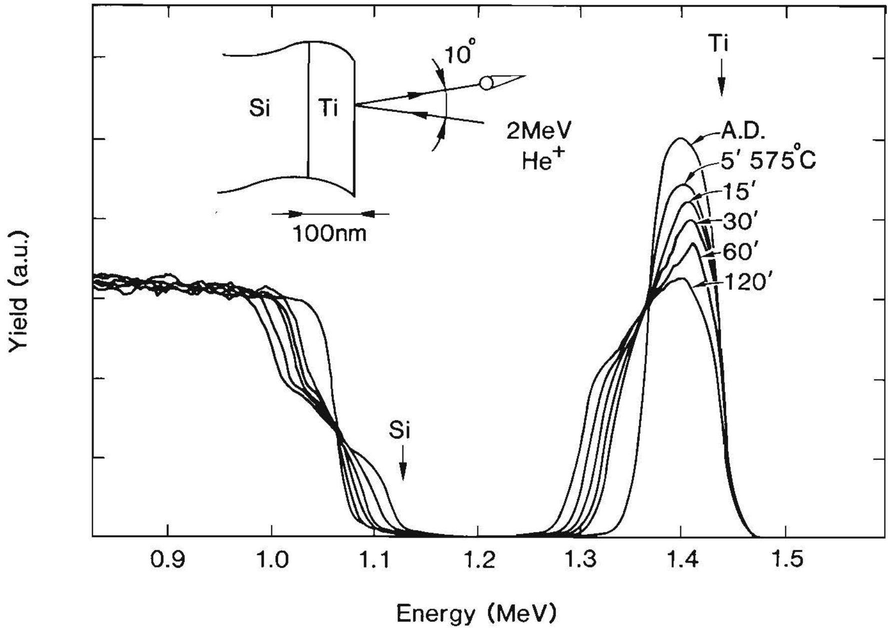

Fig. 5.19. Rutherford backscattering spectra for a single 100 nm Ti layer on crystalline Si heated *in-situ* in the RBS target chamber showing the high temperature reaction. Note the roughening of the interfaces after the first reaction step (5 min. at 575 °C).

sometimes about 100 nm. Small rectangular (10 * 20 mm^2) samples were cut from the wafers. These samples could be heated in the Rutherford backscattering target chamber by passing current through the samples. The temperature was measured with an infrared pyrometer set for the emissivity of pure Ti ($\epsilon \approx 0.35$) [Tou70]. The residual gas pressure in the (unbaked) target chamber during heating was about 10^{-4} Pa, the main component being water vapour. An advantage of heating our samples in the RBS target chamber is that many of the reproducability problems will be absent. The reaction kinetics can be studied by doing several measurements at nearly the same location on the same specimen.

A typical series of backscattering spectra is presented in Fig. 5.19. The reaction of a nominally 100 nm Ti layer and monocrystalline Si at a temperature of 575 °C is shown as a function of anneal time. (Samples were cooled between the anneals.) After the first heating cycle (5 min at 575 °C) changes in the low energy side of the Ti signal and the high energy side of the Si signal evidence a reaction at the Ti - xSi interface. The shape of the RBS signals and the absence of a clear plateau indicate that the reaction is associated with a considerable roughening of the interfaces.

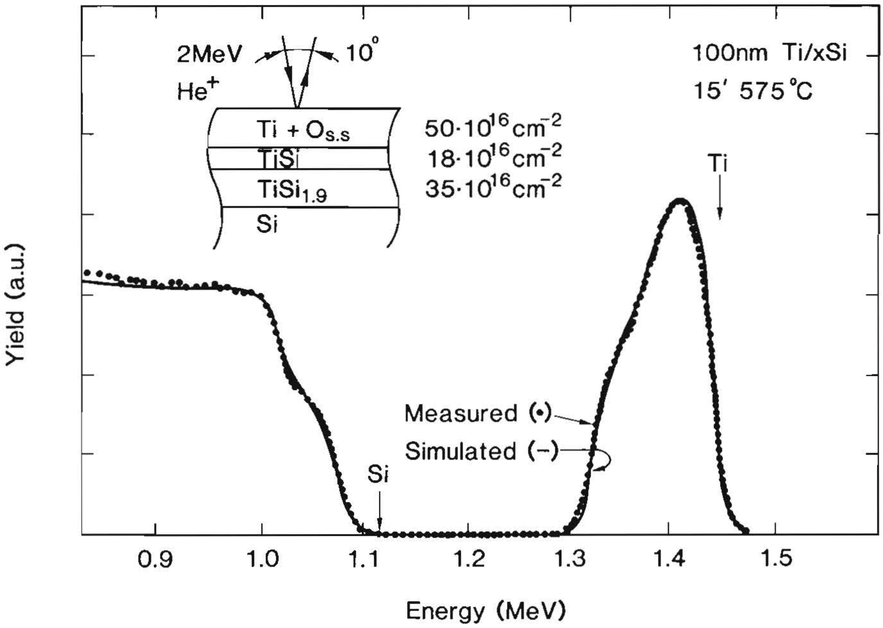

Fig. 5.20. Measured (dots) and simulated (solid line) Rutherford backscattering spectra for a Ti layer on crystalline Si annealed during 15 min. at 575 °C. The simulation is performed with the layer structure as indicated in the figure. Numbers denote the total number of atoms in the layer.

The RBS spectrum of the reacted samples was simulated in terms of the layer structure depicted in Fig. 5.20. The part of the RBS spectrum corresponding to the silicide usually could be simulated satisfactory with two silicide layers: a layer with a composition of about 50 at.% Si (TiSi) on top of a layer with a composition of about 67 at. % Si ($TiSi_2$) next to the Si substrate. The introduction of (a constant and small amount of) straggling [Doo85] in the simulation was necessary to obtain a good fit to the spectra of the reacted samples. From comparison of the measured and simulated spectrum (for example that shown in Fig. 5.20). it appears that the total amount of reacted Si is a very critical parameter in the fit. Usually it can be determined with a relative inaccuracy of about 10 %, except for the slightly reacted samples where the inaccuracy is somewhat larger. The layer thickness of the TiSi layer could not be obtained very accurately. Some monosilicide could be traded for the disilicide without affecting the fitted spectrum very much. Usually the TiSi layer thickness was found to correspond to 3 to 6 * 10^{16} at/cm^2 (10 to 20 nm). It was found convenient to derive the total amount of reacted Si from the simulation and to treat this as a representative measure of the amount of silicide formed.

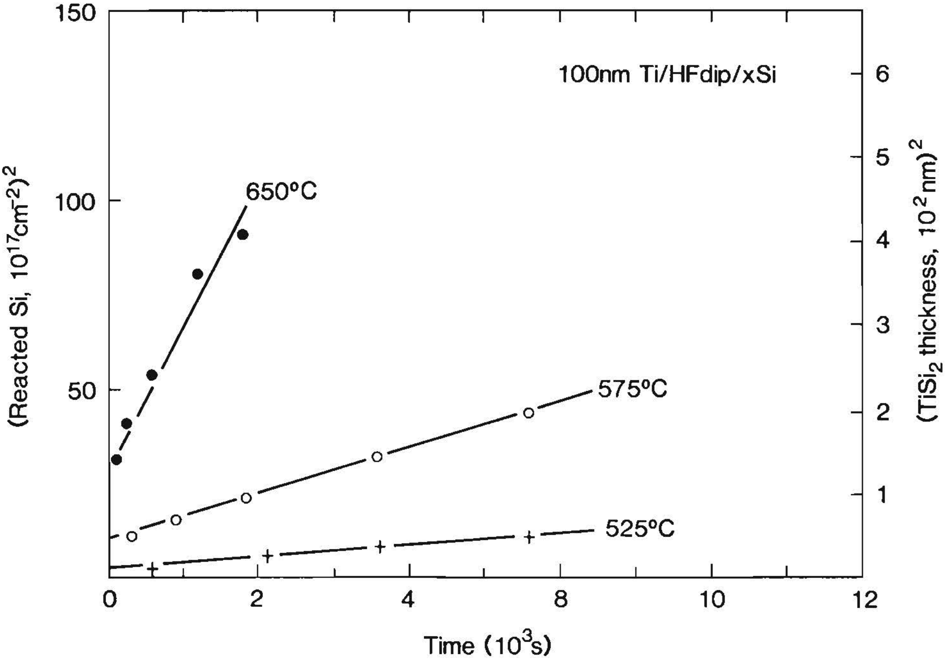

Fig. 5.21. Squared reacted amounts of Si as a function of reaction time determined from simulations of Rutherford backscattering spectra. A 100 nm Ti layer on crystalline Si was used. A straight line would indicate a diffusion controlled reaction. Note the fast initial reaction.

Fig. 5.21 shows the square of the amount of reacted Si as a function of anneal time. It is assumed that all reacted Si is present as Si in the disilicide. The thickness of the disilicide layer can then be derived using the molar volume of the disilicide phase. Using the value of bulk $TiSi_2$ ($V_m^{TiSi_2} = 42.4 * 10^{-24}$ cm^{-3}) one obtains the thickness scale as indicated on the right hand side abscis of Fig. 5.21. The error due to the presence of some monosilicide is expected to be small.

From Fig. 5.21 it can be concluded that the growth of the silicide is diffusion controlled, at least in the later stages of the reaction were a single straight line fits the measured data. From the slope of the straight lines one derives an effective chemical inter-diffusion coefficient $\tilde{D}$ as defined by the equation:

$$\frac{dx}{dt} = \frac{\tilde{D}}{x} \qquad or \qquad \tilde{D} = \frac{x^2}{2\,t} \tag{5.3}$$

where x is the reacted layer thickness. The measured values of the effective inter-diffusion coefficient as a function of temperature are presented in the Arrhenius plot of Fig. 5.22. Also shown are the values of the inter-diffusion coefficient as measured by Hung et al. [Hun83] for the reaction of Ti with

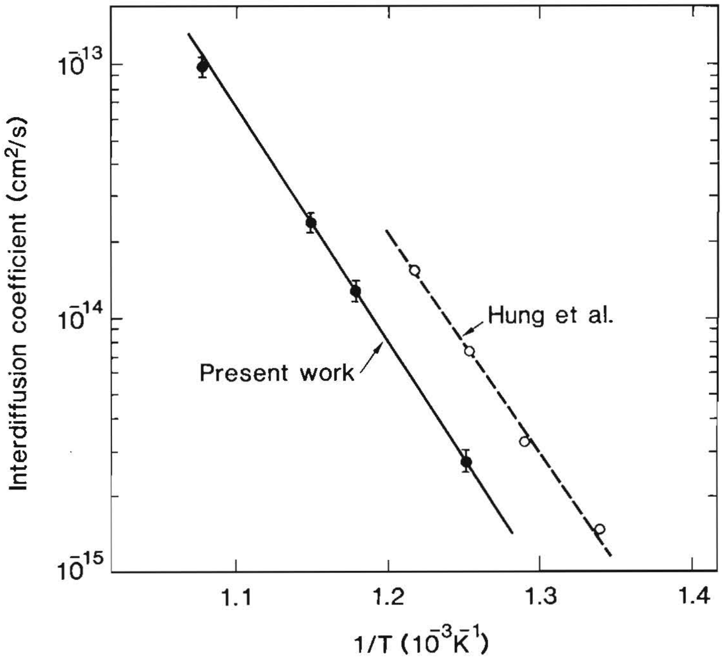

Fig. 5.22. Effective chemical inter-diffusion coefficients as a function of reciprocal temperature. Solid dots: derived from Figs. 5.21 and 5.23; open dots: derived from the work of Hung et al. [Hun83].

amorphous Si. From the slope of the solid straight line an effective activation energy of (1.9 ± 0.1) eV can be derived which agrees with that derived from Hung's data (1.8 ± 0.1 eV). The difference in absolute magnitude of the diffusion coefficient may be caused by differences in temperature calibration ($\approx 25^oC$).

In Fig. 5.21 it can be observed that before the diffusion controlled stage of the reaction sets in, the reaction proceeds with a much faster rate in the initial stages. We tried to obtain a more detailed picture of these initial stages of the reaction and the transition to the diffusion controlled stage by annealing many samples at the same temperature (600 °C) during different times. A Ti layer of 50 nm nominal thickness was used. The amount of reacted Si was determined as before.

The square of the amount of reacted Si is shown as a function of anneal time in Fig. 5.23. Different samples of the same wafer were found to give sometimes drastically different silicide thicknesses. Cleaning the samples *in-situ* with a sputter-etch in the deposition chamber just prior to Ti deposition did not yield the expected improvement in reproducibility. On some sputter-cleaned samples an intermediate, very thin (about 5 nm), co-

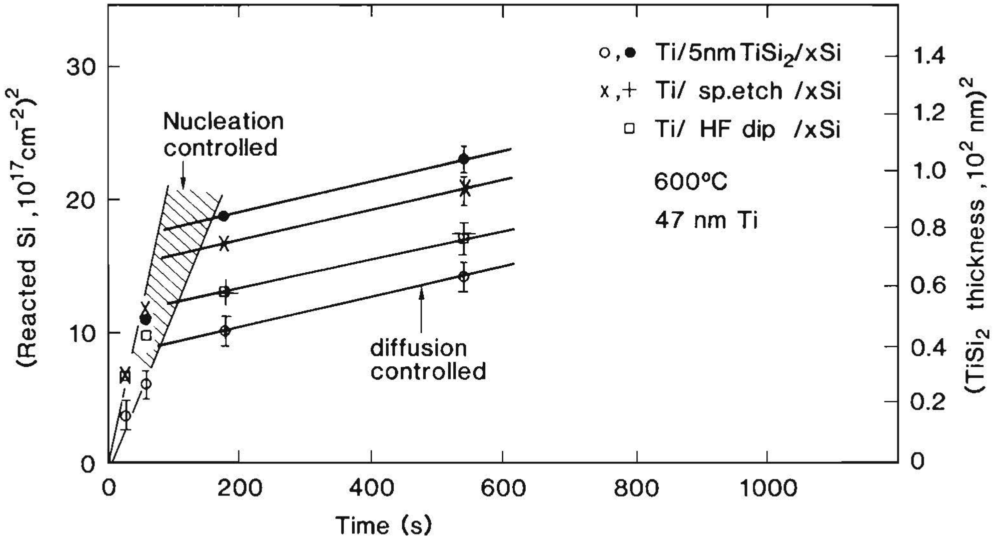

Fig. 5.23. Squared reacted amounts of Si as a function of anneal time at a temperature of 600 °C. The initial fast reaction step is thought to be controlled by nucleation, while the slower reaction is controlled by diffusion. The measurements are for different conditions of the interface. HF dip: only wet chemically cleaned; sp.etch: with an additional *in-situ* sputter-etch; 5 nm $TiSi_2$: sputter-etch and deposition of a thin intermediate layer of the stoichiometric $TiSi_2$ composition.

sputtered layer of composition Ti/Si = 1/2 (as described in chapter 2) was deposited. The latter samples yielded no improvement in reproducability either, and the presence of such a thin $TiSi_2$ layer at the Ti - xSi interface apparently does not influence the kinetics of the reaction.

A more detailed inspection of Fig. 5.23 shows that the slope of the straight lines in the diffusion controlled part of the reaction does reproduce from sample to sample, and that diffusion coefficients derived from the slope of these lines agree closely with the values of the chemical inter-diffusion coefficient as measured in the entirely diffusion controlled reaction of Ti with amorphous Si (Fig. 5.22). We conclude that the irreproducibility is concentrated in the initial stages of the reaction or, more specifically, in the position of the transition point of the fast initial reaction to the diffusion controlled reaction and possibly the rate of the fast initial reaction itself.

Such an irreproducible behaviour of Ti - crystalline Si thin film diffusion couples as compared to the reproducible behaviour of Ti - αSi diffusion couples has been noted by other investigators too [Hun83]. Moreover, a fast initial reaction or a positive abscis intercept of the squared reacted thickness versus time plot can also be noted from the work of Iyer et al. [Iye85], Aumann et al. [Aum85] and Pico et al. [Pic86].

The differences between the reaction of Ti with αSi and xSi have been attributed [Hun83] to the αSi - Ti interface being considerably cleaner than the xSi - Ti interface. From the previous section it can be concluded that the common interfacial impurities like C and O do not inhibit the Ti - xSi reaction very much at low temperatures (about 400 °C). It is not expected that they will affect the reaction in the high temperature regime much more. An alternative explanation for the bad reproducibility of the Ti - xSi reaction is based on the nucleation difficulties of the disilicide on a xSi - monosilicide interface due to the small heat of reaction when forming the disilicide as was introduced in section 5.4.1. The considerable roughening of the layer during the reaction may also be an indication that nucleation plays a significant role in the early stages.

The nucleation rate will be very sensitive to interfacial energies, heat of reaction, stress, and the presence of heterogeneous nucleation sites as interfaces and grain boundaries. The magnitude of these parameters will be influenced by for example the presence of minute amount of impurities which hardly can be avoided in practical experiments. Irreproducability is then easily explained from the combination of the sensitivity of the nucleation process to the prevailing conditions and the presence of probably unavoidable impurities in the Ti, in the Si, at grain boundaries, surfaces and interfaces.

It is reported that annealing of a thin Ti layer on xSi in ultra high vacuum results in the surface segregation of Si long before a bulk silicidation reaction occurs [But84,Idz86]. Moreover, when a Ti layer is deposited on an oxidized Si wafer, which contains contact holes to bare Si and annealed in vacuum, lateral formation of silicide over the oxide edges occurs. The rate of this lateral diffusion process is much faster than the rate which is dictated by normal diffusion controlled growth [Hov88]. The rapid lateral silicidation and the segregation of Si at the surface are both thought to be indications of the presence of fast interphase grain boundary material transport paths in Ti - Si diffusion couples. Nucleation of a new phase always requires the creation of interphase boundaries. The presence of these interphase boundaries in the nucleation controlled part of the silicidation process might explain the fast reaction rate in the initial reaction stage. The rate of this fast transport mechanism is likely to be very sensitive to the presence of minute amounts of impurities at the interphase boundaries, and might attribute to the irreproducible behaviour of a Ti - xSi diffusion couple.

The importance of nucleation and the presence of fast interphase diffusion paths leads to the following model to explain the behaviour of Ti - xSi diffusion couples (see Fig. 5.24).

(i) At low temperatures (400 °C to 500 °C) a mixed planar layer of approximately equiatomic composition is formed (Fig. 5.24b). The growth of this layer is probably controlled by diffusion through that layer.

(ii) At a temperature of about 525 °C the C49 $TiSi_2$ phase nucleates (Fig. 5.24c), probably heterogeneously on the Si - monosilicide interface.

(iii) The separate nuclei grow by fast transport along the Si - C49 $TiSi_2$ interphase boundary (Fig. 5.24c), the TiSi - C49 $TiSi_2$ interphase boundary or both.

(iv) Finally the nuclei coalesce into a continuous $TiSi_2$ layer (Fig. 5.24d), and the silicide grows controlled by diffusion through the silicide layer itself. This growth stage corresponds to the straight lines in Fig. 5.21 and 5.23.

Initially, some monosilicide will remain in the stages *(iii)* and *(iv)*. Later in the reaction this monosilicide may disappear in favor of the faster growing disilicide. The difference in behaviour of a Ti - αSi and a Ti - xSi diffusion couples is essentially caused by the much lower nucleation temperature of the disilicide phase in the αSi case. The lower nucleation temperature of the disilicide on an αSi surface leads to a continuous layer at a much lower thickness.

We conclude that the non-reproducability of the Ti - xSi reaction is not directly due to the presence of some monolayers of interfacial impurities after common cleaning procedures The alternative explanation based on the nucleation difficulties of the disilicide is more consistent with the behaviour of impurities at low temperatures and the observed low temperature intermixing of Ti with αSi and xSi. In a conventional salicide process involving rapid thermal annealing in N_2 an undesirable dependence of silicide thickness on dopant level and type in contact holes is frequently observed [Hov88,Bey87]. One might anticipate that this effect too is related to the nucleation phenomena as described in this section. Similarly, the typical roughness observed for silicidized Ti contacts [Hov88] probably is not caused by the presence of a native oxide on xSi after typical cleaning procedures, but rather will be related to the nucleation difficulties of the disilicide on a xSi substrate [Heu88].

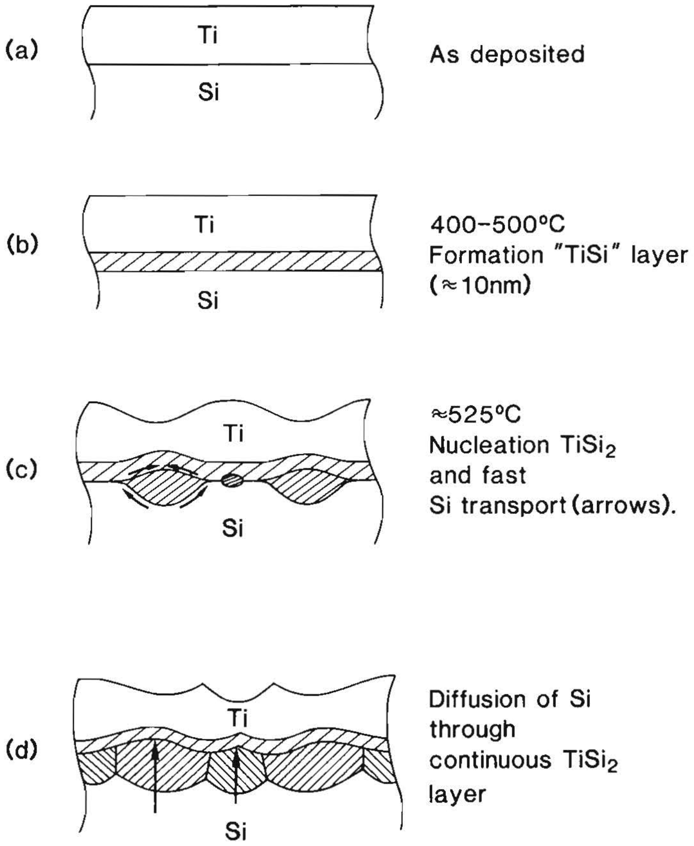

Fig. 5.24. Model for the nucleation and growth of silicides in a Ti - xSi diffusion couple. (a) as-deposited, some limited interaction may have taken place already in this stage of the process (not indicated); (b) formation of a reacted layer of approximately equiatomic composition; (c) nucleation of the disilicide, the typical distance between the nuclei is of the order of 10 nm; (d) diffusion controlled growth of $TiSi_2$.

5.5 Conclusions

In this work the reactions in various sputter-deposited Ti - Si diffusion couples were investigated in the temperature range of 300 °C to 700 °C. Both the reaction of Ti with crystalline Si as well as the reaction with sputter-deposited αSi has been addressed

In the case of reaction of Ti with αSi it has been shown that, before any crystalline silicides formed, the polycrystalline Ti layer reacts with the αSi layer to form an amorphous silicide. inter-diffusion of the Si and Ti layers occurred at temperatures as low as 350 °C, while a crystalline silicide (C49 $TiSi_2$) only formed at temperatures of 500 °C and higher. The average composition of the amorphous silicide ($\alpha TiSi_x$) was close to equiatomic. It was found from Auger depth profiling that a large composition gradient exists over the growing amorphous silicide, the silicide being very Si–rich near the Si - silicide interface ($c_{Si} \approx 0.7$) and Si poor near the silicide - Ti interface ($c_{Si} \approx 0.2$). A calculation of the free energy diagram of the Ti - Si system showed that such a large phase field is to be expected from thermodynamical arguments.

The $\alpha TiSi_x$ layer could be grown thermally to quite large thicknesses: a layer of Ti could be reacted with amorphous Si to form about 18 nm of amorphous silicide. The growth of the amorphous phase was accompanied by the nucleation and growth of Kirkendall voids at the αSi - $\alpha TiSi_x$ interface, indicative of a high mobility of Si and a low mobility of Ti at these low temperatures. The growth of the amorphous silicide was consistent with a diffusion controlled process in the initial stages. The inter-diffusion coefficient was consistent with extrapolations from those derived from the reaction rate at higher temperatures. The growth and coalescence of the Kirkendall voids at the αSi - $\alpha TiSi_x$ interface eventually causes a deviation from diffusion limited growth to occur by suppressing the Si flux to the growing layer. The interfacial contact area will be reduced until the growth virtually stops at a thickness of 18 nm.

When a Ti layer is reacted with monocrystalline Si the reaction proceeds very similar to the reaction with αSi at low temperatures (≤ 450°C) in that a reacted layer $TiSi_y$ of approximately equiatomic composition is formed. Preliminary electron diffraction experiments revealed no differences between the $TiSi_y$ layer formed from xSi and the $\alpha TiSi_x$ layer formed from αSi. The reaction rate is approximately equal to the reaction rate with αSi. The Ti - xSi interface and the Ti - αSi interface appear about equally reactive, even if some interfacial impurities like C and O are present on the Ti - Si interface. At a reaction temperature of about 500 °C profound differences between the Ti - xSi and Ti - αSi reaction were noticed.

Whereas on *amorphous* Si the disilicide (C49 phase) nucleates readily, it does not nucleate on *crystalline* Si.

These nucleation difficulties are reflected in the behaviour of a Ti - xSi diffusion couple at normal growth temperatures (550 °C to 700 °C). The reactions are studied in detail with Rutherford backscattering spectrometry and *in-situ* annealing in the target chamber. Two distinct regimes of reaction were noticed. Firstly a fast initial reaction is ascribed to the nucleation of the disilicide and the presence of a fast interphase boundary transport mechanism. Secondly, as soon as the nuclei coalesce into a continuous layer of the disilicide, the reaction proceeds with a normal and very reproducable diffusion controlled rate. The irreproducible behaviour of Ti - Si diffusion couples can now be explained from the sensitivity of the nucleation rate and the rate of the fast interphase transport mechanism to the prevailing conditions.

Bibliography

[Abd86] M.O. Abdoelfotoh and K.N. Tu, Phys. Rev. B **34**, 2311 (1986).

[Aum85] C.E. Aumann, J.R. Jacobs, M.S. Phipps, C. Pico, N.C. Tran and M.G. Lagally, Proc of the VLSI Multilevel Conf., Santa Clara (1985) (Inst. El. Electron. Eng., New York 1985).

[Bar52] J. Bardeen and C. Herring in 'Imperfections in Nearly Perfect Crystals' ed. by W. Shockley, J.C. Hollomon, R. Maurer and F. Seitz (Wiley, New York 1952).

[Bar86] J.C. Barbour, Phys. Rev. Lett. **48**, 1436 (1986).

[Bar87] J.C. Barbour, R. de Reus, A.W. Denier van der Gon and F.W. Saris, J. Mater. Res. **2**, 168 (1987).

[Ben85] G.G. Bentini, R. Nipoti, A. Armigliato, M. Berti, A.V. Drigo and C. Cohen, J. Appl. Phys. **57**, 270 (1985).

[Ben87] R.W. Bené, J. Appl. Phys. **61**, 1826 (1987).

[Ber84] M. Berti, A.V. Drigo, C. Cohen, J. Siejka, G.G. Bentini, R. Nipoti and S. Guerri, J. Appl. Phys. **55**, 3558 (1984).

[Bey85] R. Beyers and R. Sinclair, J. Appl. Phys. **57**, 5240 (1985).

[Bey87] R. Beyers, D. Coulman and P. Merchant, J. Appl. Phys. **61**,5110 (1987).

[Bos87] Internal report nr. **447/87** (Philips Research Laboratories, Eindhoven, the Netherlands 1987).

[Bra86] D. Brasen, R.H. Willens, S. Nakahara and T. Boone, J. Appl. Phys. **60**, 3527 (1986).

[Bru61] C. Brukl, H. Nowotny, O. Schob and F. Benesovsky, Mh. Chem. **92**, 781 (1961).

[Bus81] K.H.J. Buschow, J. Appl. Phys. **52**, 3319 (1981).

[Bus82] K.H.J. Buschow, Solid State Commun. **43**, 171 (1982).

[But83] R. Butz, G.W. Rubloff and P.S. Ho, J. Vac. Sci. Technol. **A1**, 771 (1983).

[But84] R. Butz, G.W. Rubloff, T.Y. Tan and P.S. Ho, Phys. Rev. **B30**, 5421 (1984).

[Cha80] B. Chapman, 'Glow Discharge Processes' (Wiley, New York 1980).

[Chu74] W.K. Chu, H. Krautle, J.W. Mayer, H. Muller, M.A. Nicolet and K.N. Tu, Appl. Phys. Lett. **25**, 454 (1974).

[Cob74] J.W. Coburn and E. Kay, CRC Crit. Rev. Sol. State Sci. **4**, 561 (1974).

[Cot56] P.G. Cotter, J.A. Kohn and R.A. Potter, J. Am. Cer. Soc. **39** 11 (1956).

[Doo85] L.R. Doolittle, Nucl. Instr. Methods **B9**, 344 (1985).

[Fan81] J.C.C. Fan and H. Anderson, J. Appl. Phys. **52**, 4003 (1981).

[Geg80] Ya.Ye. Geguzin, Yu. S. Kaganovskiy, L.M. Paritskaya and V.I. Solunskiy, Phys. Met. Metall. **47**, 127 (1980).

[Gos82] U. Gósele and K.N. Tu, J. Appl. Phys. **53**, 3252 (1982).

[Hen72] R.C. Henderson, J. El. Chem. Soc. **119**, 772 (1972).

[Hen87] J.C. Hensel, J.M. Vandenberg, F.C. Unterwald and A. Maury, Appl. Phys. Lett. **51**, 1100 (1987).

[Heu88] F.M. d'Heurle, J. Mater. Res. **3**, 167 (1988).

[Hof80] S. Hofmann, Surf. Interf. Analysis **2**, 148 (1980).

[Hol87] K. Holloway and R. Sinclair, J. Appl. Phys. **61**, 1359 (1987).

[Hou86] H.J.W. van Houtum and I.J.M.M. Raaijmakers, Mat. Res. Soc. Symp. Proc. **54**, 37 (1986) (Materials Research Society, Pittsburgh).

[Hou87] H.J.W. van Houtum, I.J.M.M. Raaijmakers and Th.J.M. Menting J. Appl. Phys. **61**, 3116 (1987).

[Hou88] H.J.W. van Houtum, A.A. Bos, A.G.M. Jonkers and I.J.M.M. Raaijmakers, accepted for publication in J. Vac. Sci. Technol. **B XX**, xxx (1988).

[Hov88] L. Van Den Hove, PhD Thesis, University of Leuven (Leuven, Belgium 1988).

[Hun80] L.S. Hung, S.S. Lau, M. von Allmen, J.W. Mayer, B.M. Ullrich, J.E. Baker, P. Williams and W.F. Tseng, Appl. Phys. Lett. **37**, 909 (1980).

[Idz86] Y.U. Idzerda, E.D. Williams and R.L. Park, Surf.Sci.Lett. **177**, L1028 (1986).

[Iye85] S.S. Iyer, C.Y. Ting and P.M. Fryer, J. Electrochem. Soc. **132**, 2240 (1985).

[Jac86] J.W.M. Jacobs and J.F.C.M. Verhoeven J. Microscopy **143**, 103 (1986).

[Jay86] D.C. Jay, A.D. Romig jr.,J.I. Goldstein eds, 'Principles of Analytical Electron Microscopy' (Plenum, New York, 1986).

[Joh86] W.L. Johnson, Progr. Mat. Sci. **30**, 81 (1986).

[Jon87] A.G.M. Jonkers, H.J.W. van Houtum and A. Moet, Proc. Workshop on Refr. Metals and Silicides. Aussois (France) 1987, published in: le Vide, les Couches Minces **42**, 103 (1987).

[Kau73] L. Kaufman and H. Nesor in 'Titanium Science and Technology', ed. by R.I.Jaffe and H. Burte (Plenum Press, New York 1973).

[Kau79] L. Kaufman, CALPHAD **3**, 45 (1979).

[Kem82] M.J.H. Kemper and P.H. Oosting, J. Appl. Phys. **53**, 6214 (1982)

[Ker72] W. Kern, Solid State Technol., Januari, 34 (1972).

[Kik87] A. Kikuchi and T. Ishiba, J. Appl. Phys. **61**, 1891 (1987).

[Lau82] S.S. Lau, C.S. Pai and C.S. Wu, Appl Phys. Lett. **41**, 77 (1982).

[Lav39] F. Laves and H.J. Wallbaum, Z. Kristallogr. **101** 78 (1939).

[Lin84a] C.D. Lien and M.A. Nicolet, J. Vac. Sci. Technol. **B2**, 738 (1984).

[Lin84b] C.D. lien, M.A. Nicolet and S.S. Lau, Appl. Phys. A **34**, 249 (1984).

[Lin84c] C.D. lien, M.A. Nicolet and S.S. Lau, Phys. Stat. Solidi A **8**, 123 (1984).

[Lin86] C.D. lien, M.A. Nicolet and S.S. Lau, Thin Solid Films **143**, 63 (1986).

[Lir85] M. Liehr, F.K. Legoues, G.W. Rubloff and P.S. Ho, J. Vac. Sci. Technol. **A3**, 983 (1985).

[Liu79] Y.C. Liu, C.J. Lin and J.S. Maa, Jpn. J. Appl. Phys. **18**, 991 (1979).

[Loe85] E.J. van Loenen, PhD Thesis, University of Utrecht (Utrecht, the Netherlands 1985).

[Mae86] K. Maex, R.F. de Keersmaecker, M. van Rossum, W.F. van der Weg and G. Krooshof, proc. conf. Ion Beam Mixing and Modification of Materials, Catania (Italy) (1986).

[Mae87] K. Maex, R.F. de Keersmaecker, M. van Rossum, W.F. van der Weg and G. Krooshof, Proc. Workshop on Refr. Metals and Silicides Aussois (France) 1987, published in: le Vide, les Couches Minces **42**, 141 (1987).

[Mae88] K. Maex, PhD Thesis, University of Leuven (Leuven, Belgium 1988).

[May82] E.A. Maydell-Ondrusz, P.L.F. Hemment, K.G. Stephens and S. Moffat, Electronics Letters **18**, 754 (1982).

[Mer84] P. Merchant and J. Amano, J. Vac. Sci. Technol. **B2**, 762 (1984).

[Mie88] A.R. Miedema and A.K. Niessen, to be published, J. Jap. Met. Soc. (1988).

[Mur83] S.P. Murarka, 'Silicides for VLSI Applications' (Ac. Press, New York 1983).

[Mur80] S.P. Murarka and D.B. Fraser, J. Appl. Phys. **51**, 342 (1980).

[Nem85] R.J. Nemanich, R.T. Fulks, B.L. Stafford and H.A. Vander Plas, J. Vac. Sci. Technol. **A3**, 938 (1985).

[New86] S.B. Newcomb and K.N. Tu, Appl. Phys. Lett. **48**, 1436 (1986).

[Nic83] M.A. Nicolet and S.S. Lau, in VLSI Electronics,**6**, edited by N.G. Einspruch (Academic, New York, 1983) .

[Ost83] M. Óstling, C.S. Petersson, C. Chatfield, H. Norstróm, F. Runovc, R. Buchta and P. Wiklund, Thin Solid Films **110**, 281 (1983).

[Pic86] C.A. Pico, N.C. Tran, J.R. Jacobs and M.G. Lagally, Mat. Res. Soc. Symp. Proc. **54**, 315 (1986) (Materials Research Society Pittsburgh).

[Pre78] R. Pretorius, J.M. Harris and M.A. Nicolet, Solid State Electron. **21**, 667 (1978).

[Pre84] R. Pretorius, Mat. Res. Soc. Symp. Proc. **25**, 15 (1984).

[Raa86] The heat of crystallization of a $TiSi_2$ alloy was measured by differential scanning calorymetry. It was found to be (11 ± 2) kJ/mol (unpublished result 1986).

[Raa87a] I.J.M.M. Raaijmakers, A.H. Reader and H.J.W. van Houtum. J. Appl. Phys. **61**, 2527 (1987).

[Raa87b] I.J.M.M. Raaijmakers, A.H. Reader and H.J.W. van Houtum, Proc. Workshop on Metals and Silicides, Aussois (France) 1987, published in: le Vide, les Couches Minces **42**, 75 (1987).

[Raa88c] Preliminary secondary ion mass spectroscopy depth profiles of a typical diffusion couple showed some F at the Ti - Si interface. Using a known F implantation in Si as a standard the integrated amount of F was estimated to be smaller than 10^{13} cm^{-2}. (unpublished result 1988).

[Rho80] E.H. Rhoderick, 'Metal Semiconductor Contacts' (Clarendon Press, Oxford 1980).

[Ron83] M. Ronay, Appl. Phys. Lett. **42**, 577 (1983).

[Ros84] M. Van Rossum, M.A. Nicolet and W.L. Johnson, Phys. Rev. **B29**, 5498 (1984).

[Rub86] G.W. Rubloff, R.M. Tromp and E.J. van Loenen, Appl. Phys. Lett. **48**, 1600 (1986).

[Sar86] F.W. Saris, L.S. Hung, M. Nastasi and J.W. Mayer, Mater. Res. Soc Symp. Proc. **54**, 81 (1986).

[Sch85] H. Schroeder, K. Samwer and U. K ster, Phys. Rev. Lett. **54**, 197 (1985).

[Sin88] W.C. Sinke, S. Roorda and F.W. Saris, submitted for publication in J. Mater. Res. (1988).

[So 86] F.C.T. So, C.D. Lien and M.A. Nicolet, J. Vac. Sci. Technol. **A3**, 2284 (1985).

[Sun86] C. Sunyanarayana , A. Inoue and T. Masemoto, J. Mat. Sci. **15**, 1993 (1980).

[Tau82] M.A. Taubenblatt and C.R. Helms, J. Appl. Phys. **53** 6308 (1982).

[Tau85] M.A. Taubenblatt, Thesis Stanford university, Stanford (1985).

[Tau86] M.A. Taubenblatt and C.R. Helms, J. Appl. Phys. **59** 1992 (1986).

[Tou70] Y.S. Touloukian and C.Y. Ho, 'Thermal Radiative Properties' Thermophysical Properties of Matter **7** (Plenum, New York 1970).

[Wal76] R.M. Walser and R.W. Bené, Appl. Phys. Lett. **28**, 624 (1976).

[Wil86] D.S. Williams, R.A. Rapp and J.P. Hirth, Thin Solid Films **142**, 47 (1986).

[Won87] S.S. Wong, D.C. Hen, P. Merchant, T.R. Cass and J. Amano, IEEE Transactions on Electron Devices **ED34**, 587 (1987).

[Zie73] J. Ziegler, J. Mayer, C. Kircher and K.N.Tu, J. Appl. Phys. **44**, 3851 (1973).

Chapter 6

Summary

In order to alleviate the problems associated with downscaling and increasing complexity of integrated circuits, the development of novel high temperature resistant contact and interconnect materials with a low electrical resistivity is needed. Silicides, i.e. compounds between a (transition) metal and silicon are very interesting materials for application in integrated circuits. Therefore, the formation mechanisms and properties of silicides have been studied extensively in the last decade. However, much remains to be done before a complete picture of the reactions of metals with Si is obtained.

This thesis describes formation mechanisms and electrical properties of titanium silicide, the silicide which is certainly going to be applied in integrated circuits. Titanium silicide ($TiSi_2$) is fitted in the process flow of integrated circuits by essentially two preparation methods: *(i)* heat treating a co-sputtered amorphous alloy of Ti and Si which causes a crystallization reaction to occurr and *(ii)* heat treating a Ti - Si diffusion couple which causes compound growth by chemical inter-diffusion. In chapters 2 to 4 silicide formation with the first method is described while in chapter 5 the formation mechanisms corresponding to the second preparation method are treated.

In chapter 2 it is described how the crystallization of Ti - Si binary amorphous alloys is studied by annealing ***in-situ*** in a transmission electron microscope. This method offers a nice way to separately observe the nucleation and growth of silicide crystals in an amorphous matrix in real time. We observed the alloys to crystallize through a random nucleation and growth process with constant rates (at a particular temperature). A high degree of faulting was noted in the crystalline material. An investigation of the nature of these faults showed these defects to be stacking faults, the presence of which could be related to the crystal structure of the silicide.

An investigation of the effects of these faults on the resistivity is reported in chapter 3. For that purpose the resistivity of co-sputtered Ti - Si alloy thin films was measured during the reactions. Three different reaction stages were easily recognized: *(i)* nucleation and growth of the so-called C49 $TiSi_2$ at a temperature of about 300 °C; *(ii)* a hitherto unidentified precipitation reaction in the temperature regime of 300 °C to 750 °C; and *(iii)* a polymorphic phase transition from the C49 to the so-called C54 phase at temperatures of about 800 °C.

During the course of a typical anneal process a large but sluggish decrease in resistivity of the crystalline material occurs during the precipitation reaction. This resistivity decrease could only partly be explained from a decrease in density of the above mentioned stacking faults. For the first time it was shown that the phase field of the C49 $TiSi_2$ phase (which is a particular crystalline form of the disilicide) may be of substantial width. A decrease in the density of point defects, due to stoichiometry deviations, explained the other part of the observed resistivity decrease. At temperatures exceeding 750 °C a phase transformation occurs from the C49 phase to the C54 $TiSi_2$ phase. This transformation is beneficial from a technological point of view, because it happens to be associated with the elimination of practically all faults and point defects from the silicide, thus creating a material with a reproducably low resistivity.

The overall kinetics of the different phase transformations in the Ti - Si system are conveniently measured with *in-situ* resistivity measurements. Such kinetic studies are reported in chapter 4. Both the crystalization reaction and the C49 - C54 phase transformation could be described remarkably well with a constant (random) nucleation rate and a constant linear growth rate in terms of the so-called Johnson–Mehl–Avrami equation. The effective activation energies can be determined from an analyses of the reaction kinetics. The activation energy of the C49 - C54 transformation was so high that it was concluded that nucleation of this phase is the difficult reaction step.

Crystallization temperatures were reported as a function of composition in chapter 4 too. Amorphous Ti - Si alloys with compositions corresponding to the central or Ti–rich part of the phase diagram (Si concentration between 0.2 and 0.6) crystallized at temperatures of about 500 °C. This temperature appeared to be higher than the temperatures at which first reactions occurred in Ti - Si diffusion couples. Consequently, it was possible to react Ti and Si to an amorphous phase (see further). A marked depression of the stability of the amorphous alloy was found for compositions near that of $TiSi_2$. Values of the crystallization temperature as low as 270 °C were measured. These phenomena were discussed in terms of existing models for crystallization of amorphous alloys.

In chapter 5 reactions in Ti - Si diffusion couples were described in the temperature regime from 300 to 700 °C. A review from the literature revealed many ambiguities and the absence of a detailed study towards the kinetics of silicide formation in a Ti - crystalline Si diffusion couple. Differences in the reaction of Ti with Si in an *amorphous* or *crystalline* state are reported for which a solid explanation is still sought. Reactions were studied with Auger electron spectroscopy, Rutherford backscattering and cross-section transmission electron microscopy.

At low temperatures (smaller than about 475 °C) the reaction of Ti with αSi and xSi proceeded very similar. At these low temperatures no equilibrium silicide phases were formed, rather, an amorphous metastable alloy of about equiatomic composition forms. Differences between the reaction of Ti with αSi or xSi are found after anneal at higher temperatures (about 500 °C). While on amorphous Si the disilicide nucleates readily, it does not so on crystalline Si. The nucleation difficulties of $TiSi_2$ on xSi were ascribed to the contribution of the heat of crystallization of αSi to the total heat of reaction.

The above identified nucleation difficulties are also reflected in the behaviour of Ti - xSi diffusion couples at slightly larger growth temperatures which are normally used in salicide processing (550 °C to 700 °C). In this temperature regime the reaction could be separated in a nucleation controlled initial part, and a normal diffusion controlled part. It was shown that many reproducibility problems in the Ti - xSi reaction are primarily due to the nucleation controlled kinetics in the initial reaction stages.

This study was intended to contribute to the knowledge of Ti–silicides and reactions occurring in the Ti - Si system. Important from a technological point of view is the profound presence of nucleation difficulties. These difficulties occurr as well during the formation of C49 $TiSi_2$ on a crystalline Si substrate as during C54 - C49 phase transformation This knowledge may lead to new ways of tackling technological problems.

From a scientific point of view, it seems worthwile to study the crystallization reactions in different co-deposited (amorphous) silicides in a more systematic way. Interesting findings in such amorphous films are the decrease in crystallization temperature for compositions near that of $TiSi_2$. Since we have demonstrated that a solid state amorphization reaction occurs readily in the Ti - Si system knowledge on crystallization reactions may also improve our basic understanding of metal - Si reactions and first phase nucleation rules.

Curriculum Vitae

De schrijver werd geboren op 29 juli 1957 te Almelo. In juni 1975 behaalde hij het diploma Atheneum B aan het Willibrordus college te Goes. In hetzelfde jaar is hij aangevangen met de studie Technische Natuurkunde aan de Technische Hogeschool (nu: Technische Universiteit) te Eindhoven. In oktober 1982 behaalde hij het Ingenieurs diploma in de technische natuurkunde, het afstudeerwerk betrof een theoretisch en experimenteel onderzoek aan afwijkingen van locaal thermodynamisch evenwicht in inductief gekoppelde argon plasmas. Het onderzoek werd uitgevoerd in het Philips Natuurkundig Laboratorium onder leiding van Prof. Dr. Ir. D.C. Schram (TUE) en Dr. P.W.J.M. Boumans (Philips). Sinds oktober 1982 is hij werkzaam in het Philips Natuurkundig Laboratorium in de Groep Silicium Technologie. Hij onderneemt daar materiaalkundig onderzoek op het gebied van reacties in dunne films (silicides), groei van dunne films (aluminium) en magnetron kathode verstuiving.

Stellingen bij het proefschrift:

FUNDAMENTAL ASPECTS OF REACTIONS IN TITANIUM–SILICON THIN FILMS FOR INTEGRATED CIRCUITS

Ivo J.M.M. Raaijmakers,

8 november 1988
TU Eindhoven

1. Slecht reproduceerbaar gedrag van de reactie tussen titaan en kristallijn silicium zoals gerapporteerd door Hung e.a. is niet primair te wijten aan onzuiverheden op het Ti - Si grensvlak.

   Dit proefschrift, hoofdstuk 5.
   L.S. Hung, J. Gyulai, J.W. Mayer, S.S. Lau en M.A. Nicolet, J. Appl. Phys. 54, 5076 (1983).

2. De kinetiek van het vormen van holtes in, en uitstulpingen op, aluminium geleidespoortjes tengevolge van electromigratie is tot op heden slecht beschreven. Het verdient aanbeveling om de beschrijving van deze kinetiek in termen van de Johnson–Mehl–Avrami vergelijking nader te bestuderen.

   K.P. Rodbell, M.V. Rodriguez en P.J. Ficalora, J. Appl. Phys. 61, 2844 (1987).

3. Een hoge restweerstand van de C49 $TiSi_2$ fase wordt veroorzaakt door zowel stapelfouten als puntfouten.

   Dit proefschrift, hoofdstuk 3.

4. Diffusie gekontroleerde groei van een intermetallische fase in een diffusiekoppel wordt dikwijls geanalyseerd met behulp van de volgende groeivergelijking:

   $$\frac{dx}{dt} = \frac{\tilde{D}}{x}$$

   waarin $\tilde{D}$ een konstante en x de laagdikte. Het is echter niet konsekwent om de meetresultaten te analyseren in een grafiek van x tegen $\sqrt{t}$.

5. Er is op het moment geen afdoende bewijs wat aantoont dat $TiSi_2$ in de C49 kristalstruktuur inderdaad een metastabiele fase is. Analoog aan het bestaan van tetragonale en hexagonale structuren van $MoSi_2$ en WSi_2 kan de C54 structuur als een hoge temperatuur modificatie van de C49 struktuur gezien worden.

   Dit proefschrift, hoofdstuk 1
   R. Beyers en R. Sinclair, J. Appl. Phys. 57, 5240 (1985).

6. De kwalitatieve evolutie van tennisrackets naar "midsize" formaat heeft ten onrechte niet geleid tot een vergelijkbare evolutie van het bespanningsmateriaal.

7. De stabiliteit van een amorfe diffusiebarriere in een geintegreerd circuit is in het algemeen niet gelimiteerd door een te lage kristallisatie-temperatuur maar door een te lage reactietemperatuur met het aangrenzende silicium of metaal.

   M.A. Nicolet, I. Suni en M. Finetti, Solid State Technol. p. 129, december (1983).
   L.S. Hung, F.W. Saris, S.Q. Wang en J.W. Mayer J. Appl. Phys. 59, 2416 (1986).

8. Het model van Vincent voor de beschrijving van driedimensionale groei van dunne films geeft een verrassend goede weergave van de realiteit als tweede orde kiemen niet geteld worden.

   R. Vincent, Proc. Roy. Soc. Lond. A 321, 53 (1971).

9. Er bestaat geen eenduidige relatie tussen de gemiddelde ruwheid van een reflecterend oppervlak en de ellipsometrische hoeken Ψ en Δ.

   I.J.M.M. Raaijmakers en M.J. Verkerk, Appl. Opt. 25, 3610 (1986).
   J.R. Blanco, P.J. McMarr en K. Vedam, Appl. Opt. 24, 3773 (1985).

10. Acupunctuur hoeft in het algemeen niet de oorzaak te zijn van het daadwerkelijk stoppen met roken na een behandeling door een acupuncturist.

11. De zogenaamde "gemiddelde faaltijd" tengevolge van electromigratie in een geleidespoortje van een bepaald materiaal is geen goede representant van de eigenschappen van dat materiaal.

    F.M. d'Heurle en P.S. Ho in "Thin Films: Interdiffusion and Reactions" red. J. Poate, K.N. Tu en J.W. Mayer, (Electrochem. Soc., Princeton NJ 1978).